A NEW APPROACH TO IMPROVE LITHIUM-ION BATTERY LIFETIME IN A RENEWABLE HOME ENERGY STORAGE SYSTEM

A NEW APPROACH TO IMPROVE LITHIUM-ION BATTERY LIFETIME IN A RENEWABLE HOME ENERGY STORAGE SYSTEM

BY

MEHDI ALIMARDANI

A THESIS

SUBMITTED TO THE DEPARTMENT OF ELECTRICAL AND COMPUTER ENGINEERING AND THE SCHOOL OF GRADUADE STUDIES OF MCMASTER UNIVERSITY

IN PARTIAL FULFILMENT OF THE REQUIREMENTS FOR THE DEGREE OF

MASTER OF APPLIED SCIENCE

Master of Applied Science (2018) McMaster University

(Electrical & Computer Engineering) Hamilton, Ontario, Canada

TITLE: A NEW APPROACH TO IMPROVE LITHIUM-ION BATTERY LIFETIME IN A RENEWABLE HOME ENERGY STORAGE SYSTEM

AUTHOR: Mehdi Alimardani
McMaster University, Hamilton Canada

SUPERVISOR: Dr. M. Narimani
CO-SUPERVISOR: Dr. N. Al-Mutawaly

NUMBER OF PAGES: xvi, 131

I would like to dedicate this thesis to my wife, Hanie, who has been an endless source of encouragement and support during my graduate studies. Thank you so much my Love! Also, I would like to dedicate this thesis to my son, Daniel, and my daughter, Niki, who gave me the courage and hope to peruse my dreams. I love you my Sweet Hearts!

Abstract

This thesis suggests a new approach to extend the lifetime of Lithium-ion batteries for a Home Energy Storage System equipped with a renewable energy source. The new configuration improves the lifetime of the energy storage device by using the pulsed charge-discharge method. The batteries in this system can be charged either using solar panels when solar energy is available or by the grid power during off-peak hours when the electricity cost is at its lowest rate. In the new configuration, the battery bank is split into two equal sections to employ pulsed charge-discharge method. Interrupting the charge or discharge current provides a relaxation time for the lithium ions to diffuse gradually into the electrodes material of Lithium-ion batteries, this reduces the damage in the microstructure of the electrodes and thus it helps to prolong the battery lifetime. The spilt bank strategy improves the longevity of Lithium-ion batteries while maximizing the solar energy utilization. This strategy leads to reduce the reliance on the grid power which decreases the consumer's total energy cost as well. To show the usefulness of the new approach, different modes of operation are discussed in details along with simulation results. An experimental setup is also developed to evaluate the effectiveness of the new approach in extending the Lifetime of Lithium-ion batteries.

Acknowledgements

I would like to thank all people who helped me in different ways during my graduate studies. First and foremost, I would like to express my utmost gratitude to my supervisor Dr. Mehdi Narimani, for all his invaluable guidance and support during my study and research at McMaster University.

I would like to appreciate my co-supervisor Dr. Nafia Al-Mutawaly as my mentor who encouraged me to study on smart grid and choose the topic of energy storage systems.

Next, I would like to thank Dr. Nigel Scofield as my former supervisor who helped me at the beginning of this academic work.

Also, I would like to thank W Booth School of Engineering Practice and Technology at McMaster University especially Dr. Ishwar Singh for providing the support and Mohammad Waleed for assisting me in implementing of the prototype for the new Home Energy Storage System.

Notations and abbreviations

AC	-	Alternative Current
Ah	-	Ampere-hour
BMS	-	Battery Management System
CC	-	Constant Current
CV	-	Constant Voltage
CCCV	-	Constant Current Constant Voltage
CT	-	Current Transformer
DAC	-	Digital To Analog Converter
DC	-	Direct Current
DCCT	-	DC Current Transformer
DOD	-	Depth of Discharge
DGS	-	Distributed Generation Stations
EIS	-	Electrochemical Impedance Spectroscopy
EKF	-	Extended Kalman Filter
EOL	-	End of Life
ESS	-	Energy Storage System
EV	-	Electrical Vehicle
FF	-	Fill Factor
HESS	-	Home Energy Storage System
IGBT	-	Isolated Gate Bipolar Transistors
Imp	-	Maximum Power Current
LA	-	Lead-Acid

LabVIEW	-	Laboratory Virtual Instrument Engineering Workbench
LDC	-	Local Distribution Company
Li-ion	-	Lithium-Ion
MPP	-	Maximum Power Point
MPPT	-	Maximum Power Point Tracking
NiCd	-	Nickel Cadmium
OCV	-	Open Circuit Voltage
P&O	-	Perturb and Observe
PT	-	Potential Transformer
PV	-	Photovoltaic
p.u	-	Per Unit
RESS	-	Residential Energy Storage System
SOC	-	State of Charge
SOC_o	-	State of Charge initial value
SOH	-	State of Health
THD	-	Total Harmonics Distortion
NaS	-	Sodium Sulfur
TOU	-	Time of Use
UPS	-	Uninterrupted Power Supplies
Vmp	-	Maximum Power Voltage
VI	-	Virtual Instrument
η_c	-	Charger efficiency
η_d	-	Discharge (Inverter) efficiency

Table of Contents

List of Figures

List of Tables

Chapter 1 : Introduction

1.1 Motivation and Background

Recently, many vendors have shown more interest in energy storage systems using rooftop solar panels for household applications to reduce the dependency to the grid power. An energy storage system can be built without or with a green energy source. A home energy storage system (HESS) without green energy source utilizes the electrical power from the grid to charge its battery bank and use the stored energy when it is required. Uninterrupted power supply (UPS) is an example for such a system when the battery bank provides power to the critical loads during a power outage. They can also be used to reduce the energy cost in the areas that the electricity cost is variable. The energy storage system without green energy source charges the battery bank when the electricity price is low and discharges the battery bank when the electricity price is high. [1] [2]

The disadvantage of an energy storage system without renewable energy source is the increase in the net produced CO_2, SO_2, and NO_x emissions due to storage system inefficiencies. Therefore, home energy storage does not reduce the emissions and energy consumption unless a renewable energy source such as solar or wind energy is integrated in the system. [2] [3]

Energy Storage systems allow self-consumption of electricity generated for household applications using photovoltaic solar panels. This helps to reduce the extra stress on the local grid equipment during peak hours. [4] [5] Also, it helps to reduce the energy cost either by storing low cost energy during off-peak hours or free solar energy at any time of the day. [5] [6] A number of

charge and discharge scenarios can be used to enhance the utilization of energy storage system based on the time of use (TOU) which it varies by jurisdiction.

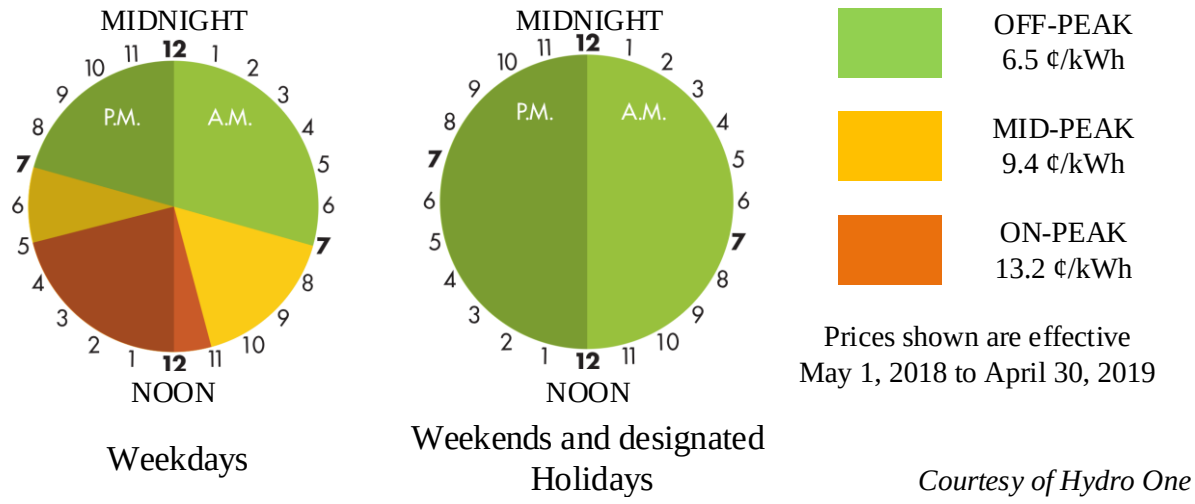

Fig. 1.1: Time of Use in Ontario for summer 2018 [7]

Fig.1.1 illustrates the electricity price per kWh and time schedule for on-peak, mid-peak and off-peak hours in Ontario in summer 2018. [7]

In the recent years, many electrical utilities have started converting the regular meters to smart meters for residential areas. Basically, the smart meters record the consumed electric energy and the time of measurement continuously. They send this information to a central system for billing based on TOU. Due to electricity cost difference between off-peak hours and on-peak hours, an energy storage system can be used to charge the battery bank during off-peak hours when the electricity cost has the lowest rate. During on-peak hours, when the electricity cost is at its highest rate, the discharging cycle is enabled. This method helps reducing the grid energy cost. Clearly, employing an energy storage system will be more feasible and beneficial if the energy cost difference between on-peak and off-peak hour's increases. [7] [8] [9]

1.2 Challenges

Generally, unmanaged injection of electrical power to the grid boosts the grid voltage locally and can cause damages to the equipment if the injected power is significantly high, that is why electrical utilities do not allow consumers to inject power to grid without having a permit. Hence in this thesis, it is considered that the household consumer is not injecting any electrical power to the grid. In order to overcome this restriction, the HESS controller monitors the incoming power from the grid and the consumed power on the household loads continuously. Using these readings, HESS controls the Grid-Tie inverter output power to prevent injecting electricity to grid at any time.

Most of the energy storage systems use electrochemical batteries as their energy reservoirs. For household application, Battery energy storage systems still need to overcome some barriers to be able to integrate into the power systems. High battery cost, lack of financial compensations, and safety are some of these barriers. [10]

The battery storage system should be capable for supplying long charge or discharge cycles. So that, Deep-Cycle batteries would be good candidates for such a system. Also it should have the capability for high number of charge-discharge cycles. In other words, the life time of the batteries should be long enough as the battery bank is generally the most expensive component of an energy storage system. Hence, the longer battery life time or the higher end of life (EOL) renders the more feasible system. For these reasons, Lithium-ion battery would be a good choice due to its advantages versus the lead acid batteries. [11] [12]

The existing home energy storage systems generally utilize a single battery bank. Although, they can improve the life time of the batteries by reducing the charge or discharge current or the depth of discharge (DOD), this is affecting the charging time and performance of the overall

system. In this thesis a new strategy to employ the battery bank is suggested to extend the battery lifetime while maximize the utilization of the renewable energy system.

1.3 Contributions of the Thesis

In this thesis, a new approach for improving the lifetime of Li-ion batteries in a renewable home energy storage system is suggested while utilizing the maximum available renewable energy.

The contributions of this thesis are:

- A novel configuration for a Renewable Home Energy Storage System is introduced,
- The new configuration increases the lifetime of the Li-ion batteries,
- The new configuration increases the utilization of the available renewable energy,
- The new system is simulated to demonstrate the performance of the news configuration at different modes of operation,
- The new HESS with split battery banks strategy is designed and implemented,
- Stress test cycles on Li-ion battery cells is performed to prove the effectiveness of this new approach on extending the batteries lifetime.

1.4 Organization of the Thesis

This thesis is organized as follows:

Chapter 1: Motivation and background, challenges and contributions of the thesis are discussed.

Chapter 2: A feasibility study for a renewable home energy storage system is provided.

Chapter 3: The main components of a renewable home energy storage system are reviewed.

Chapter 4: Conventional HESS and new HESS are compared along with modes of operation and simulations results for the suggested system.

Chapter 5: The porotype system implementation in terms of hardware and software are discussed.

Chapter 6: Experimental setup and the stress test results are explained in details.

Chapter 7: Concludes the new HESS and its benefits in a renewable home energy storage system and talks about the future works.

Chapter 2 : Home Energy Storage System Feasibility Study

A typical renewable energy storage system consists of electrochemical battery bank, the electric grid as AC source, energy conversion devices, solar or wind energy source and loads.

Fig 2.1 shows a simplified diagram of a renewable home energy storage system. The battery bank as the energy storage device can be charged by using either a green energy source or the grid. The green energy source can be from photovoltaic solar panels or wind turbines or the combination of both. In this study, photovoltaic solar panels will be considered as the green energy source.

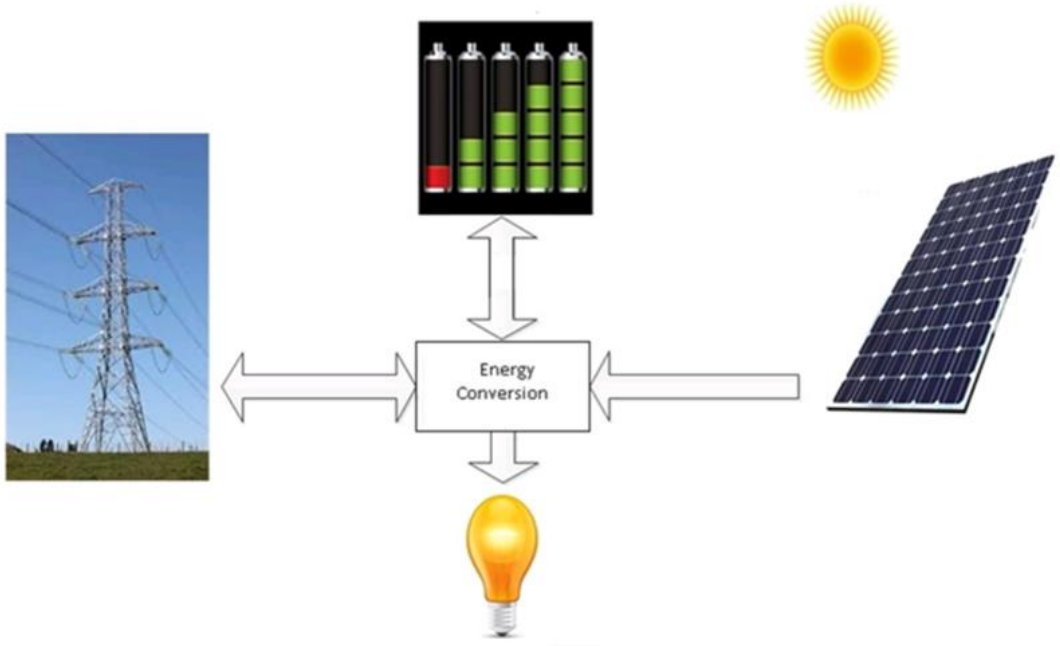

Fig. 2.1: A renewable Home Energy Storage System diagram

In order to perform feasibility study on a home energy storage system, two cases were considered. HESS without a renewable source and HESS with a renewable source.

2.1 HESS without Solar Energy -Case 1

Fig 2.2 shows an energy storage system for a house. In this system, the battery charger uses the grid electricity power during the off-peak hours to charge the battery bank. The stored energy in the battery bank is converted from DC to AC by means of a Grid-Tie inverter to feed the household loads, only during on-peak hours.

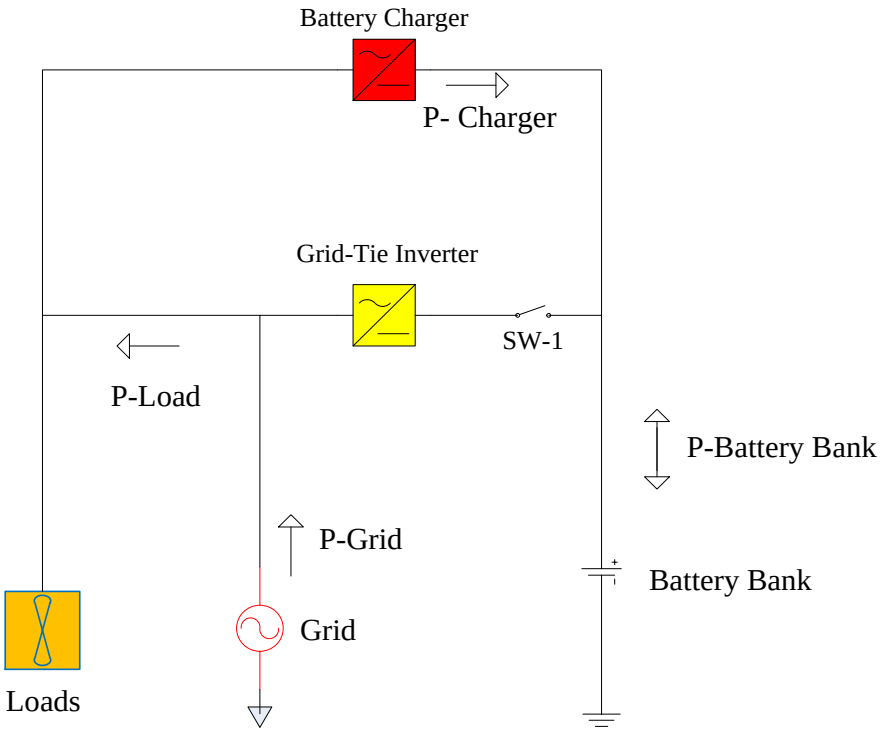

Fig. 2.2: Home Energy Storage System without renewable energy source

Since local electric utilities or local distributing companies (LDCs) have started converting the regular meters to smart meters for residential areas in the past years any power injection to grid system can be detected by these meters. This extra power can cause harm to the local grid equipment and the loads in the neighbourhood if in not controlled. So, it is assumed that the household user is not injecting electrical power to the grid at any time. Therefore, the control system has to measure the input power from grid and the load power to control the inverter output power to ensure no power is injected from the energy storage system to the grid.

In order to formulate the total electricity cost for a house, two following graphs were considered. Fig. 2.3 shows the electricity cost per kWh versus time during weekdays and Fig 2.4 shows average daily electricity consumption for a house during weekdays.

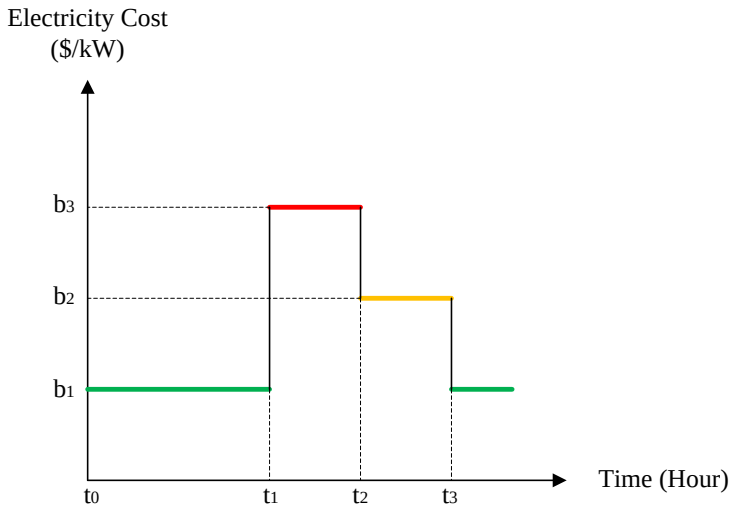

Fig. 2.3: Electricity cost per kWh versus time

Fig 2.5 shows the charging signature for a Lithium–ion battery cell. [13] As we can see from the charging current will be constant during CC charge stage when the battery voltage increases almost linearly as it stores electrical energy.

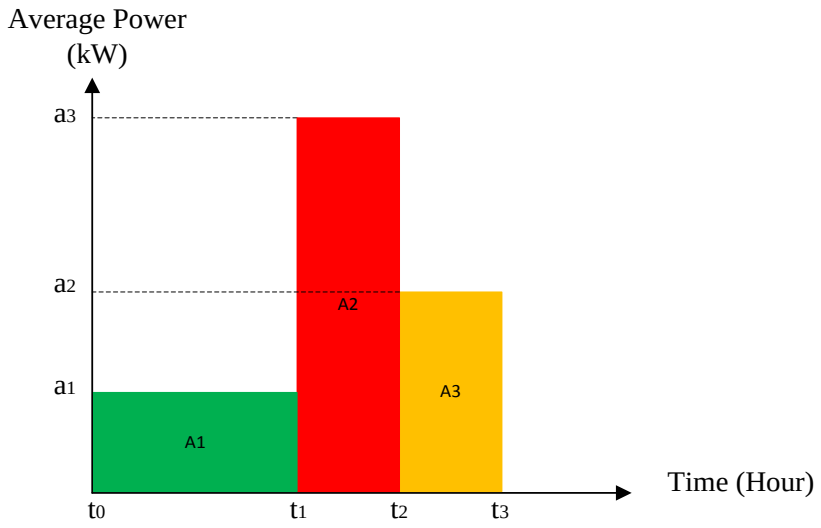

Fig. 2.4: Average power (kW) consumption per day

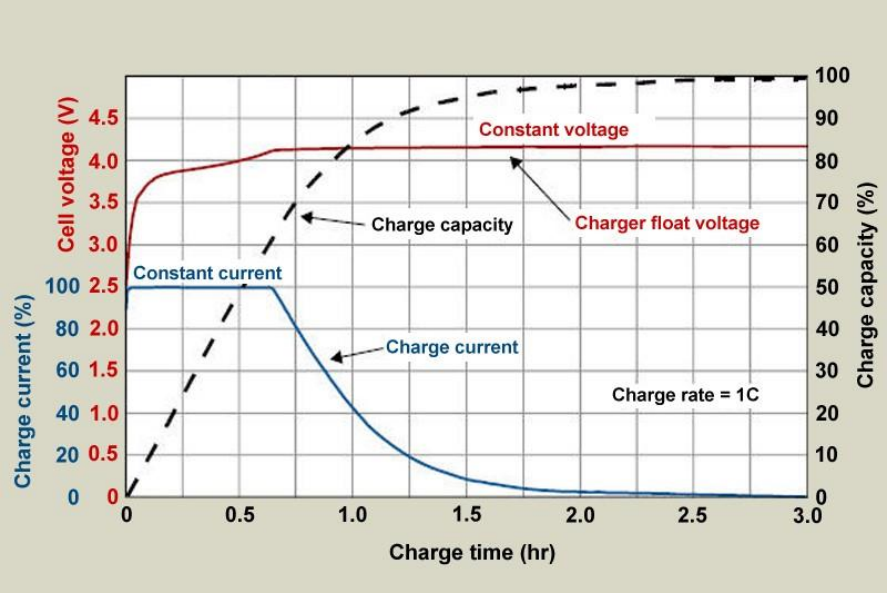

Fig. 2.5: Charging signature for a Lithium–ion battery cell [13]- *Courtesy of Cadex*

Since HESS requires deep charge and discharge cycles, the constant current operating region was considered for the Energy Storage System. The other regions are not suitable for the HESS operation due to the low efficiency and reduction in the life time.

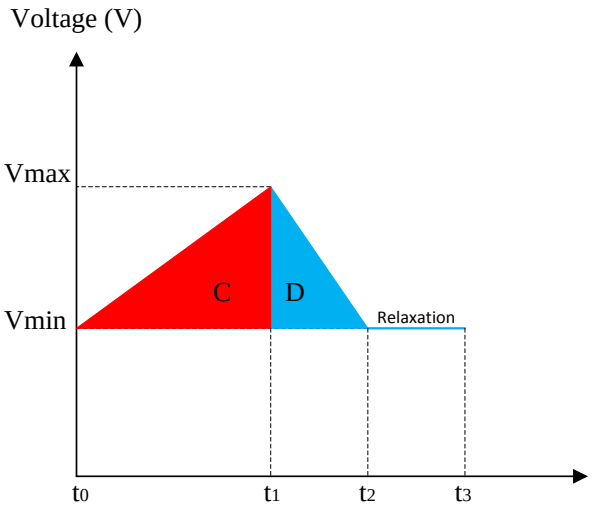

Fig. 2.6: Voltage of the battery versus Time

Fig. 2.6 represents the battery voltage value during charge and discharge cycles. Therefore, the stored energy in the battery can be determined as below:

Area C: Required energy for charging the battery to high charge level during off-peak hours (kWh) is equal to:

$$V_{average} \times I_{charge} \times P_{base} \times (t_1 - t_0) / \eta_c \qquad (2\text{-}1)$$

Where:

$$V_{average} = (V_{max} + V_{min}) / 2$$

Area D: Discharged energy to the battery low level during on-peak hours (kWh) is equal to:

$$V_{average} \times I_{Discharge} \times P_{base} \times (t_2 - t_1) \times \eta_d \qquad (2\text{-}2)$$

Where:

- $V_{average}$, I_{charge} and $I_{discharge}$ are all per unit values.
- It is considered that P_{base} is the rated battery power during on-peak hours.
- η_c and η_d are the charger and inverter efficiency values, respectively.

To utilize the maximum energy capacity of the system, we consider that the amount of charged and discharged energies should be balanced. So, we can derive equation 2-3 when the internal power loss of the battery is considered negligible.

$$I_{charge} \times (t_1 - t_0) \times \eta_d = I_{Discharge} \times (t_2 - t_1) / \eta_c \qquad (2\text{-}3)$$

Now, we can calculate the total electricity cost per day for weekdays. (Delivery and other related charges are not included yet)

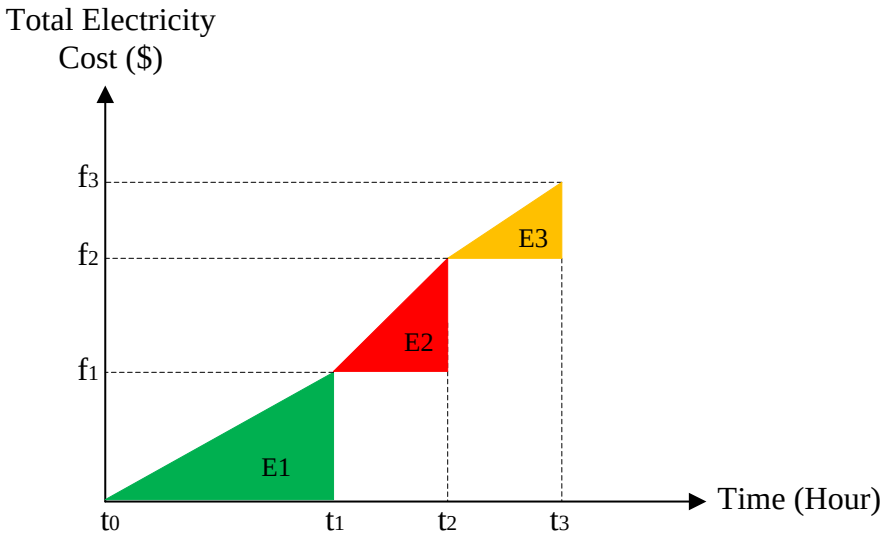

Fig. 2.7: Electricity cost without HESS

E_1, E_2 and E_3 are the electricity costs during off-peak, on-peak and mid-peak hours respectively as shown in fig. 2.7. The delivery charge is usually a combination of fixed and variable charges which is a significant portion of the electricity cost.

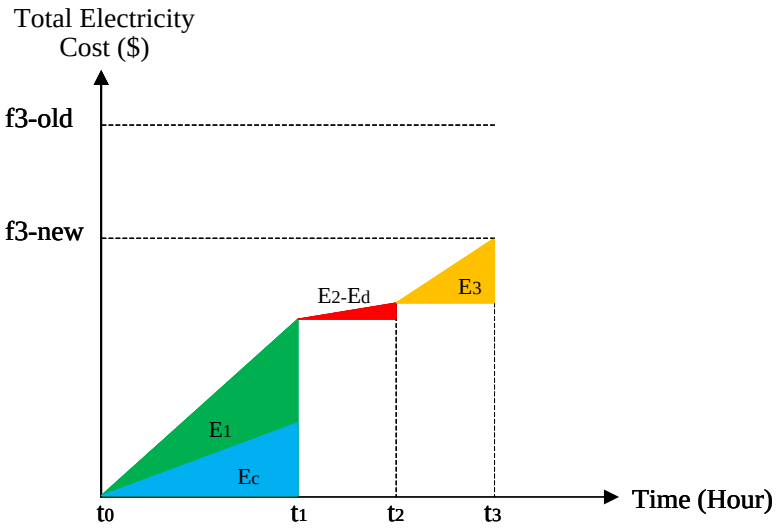

Fig. 2.8: Electricity cost with HESS

In Fig. 2.8, E_c and E_d represent the amount of energy which is transferred into and out of the battery bank during charge and discharge cycles, respectively. The total energy cost in a day for a household is represented by f_3-*old* when there is no energy storage system and f_3-*new* when the storage capability is exist. As one can observed, the total cost is expected to be reduced after adding the energy storage system.

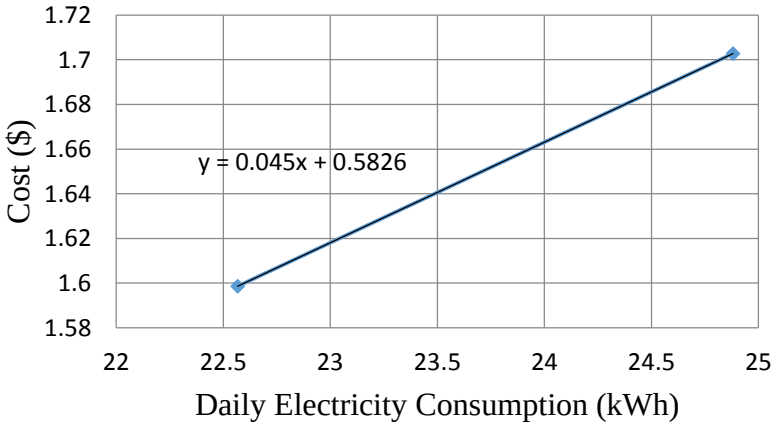

Fig. 2.9: Electricity delivery cost per kWh

Fig. 2.9 is generated based on two electricity bills for a house single family house in Ontario to derive the formula that it is used to calculate the delivery cost per day in general. Therefore, total electricity consumption in a day can be calculated by using Fig. 2.3 and Fig. 2.4 parameters as below:

$$A\ (kWh) = A_1 + A_2 + A_3 = a_1 \times (t_1 - t_0) + a_3 \times (t_2 - t_1) + a_2 \times (t_3 - t_2) \quad (2\text{-}4)$$

Therefore, the delivery cost can be calculated as below:

$$f_d(\$) = 0.045 \times A + 0.5826 \quad (2\text{-}5)$$

It should be noted that regulatory and other chargers are ignored as they are negligible. Assuming that there would be no power injection to grid, the grid power will be always positive. In other word, all the stored energy from solar panels or the grid will be consumed by the household loads. So, the total electricity cost per day, f_3-*new* and f_3-*old* can be calculated in the next step for a HESS with and without energy storage system, respectively.

The total cost per day without ESS is the summation of the electricity costs during off-peak (E_1), on-peak (E_2) and mid-peak (E_3) hours plus the total delivery charge f_d.

$$f_3\text{-}old\ (\$) = f_d + E_1 + E_2 + E_3 \quad (2\text{-}6)$$

The area of each triangle in Fig. 2.8 represents the energy cost based on the duration and the electricity rates according to the TOU schedule. For instance, the product of a_2 and b_2 represents the average power cost during the mid-peak hours.

Therefore:

$$f_3\text{-}new\ (\$) = f_d + (t_1 - t_0) \times (a_1 \times b_1) / 2 + (t_2 - t_1) \times (a_3 \times b_3) / 2 + (t_3 - t_2) \times (a_2 \times b_2) / 2 \quad (2\text{-}7)$$

Whereas, the total cost after adding the energy storage system f_3-*new*, can be calculated in the same way for f_3-*old* by adding the extra electricity cost for charging the battery bank during off-peak hours E_c and subtracting the energy cost (saving) during the on-peak hours E_d.

$$f_3\text{-}new\ (\$) = f_d + E_1 + E_2 + E_3 + E_c - E_d \quad (2\text{-}8)$$

2.2 HESS with Solar Energy-Case 2

Fig 2.11 shows the Energy Storage System with solar panels for a house. Like to the HESS without solar, the battery charger uses the grid electricity power during the off-peak hours to charge the battery bank. But when solar energy is available, the new system converts solar energy to electrical energy to either charge the battery banks or providing power to the load if the battery banks are fully charged. The solar energy and stored energy in the battery bank provide the power to the household loads by means of a Grid-Tie inverter only during on-peak hours.

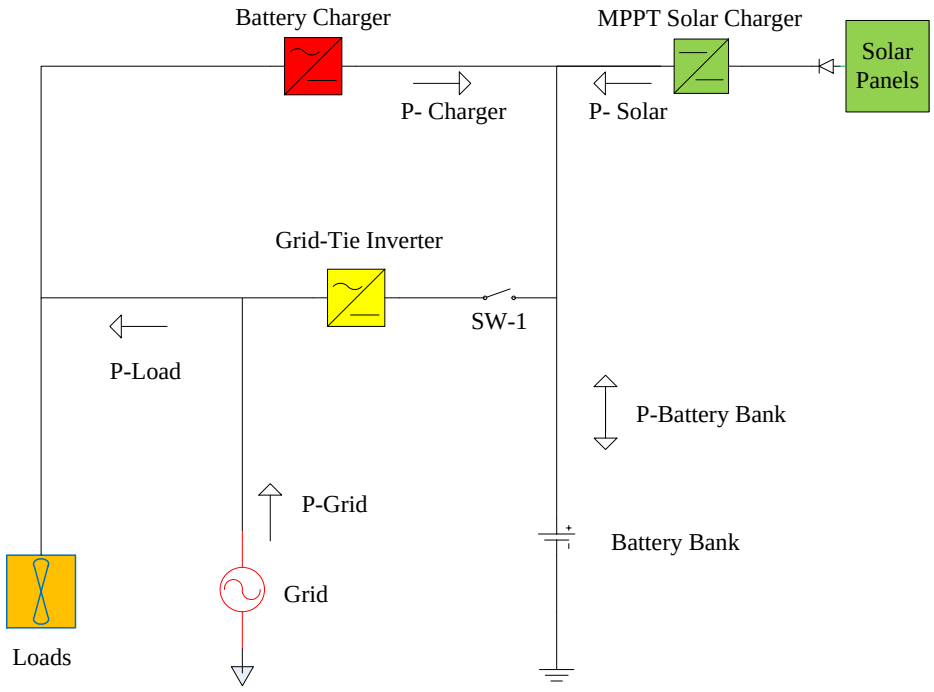

Fig. 2.10: Energy Storage System with Solar Panel

In this case, it is assumed that both battery charger and Maximum Power Point Tracking solar charge controller have the same efficiency of η_c. Therefore:

$$P_{Charge} \times 12 / \eta_c = P_{Discharge} \times 6 \times \eta_d \quad (2\text{-}9)$$

Where:

$$P_{Charge} = P_{Solar} + P_{Charger} \quad (2\text{-}10)$$

$$P_{Solar} = q \times P_{Charge} \quad (2\text{-}11)$$

$$P_{Charger} = (1\text{-}q) \times P_{Charge} \quad (2\text{-}12)$$

q is the solar power contribution ratio

Based on Toronto Hydro data for a single family house in Ontario for summer 2018, [14]

Where:

a_1= 2.6kWh/6h= 433W, a_2= 13.1kWh/12h= 1092W, a_3= 18kWh/6h= 3kW and

b_1= \$0.065/kWh, b_2= \$0.094/kWh, b_3= \$0.132/kWh

Assomptions: η_c= 95%, η_d = 96.5%;

t_0= 0, t_1= 12, t_2= 18, t_3= 24;

We can derive equation (2-15) for the total energy cost per day assuming that E_c is equal to E_d.

$$I_{Charger} \times 12 / 0.965 = I_{Discharge} \times 6 \times 0.95$$

$$I_{discharge} = 1.8335 \times I_{Charger} \quad (2\text{-}13)$$

$$f_3\text{-}new\ (\$) = f_3\text{-}old\ (\$) + V_{average} \times [(1\text{-}q) \times I_{Charger} \times P_{base} \times b_1 \times (t_1 - t_0)] / \eta_c - V_{average} \times I_{Discharge} \times P_{base} \times (t_2 - t_1) \times b_3 \times \eta_d \quad (2\text{-}14)$$

Therefore:

$$f3\text{-}new(\$) = f_3\text{-}old\ (\$) + V_{average} \times I_{Charger} \times P_{base} \times b_1 \times [(1\text{-}q) \times (t_1 - t_0) / \eta_c - 1.8335 \times (t_2 - t_1) \times \eta_d \times b_3)] \quad (2\text{-}15)$$

Assumption: $V_{average}$ = $1_{p.u}$ and P_{base} = 3kW.

Table 2.1 shows the total energy costs for different solar power contribution (q).

solar power contribution (q)	**0%**	**25%**	**50%**	**75%**	**100%**
f_3-*old* (\$/month)	142.83	142.83	142.83	142.83	142.83
f_3-*new* (\$/month)	114.35	104.28	94.20	84.12	74.05

Table 2.1: Results of different cost for a HESS with solar power contribution

By comparing the achieved results from the above example, it can be concluded that the cost saving for a home energy storage system without renewable energy source is about 20% as the total cost decreases from $142.83 to $114.35 per month. Although, we know that the electricity price increases every year. So, it will be more economical when the electricity cost difference between the on-peak and off-peak hours increases.

After adding the solar panels to the system, it is expected to achieve more cost saving as the solar energy contribution increases to about 50% ($142.83 to $74.05) when the contribution ratio is equal to unity.

In general, increasing the size of solar panels and the energy storage capacity can be considered to increase the capacity of the whole system. However, there should be a compromise between spending extra money for more solar panels or larger battery bank and reducing the total electricity cost. It should be noted that the size of the electrical loads should be considered for optimization of the energy storage system.

Chapter 3 : Home Energy Storage Components

3.1 Energy Storage Devices

The main component of an energy storage system is the storage device. Energy can be stored in different shape of energy like compressed air (Mechanical), capacitor (Electrical), Electrochemical Battery (Chemical) and others. However, the electrochemical battery technology is the oldest method for storing electricity. [15] Electrochemical batteries are divided in to different types based on their chemistries such as Lead-acid, Nickel cadmium, Sodium Sulfur, Lithium-ion batteries.

Lead-acid (LA) which is made of a lead dioxide electrode (positive), a lead electrode (negative) terminals and a sulfuric acid electrolyte. Lead acid battery is a very common storage device that is used in most of the cars, UPS and many more applications. The low cycle life, repetitive maintenance requirement and environmental issue when disposing of lead are some of the disadvantages of LA batteries that make this type not the best choice for an Energy Storage System.

Nickel cadmium (NiCd) consists of a nickel hydroxide (positive), a cadmium hydroxide (negative) terminals and an alkaline electrolyte. The nominal cell voltage of NiCd battery is 1.2 volts. These batteries are reliable and need low maintenance. Its low cycle life and cadmium disposal issue are the disadvantages of this type.

Sodium sulfur (NaS) is made of liquid sulfur, liquid sodium at the positive and negative electrodes respectively. High self-discharge of 20%, high operating temperature over 300°C are some of the disadvantage of this type.

Lithium-ion Battery consists of a Lithium Metal Oxide as the positive electrode or Cathode, a porous Carbon as the negative electrode or Anode. The ions move from the anode to the cathode during discharge and move back to anode from the cathode during charge cycle as it shown in Fig. 3.1. [16]

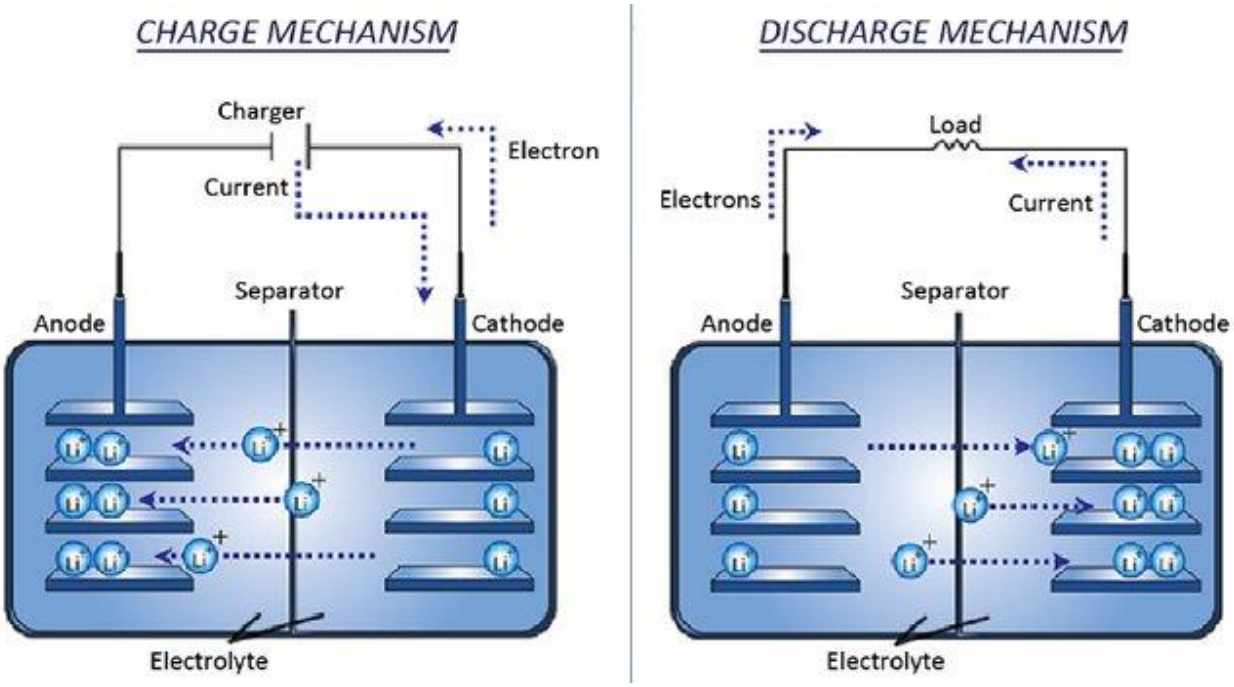

Fig. 3.1: Charge and Discharge cycles for Lithium-ion Batteries [17]

Lithium–ion battery has been considered one of the best types of electrochemical energy storage devices suitable due to the following advantages: [16]

- High energy density and capacity
- High load capabilities
- High number of charge-discharge cycles (long lifetime)
- Very low self-discharging rate
- High depth of discharge capability

- Simple charge algorithm and short charge time
- Maintenance-free

In addition to the above advantages, due to the improvement in the manufacturing and higher market demands, the Li-ion battery price is decreasing very fast which it can be considered as a new advantage over the other battery chemistry. [16]

However, the following limitations are exist in utilization of Li-ion batteries:

- Life time reduction at high temperature when stored at high voltage
- Difficult fast-charge possibility at low temperatures below zero degree Celsius
- Requires appropriate protection circuit to prevent thermal runaway

According the above advantages, Li–ion battery chemistry is the best choice for energy storage system for residential houses, distributed generation stations (DGS), and electric vehicle (EV) applications.

3.1.1 Definitions

- **Capacity** is a measure of stored energy in the battery and is calculated by multiplying the current (in Amperes) and the discharge time (in hours). In other word, the battery capacity represents the maximum amount of energy that can be extracted from the battery. [18]
- **C-Rate** is a measure of the rate at which a battery is discharged relative to its maximum capacity. [19] The capacity of a battery is usually rated at 1C which it means that a fully charged battery at 1Ampere-hour (Ah) provides 1A for one hour. [20]

Fig. 3.2 shows the discharge curves of a 12V Lithium-ion battery at different C-rates.

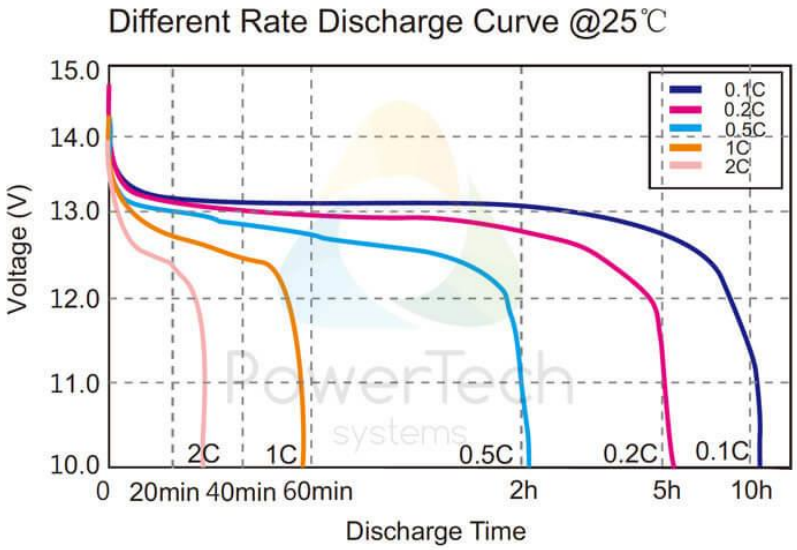

Fig. 3.2: Discharge curves of a 12V Li-ion battery [21]- *Courtesy of PowerTech Systems*

- **State of Charge (SOC)** is "an expression of the present battery capacity as a percentage of maximum capacity". [19] SOC value cannot be measured by a simple sensor. Instead, SOC is an estimated value which it is determined from some physical measurements and use an algorithm. [22]

  There are different methods and algorithms to estimate the SOC value of a battery. Some of them are Open-Circuit Voltage, Coulomb Counting, Electrochemical Impedance Spectroscopy, Extended Kalman filter (EKF). Coulomb Counting based algorithm is often used to estimate SOC value in Battery Management Systems (BMS). In this method, the SOC is stated by the ratio of the available capacity to the nominal capacity. The available capacity is calculated by measuring the battery current and integrating it over a time interval.

Equation (3-1) is the common equation to calculate the SOC, where I_{bat} represents the charging current, Δt is the time interval, SOC_o is the initial SOC value and the Q is the nominal capacity of the battery. [21]

$$SOC=SOC_o+\frac{\int_{to}^{to+t} I_{bat}\Delta t}{Q}*100 \qquad (3\text{-}1)$$

This method calculates the approximate value of SOC due to the inaccuracy of initial SOC value and cumulative errors. These issues can be corrected by different solutions. [23]

- **Depth of Discharge (DOD)** is a percentage of the battery capacity that has been discharged from maximum capacity. A discharge to at last 80% DOD is referred to as a deep discharge. [19] DOD can be calculated for any given SOC value as Equation (3-2) shows.

$$DOD\ (\%) = 100 - SOC\ (\%) \qquad (3\text{-}2)$$

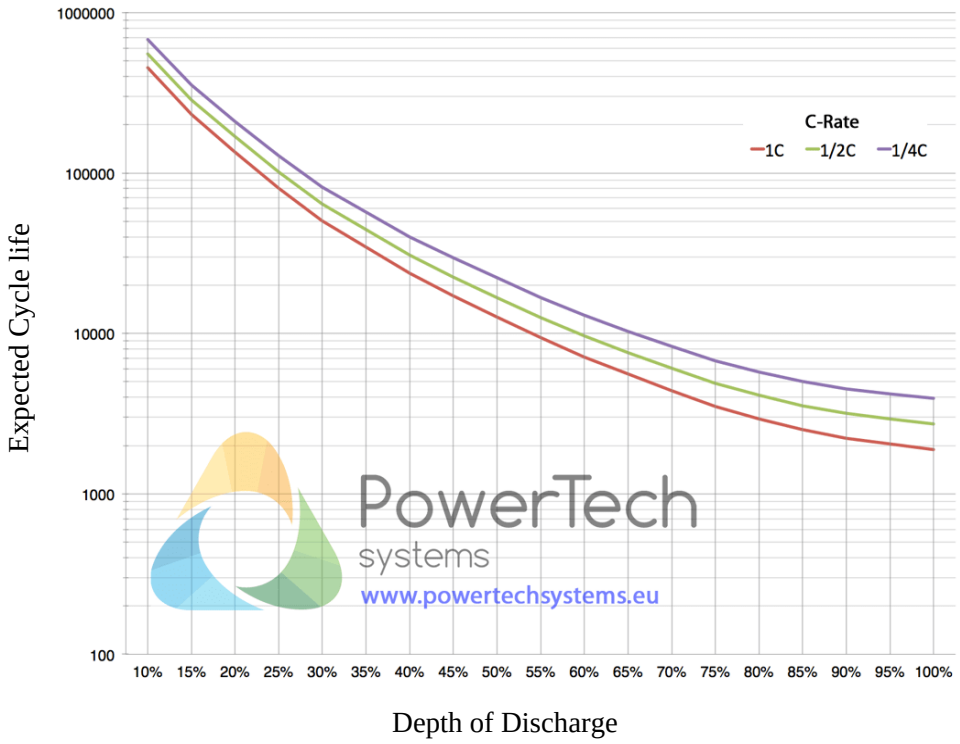

Fig. 3.3: Lithium Iron Phosphate Cycle life [24]- *Courtesy of PowerTech systems*

- **Cycle Life** is the number of charge-discharge cycles that a battery can operate before it fails. This value can be changed because of many conditions such as humidity, temperature, DOD and current intensity. For instance, the higher DOD, the lower the cycle life.

  Fig. 3.3 shows the estimation of the life-cycle based on the depth of discharge and discharge rate.

- **State of Health (SOH)** is a measure that reflects the condition of a battery and its capability to perform when it is compared with a fresh battery. SOH is an estimated value that indicates how much of the lifetime of the battery has been consumed. It can be compared to the odometer display of a car that shows how many kilometers the car has been driven.
- **Open-Circuit Voltage (OCV)** is the battery terminal voltage with no load applied. The OCV is a function of the battery SOC.

3.1.2 Equivalent circuit model of a battery

Batteries are basically nonlinear devices. They can be modeled in different shapes. A simplified electrochemical model was introduced in electrochemical theory by using mathematics to explain the internal actions of the battery. However, this model is not suitable to simulate the dynamic performance of a battery. [25]

An electrical equivalent circuit model (Thevenin's circuit-based battery model) was developed which it was capable to simulate the battery dynamic performance. [26] This model basically consists of three main components which includes a voltage source, internal resistances and capacitors. An ohmic resistance R_S and a polarization resistance R represent the internal resistance. A capacitance C in parallel with resistor R were considered to simulate the dynamic performance of a Li-ion battery approximately.

This simple model is called 1st OCV-R-RC model. With more polarization pairs of R and C, we can achieve more accurate models. Fig 3.4 represents a 2nd order OCV-R-RC-RC model (Randel's circuit). The resistor R_s is contained within an ohmic and charge transfer resistance which is a function of temperature, R1||C1 and R2||C2 accounts for diffusion which are functions of temperature and SOC.

V_{OC} value depends on SOC which represents the open-circuit voltage (OCV). OCV can be measured as the terminal voltage when there is no current flow through the resistors. In other word, the OCV can be measured when the battery is completely relaxed and there is no charge on the capacitors.

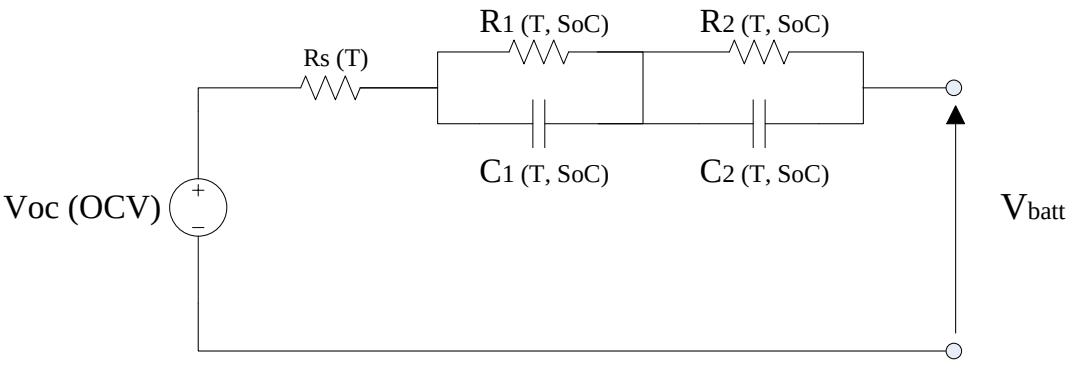

Fig. 3.4: OCV-R-RC-RC model of a Li-ion battery

3.1.3 Lithium-ion battery charging cycle

Most battery chargers usually use constant-current constant-voltage (CCCV) method to charge batteries which it combines constant current (CC) stage and constant voltage (CV) stage. In CC stage, the current is regulated to one of two values, pre-charge and fast charge. If the battery

voltage is very low, the charge current is reduced to a pre-charge level to condition the cell and prevent cell damage.

This threshold value differs with the battery chemistry and is typically determined by the cell manufacturer. Once the cell voltage rises above the pre-charge threshold, the charge increases to the fast charge current level. The maximum suggested fast charge current for typical cells is 1C which is also determined by the battery cell manufacturer. [27]

The typical charge current is about 0.8C in order to maximize the lifetime of the cell. [13] As the battery is charged, the battery voltage rises. Once the cell voltage reaches to the regulation voltage (typically 4.2 V), the charge current tapers down and the cell voltage is regulated in order to prevent overcharge.

In this mode, the current tapers off as the cell is charged. Once the current drops to a predetermined level (typically 10 percent of the fast charge current), the charge cycle is terminated. Li-ion batteries are not typically float-charged because it reduces the lifetime of the cell. [28] Fig 3.5 graphically shows a typical charge cycle for a lithium-ion battery.

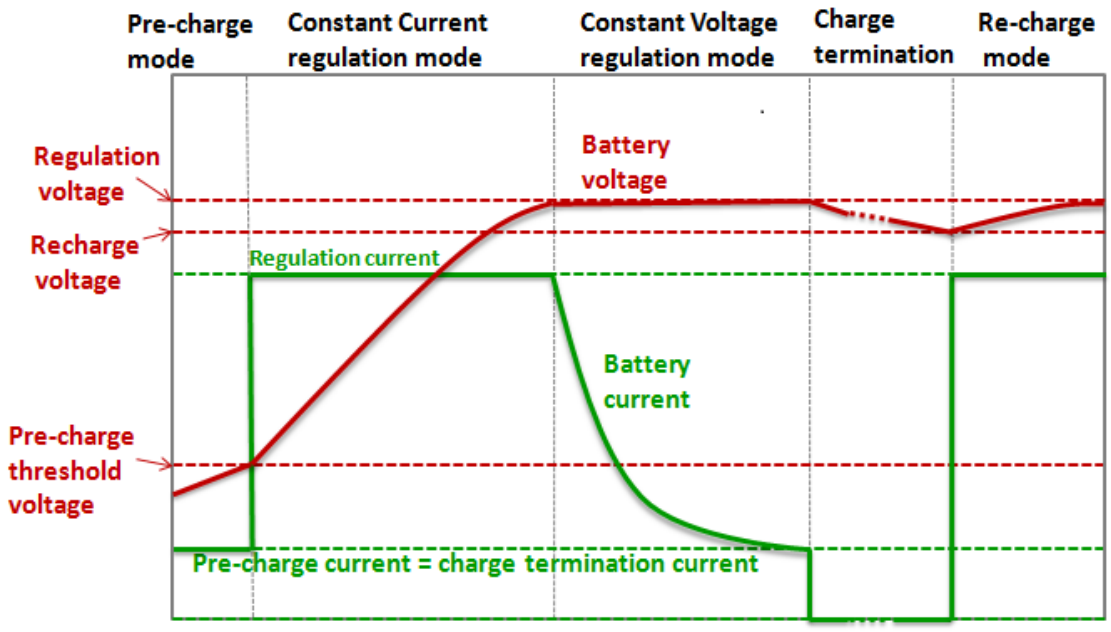

Fig. 3.5: Li-ion battery charge cycle [29]- *Courtesy of RICHTEK*

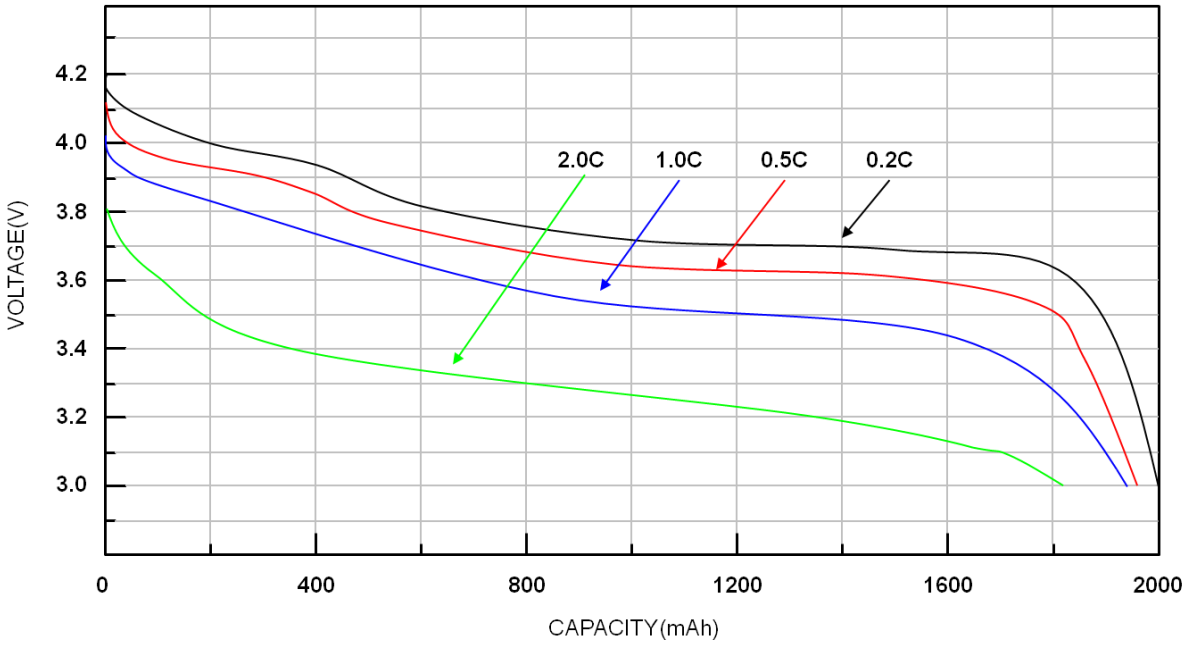

Fig. 3.6: Lithium-ion Discharge curves at different C rates [30]– *Courtesy of RICHTEK*

Fig 3.6 shows discharge characteristics of a lithium-ion battery for different discharging rates. It can be observed as the discharge current increases, the voltage decreases, assuming the battery temperature is kept constant.

3.1.4 Lifetime or Cycle Life of Li-ion batteries

There are many factors that affect the lifetime of Lithium-ion batteries. Temperature is one of them. Similar to many other electrical devices, the Li-ion batteries life time will decrease faster as the temperature increases.

Some battery types, like Lithium-ion and lead-acid batteries require integrated temperature management in the battery installation for optimal performance and safety. However, Lithium-ion batteries are generally not as sensitive to temperature as Lead-Acid batteries [29].

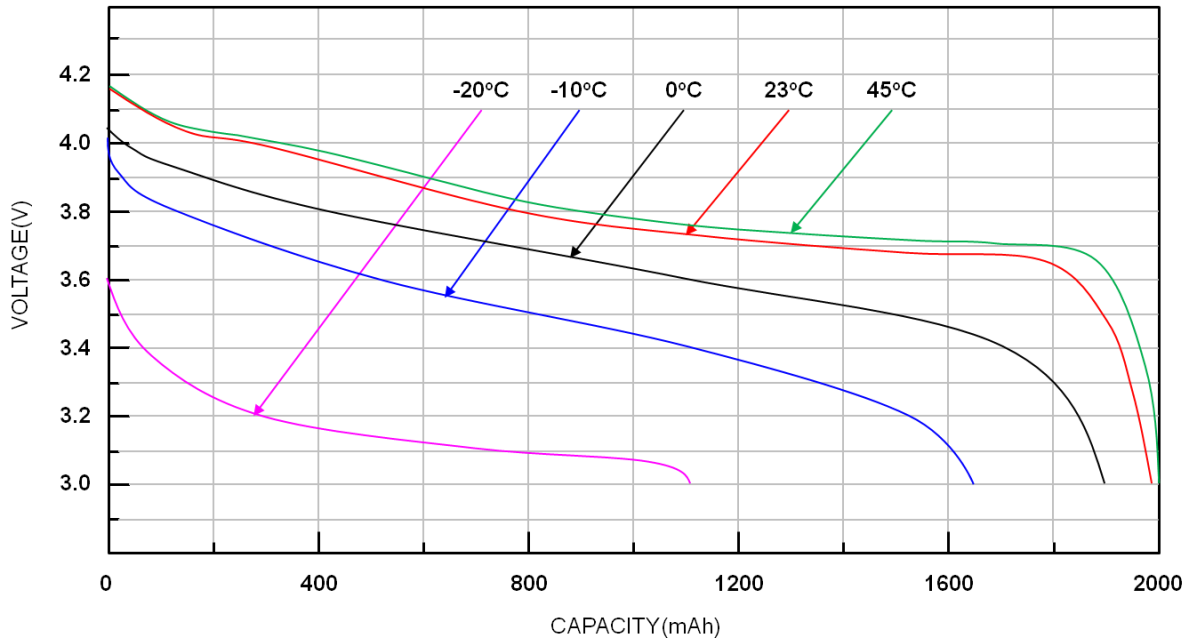

Fig. 3.7: Lithium-ion discharge curves for different temperatures [30]– *Courtesy of RICHTEK*

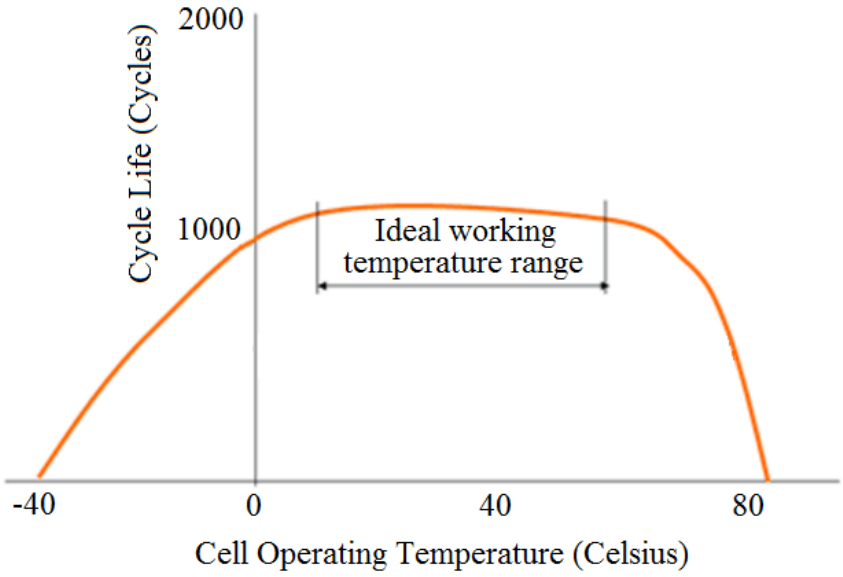

Fig. 3.8: Li-ion battery Cycle Life versus operating temperature [31]- *Courtesy of Electropedia*

A temperature controller unit can be used to keep the battery temperature constant in order to minimize the temperature impact on the battery lifetime. According to literature, for every 10℃ rise in temperature, the rate of reactions that contribute to aging is doubled. [31] Fig 3.7 and Fig 3.8 show the discharge curves and the ideal working temperature range for a Lithium-ion battery cell.

Another critical factor is the charge or discharge current rate. High charge or discharge current rate will reduced the lifetime of Li-Ion batteries. Therefore, it is very important how to charge or discharge the batteries.

Also, the Li-ion batteries lifetime suffer when they are overcharged or over discharged. Most Li-ion battery cells charge to 4.20V per cell. However, the optimal charge voltage is 3.92V per cell. Battery experts believe that this threshold eliminates all voltage-related stresses, going lower may not gain further benefits but induce other symptoms. Therefore, it is better to operate in the

ideal SOC working range from 20% to 90%. Figure 3.9 shows the charge and discharge characteristics curves for a Li-ion battery.

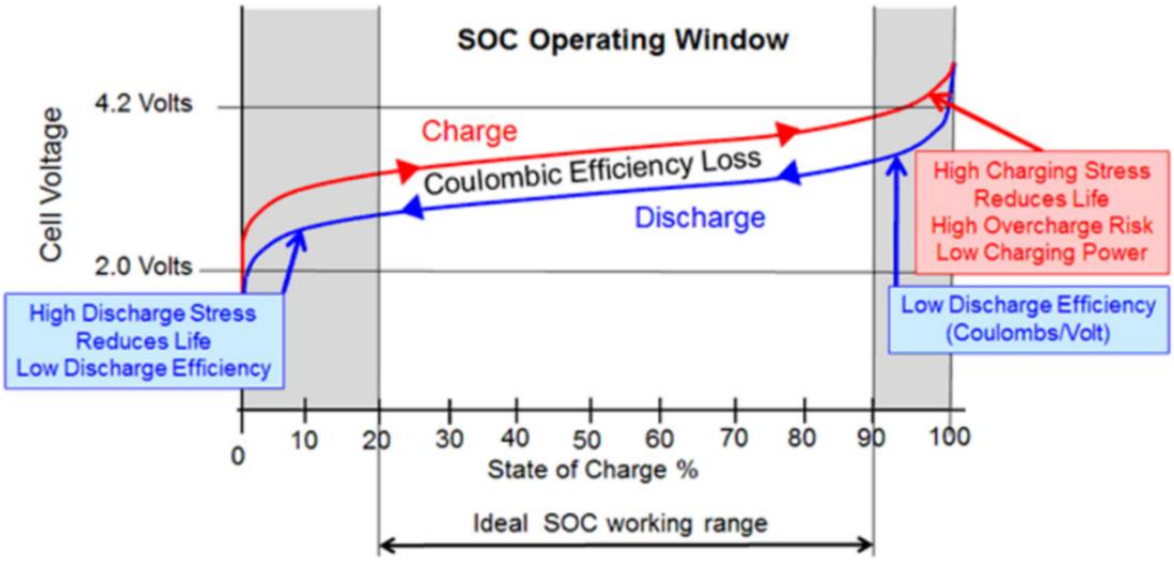

Fig. 3.9: Li-ion battery charge cycle [31]- *Courtesy of Electropedia*

3.2 Pulsed Charge and Discharge Method

3.2.1 Pulse Charging

As it was mentioned before, constant-current constant-voltage method is often used to charge the batteries. However, pulse charging employs the CCCV method but interrupts the charging current for a short period of time during the charging cycle to relax the battery cells. Based on number of studies [32] [33], this method improves the battery performance and consequently extending its battery life time.

Since this thesis is focusing on Li-ion batteries, pulse charging method and its advantages will be discussed based on Li-ion batteries.

Fig. 3.11 shows the charging cycle of a Li-ion battery. During charge cycle, the lithium ions (Li+) move from the positive electrode or Cathode to the negative electrode or Anode through the Separator and the Electrolyte to intercalate in the anode. In other word, the arriving Lithium-ions at the anode during charge cycle diffuse within, to be intercalated in to the anode material.

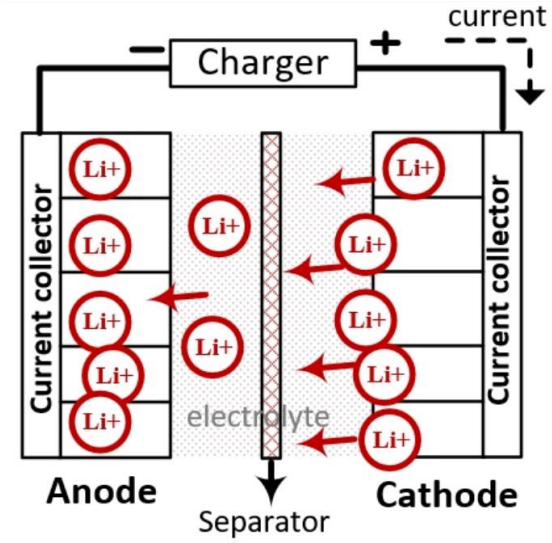

Fig. 3.10: Charging cycle diagram for a Li-ion battery [33]

Continuous charging current can cause inefficiencies in the intercalation and result in accumulation of lithium ions at the anode-electrolyte interface layer. This accumulation of ions can cause issues related to space-charge layers and also damages to the anode structure and consequently, reduction of efficiency and lifecycle. To avoid these issues, the CCCV charging method is considered as the charging algorithm but the current is interrupted for a short period of time to provide a relaxation time for allowing the lithium ions to penetrate into the anode electrode successfully to preventing dendrite formation also the benefit of improving safety.

3.2.2 Electrode microstructure

Based on a research work [32], the electrode microstructure was examined on three Lithium–ion battery cells, Fresh, 300 cycled continuous DC charging and 300 cycled pulse charging at 1C rate.

Fig. 3.11 to Fig. 3. 3 show the surface morphologies of the cathodes. It can be observed that the active material look compact after 300 cycles, but some cracks can be seen on some active material particles. By comparing the cathode surface for the fresh battery and the aged batteries, it can be claimed that the cracks in the active materials particles are not due to the mechanical force during electrode production, but are because of the stress during cycling which it proves that pulse charging causes less damage to the electrode structure in comparison with continuous charging. [32].

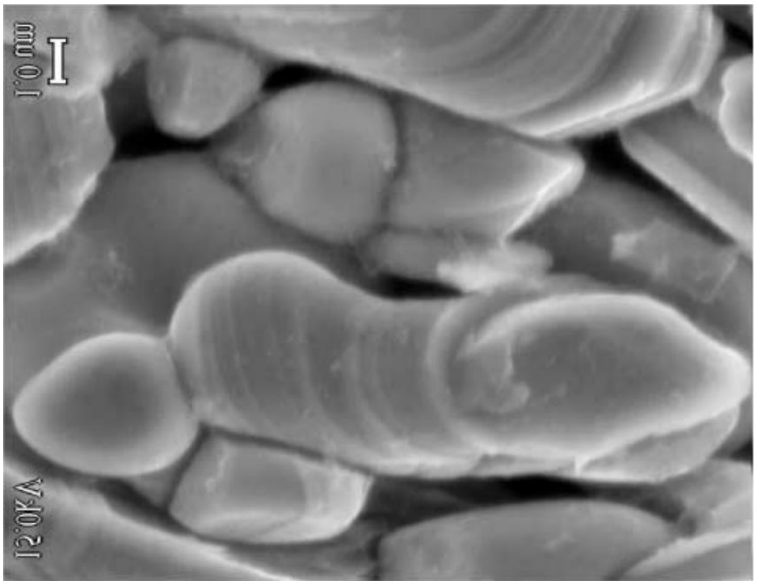

Fig. 3.11: Micrographs of cathodes in the fully discharged fresh lithium-ion battery [32]

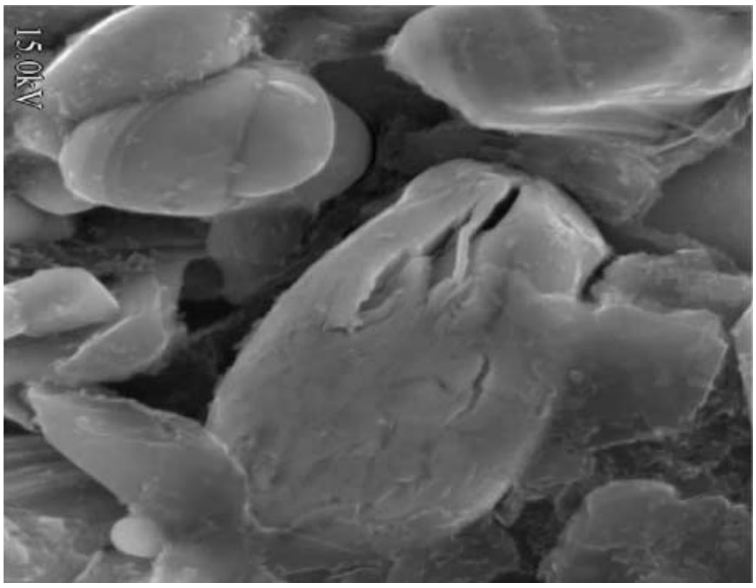

Fig. 3.12: Micrographs of cathodes in the fully discharged 300 cycled lithium-ion battery by continuous dc charging at 1 C charge–discharge rate [32]

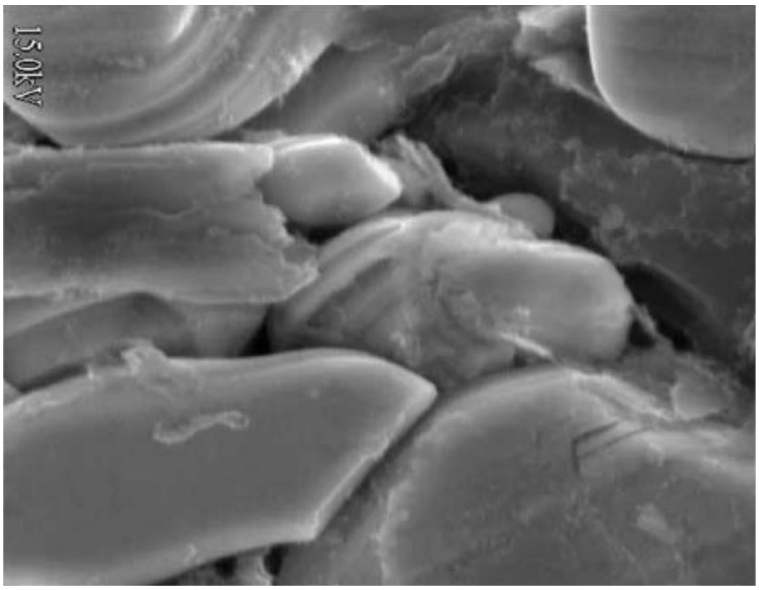

Fig. 3.13: Micrographs of cathodes in the fully discharged 300 cycled lithium-ion battery by pulse charging at 1 C charge–discharge rate [32]

The pulsed current is known in the field of electrochemistry which it has various effects at the electrode-electrolyte interface layer. This improves the active material utilization giving the battery higher charge capacity and, longer the battery lifetime. Therefore, pulsed charge-discharge is an interesting method to be considered for battery performance optimization. [34]

Fig. 3.14 shows a simple pulse charging circuits where the charging current can be interrupted by a switch. The pulsed charge current has three variables of charging current, *I*, switching frequency, *f* and the duty cycle, *D* which is the ratio of the on-time, t_{on} over the cyclic period, *T*.

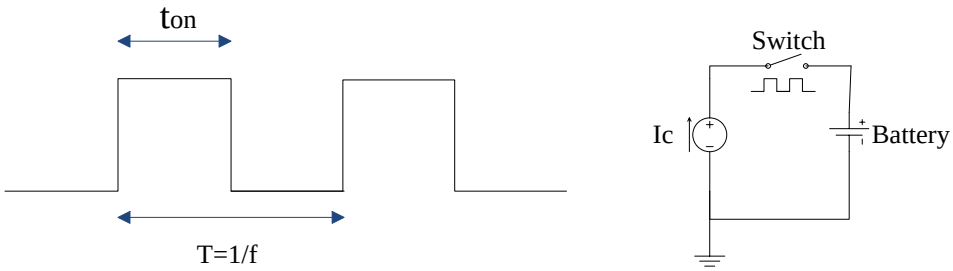

Fig. 3.14: Simple pulse chagrining circuit diagram

The lifetime of the battery and the battery impedance parameters can be impacted by changing each of these variables. Therefore, it is very important to choose the best frequency and duty cycles to achieve the best performance.

As it was discussed earlier, a battery can be modelled by an electrical equivalent circuit as it was shown in Fig 3.4 where a voltage source is in series with a resistor which represents the resistance of the electrolyte material and in series with pairs of parallel combination of a resistor and a capacitor which represent charge transfer and the charged areas, respectively.

Electrochemical impedance spectroscopy (EIS) test is a measurement method that can extract the battery impedance parameters for every SOC value. Fig. 3.15 shows an example of EIS test on two Li-ion batteries.

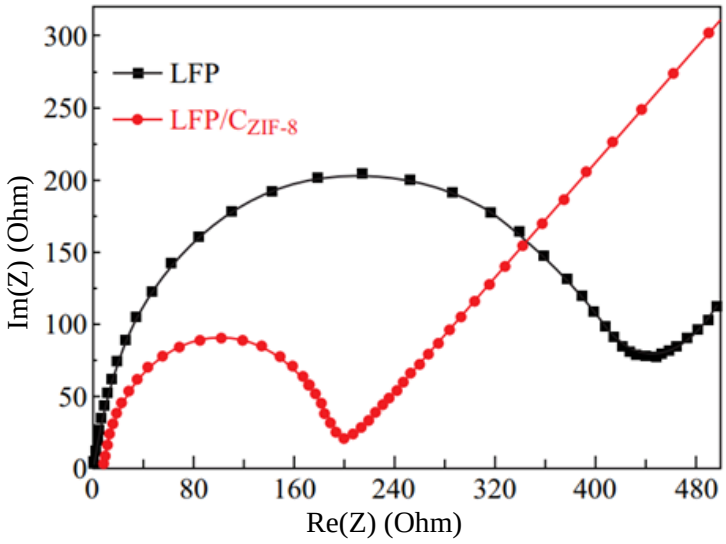

Fig. 3.15: EIS test results for two different Li-ion batteries [35]

Using the result of EIS test, one can determine the best switching frequency where the battery impedance has the lowest value which the energy losses in the battery resulting higher power transfer and efficiency. However, the battery impedance parameters depend on the SOC value of the battery during EIS test. Therefore, in normal operation, the switching frequency needs to be regulated accordingly to achieve the best result.

The charging current value depends on the demand and specification of the battery. Clearly, the lower charging current helps to extend the lifetime cycle of the battery. However, this increases the charging cycle. Therefore, there should be a compromise between the battery lifetime and the charging time.

The lower duty cycle of the charging current allows more relaxation time which it increases the charge time, and the higher duty cycles reduce the charging time. However, it reduces the relaxation time resulting less battery lifetime. Based on the experimental results [33] when the duty cycle is set to 50%, the optimal result can be achieved.

3.2.3 Pulse Discharging

During discharge the lithium ions return to cathode as the current flow is reversed. Using the same analogy of the pulse charging method, it can be expected that pulse discharging method also improves the Li-ion battery lifetime. Therefore, pulsed charge-discharge method is considered to be used in this thesis.

3.3 Split Battery Bank

The idea of splitting the battery bank in two sections is introduced in this thesis based on the pulsed charge-discharge method. It is expected to extend the lifetime of the battery bank by employing the pulsed current method while utilizing the maximum harvested energy by the solar panels.

Each battery bank contains of Lithium-ion battery cells which are connected in series during charge and discharge operations. The battery management system (BMS) estimates the state of charge (SOC) for each battery bank continuously. The SOC value of each battery bank is estimated continuously to adjust the pulsed charge-discharging duty cycle. This ensures that both battery banks are charged or discharged correspondingly. This approach will be explained in details in Chapter 4.

3.4 Cell Balancing

Since the battery banks are usually constructed by connecting a number of series cells, it is necessary to monitor and control the SOC value of each battery cell when the storage system is not in charge or discharge modes. This will utilize the maximum capacity of the battery bank.

Although the battery cells are identical and assumed with the same energy capacity, but practically they will not keep the same energy capacity value as they age. Since the cells are

connected in series, the weakest cell with the lowest capacity will be the dominant cell in the bank and it leads to lower the total battery bank energy capacity. Therefore, it is very vital to ensure all battery cells have the same SOC value for the best energy utilization despite that the HESS balances the battery banks automatically during normal charge or discharge operations. To overcome this issue, the HESS controller activates a balancing circuit when the battery banks are not in service, for example during mid-peak hours.

The HESS controller activates a passive balancing circuit which isolates the battery banks from the chargers or inverters and connects all battery cells in parallel during cell balancing mode. Fig. 3.16 shows a simple passive balancing circuit. A fuse and one low value resistor in series with each battery cell are added to protect and limit the balancing current, respectively.

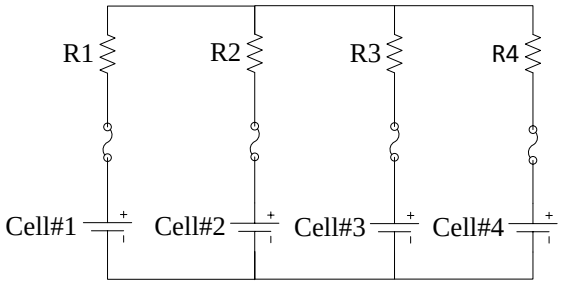

Fig. 3.16: Cells Balancing/Equalizing Passive Circuit

There are also other ways to balance battery cells. Fig. 3.17 presents an active cell balancing technique that uses a number of capacitors and switches (electronic switches) to transfer the extra charge from the cells with higher charge to the cells with lower charge. This switching process runs continuously until all battery cells reach to the same SOC value. Obviously, the power loss in the active balancing will be much less than the passive circuits. However, the complexity and higher cost of the active cell balancing circuits are the disadvantages of this type.

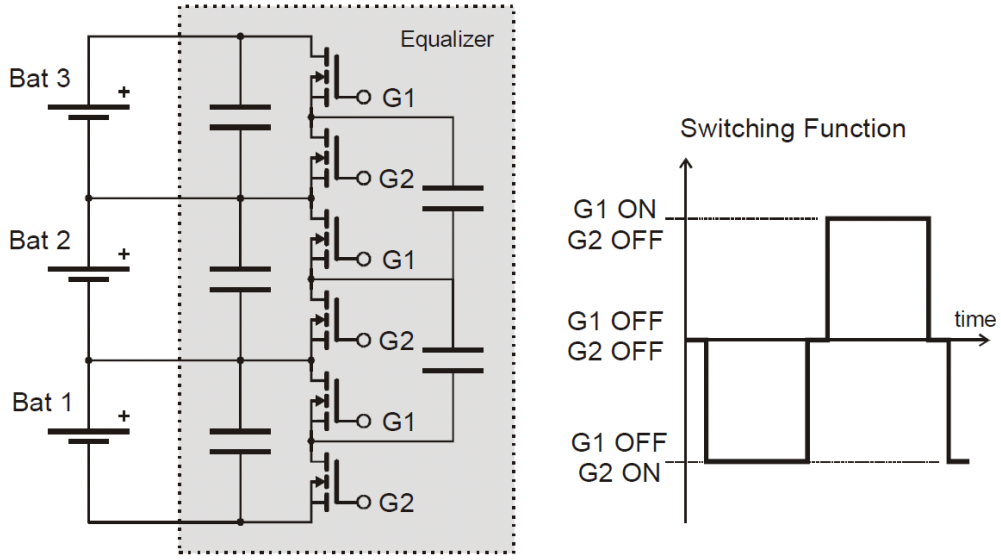

Fig. 3.17: Cells Balancing/Equalizing Active Circuit [36]

3.3 Photovoltaic Panels

One way of converting solar energy to electrical energy is to employ the photovoltaic (PV) solar panels. Each solar panel entails a group of series and parallel solar cells to provide specific voltage levels suitable for the desired application. A solar cell is an electronic device that converts the sunlight energy into electricity based on the principal of photovoltaic effect.

3.3.1 Solar Cell Characteristic Curves

Figure 3.18 shows the I-V characteristics and P-V curves for a solar cell. I-V curve describes the energy conversion capability at a sunlight level and temperature conditions. As the sunlight power decreases, the current of the solar cell decreases gradually until it reaches to the maximum power point (MPP). MPP is the peak power value and is the best operating point of the solar cell to generate the maximum power to the electrical load. Then, the current decreases suddenly to a very low value.

P-V curve is computed from I-V curve, which is the product of voltage and current values. The I_{mp} and V_{mp} values are the cell current and voltage values that is used to compute the maximum power point. When the load current is equal to zero, the cell voltage is maximum and is known as open-circuit voltage (V_{oc}). [37]

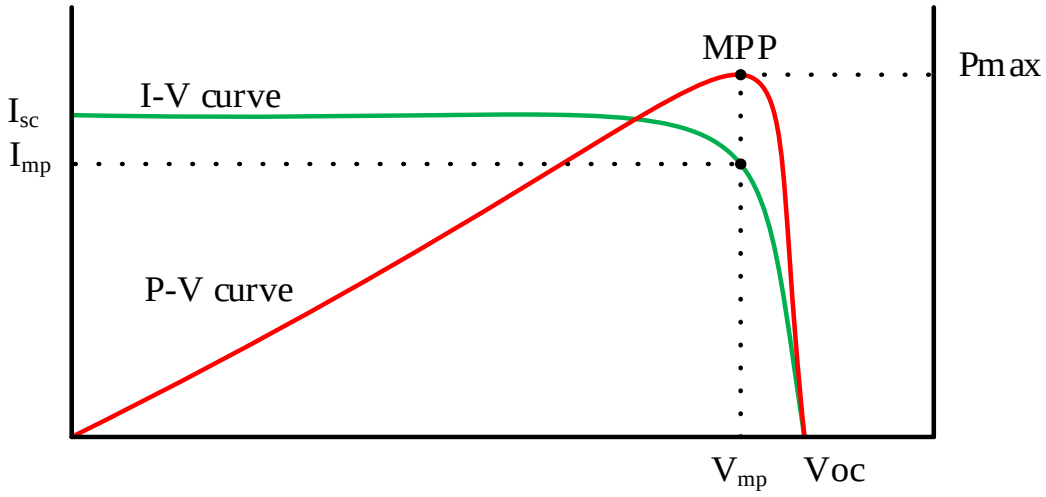

Fig. 3.18: I-V characteristics and P-V curves for a typical solar cell

Fig. 3.19 shows the equivalent circuit diagram for a solar cell. When the solar cell terminals are short circuited, the maximum current I_{sc} flows out of the positive terminal. [38]

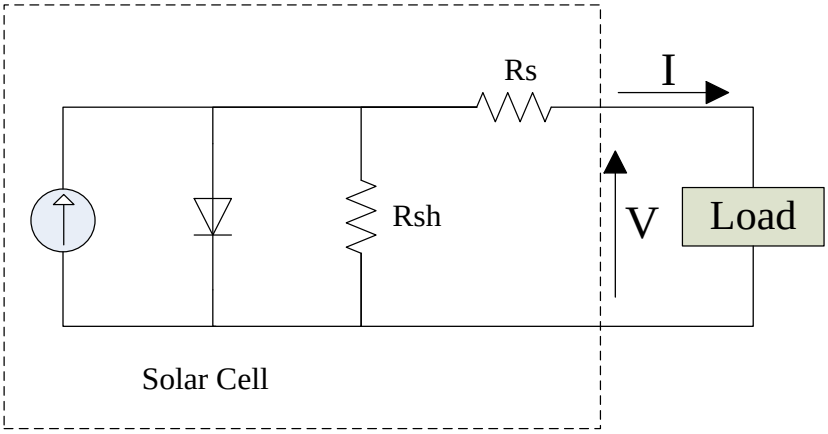

Fig. 3.19: Equivalent circuit diagram for a typical solar cell

3.3.3 Fill Factor

Fill factor (FF) of a photovoltaic panel is an important indicator that shows the rectangularity of the I-V curve. FF is the ratio of green area over the yellow area as figure 3.20 shows. Obviously, a solar panel with higher Filling Factor can produce more electricity which it makes it more efficient. [38]

The Filling Factor is calculated according to Equation 3-1.

$$FF = \frac{Imp.Vmp}{Isc.Vsc} = \frac{Pmax}{Isc.Vsc} \qquad (3\text{-}1)$$

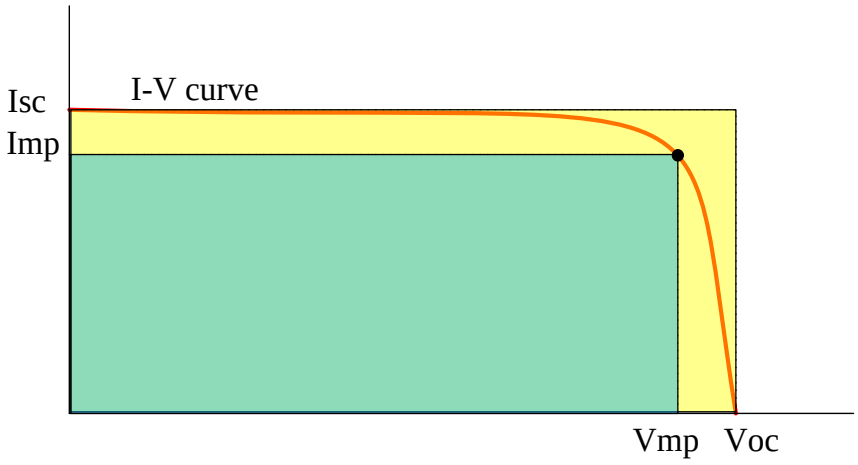

Fig. 3.20: Solar cell Filling Factor areas

3.3.4 Maximum Power Point Tracking

In order to utilize the maximum solar energy via solar panels, maximum power point tracking (MPPT) controllers are needed to be used. There are different methods to have a MPPT device. Two of these methods are incremental conductance method and perturb and observe (P&O) method. [39]

In incremental conductance method, the controller measures the PV current and voltage for two adjacent points and compares the incremental conductance $(\frac{\Delta I}{\Delta V})$ and the instantaneous conductance $(\frac{I}{V})$. depending on the results of this comparison, the operation voltage of the PV is either increased or decreased until the maximum power point is determined.

In P&O method which is the most commonly used algorithm for MPPT applications, the controller measures the PV voltage and current and calculates the slope of P-V curves. Based on the result, the controller changes the operating voltage level the way to reach MPP where the slope is zero. The operating voltage oscillates repeatedly around the maximum voltage point (V_{mp}) to

make sure that it tracks the maximum powering point. Fig. 3.21 and 22 show the flowcharts for these two methods. [40]

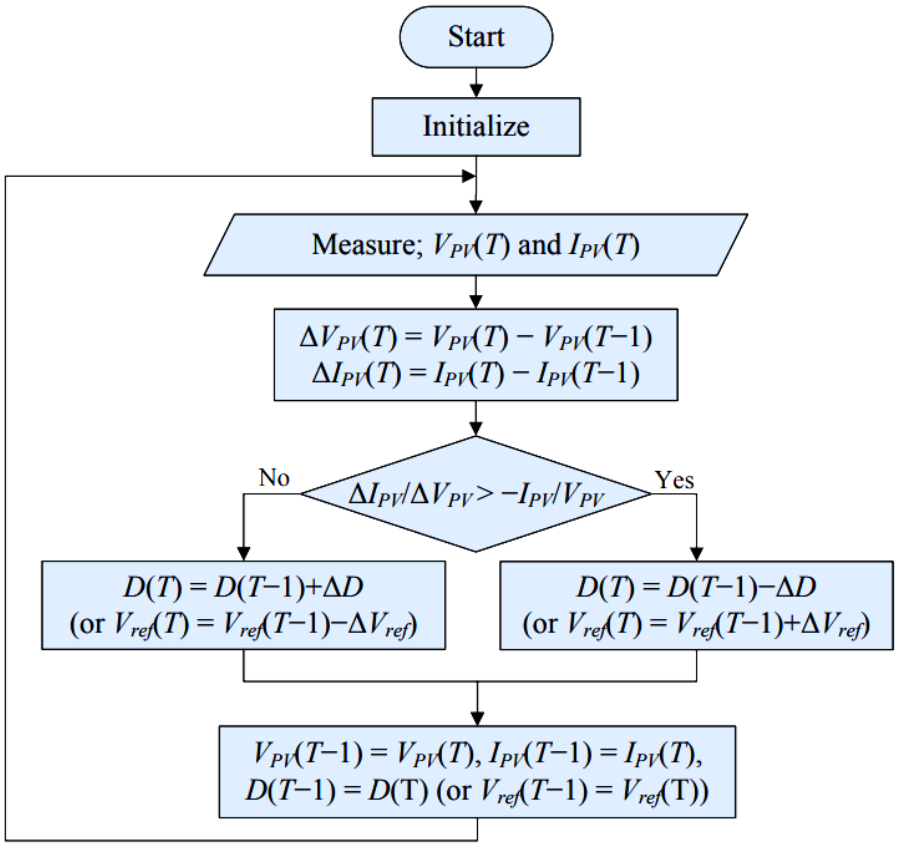

Fig. 3.21: Flowchart for Incremental conductance method [41]

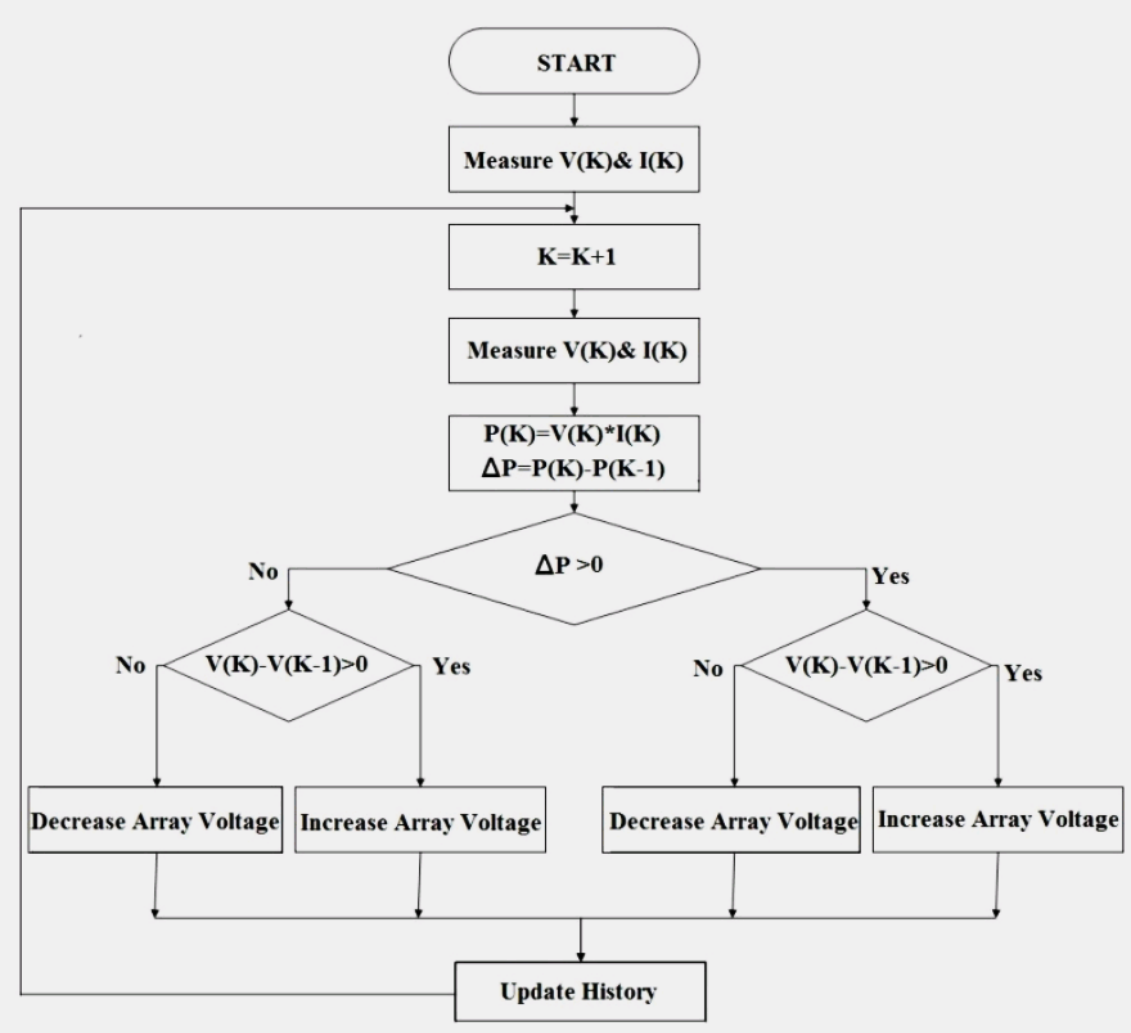

Fig. 3.22: Flowchart for P & O method [42]

Chapter 4 : Introducing New HESS, its Modes of Operation and Simulations Results

4.1 Home Energy Storage System Review

It is necessary to review some of the home energy storage system ideas that are introduced by other innovators or companies before discussing the new energy storage system for this thesis.

Fig 4.1 shows a residential photovoltaic ESS that suggests a bidirectional converter to charge the battery bank using the grid power and discharge the battery bank to feed the AC loads or to inject the excessive power to the grid. The DC-DC Converter charges the battery bank using the generated power by solar panels. If the battery bank is fully charged, the solar power is converted to AC power via the bidirectional converter. Fig. 4.2 represents the modes of operation in a day which we see that the systems injects power to grid. [43]

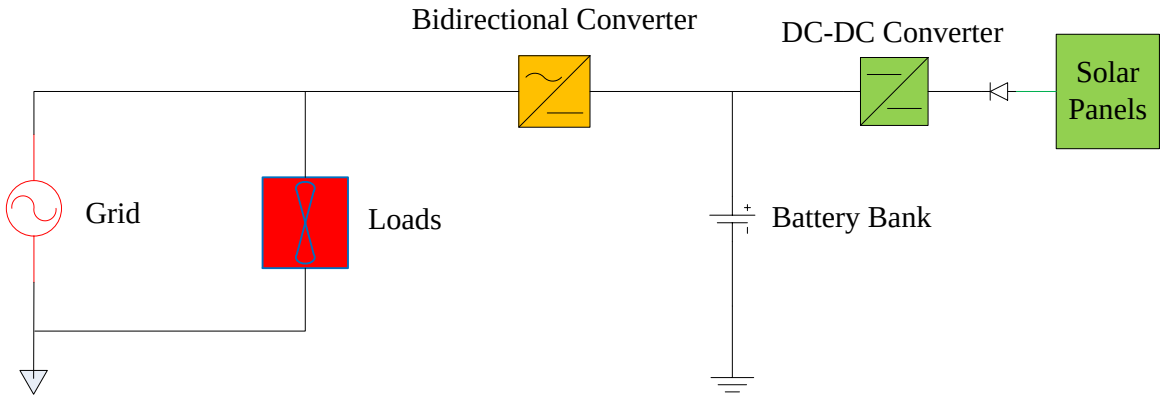

Fig. 4.1: The power circuit of the residential photovoltaic ESS [43]

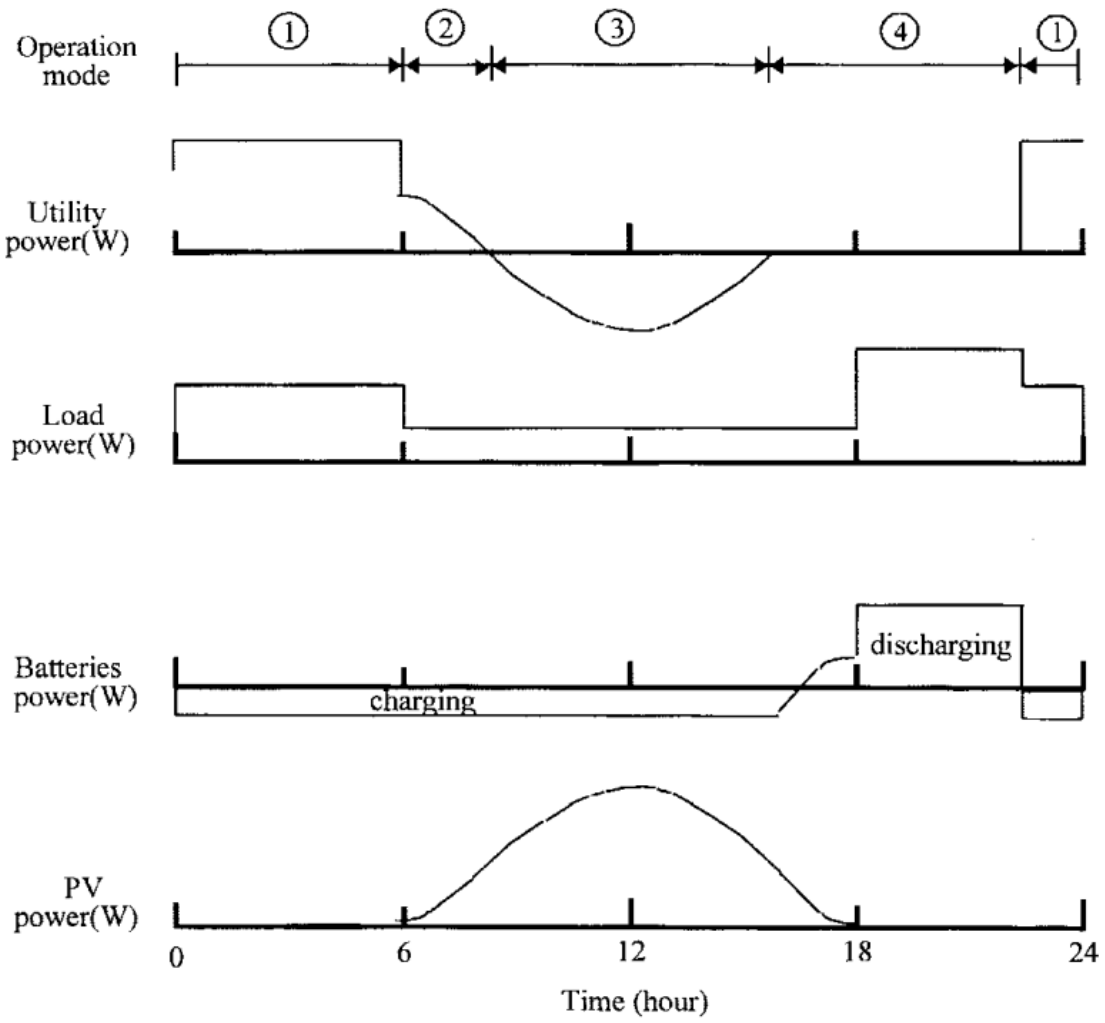

Fig. 4.2: A pattern of daily operation of the residential PV ESS [43]

Fig4.3 suggests a DC Nano grid prototype system for smart home applications where it is fed from different renewable energy sources and converters the DC power to charge the battery bank and also supply power to the loads. A bidirectional converter allows importing power from the grid or injecting power to the grid based on the demand from the loads or the generated power from the renewable sources. [44]

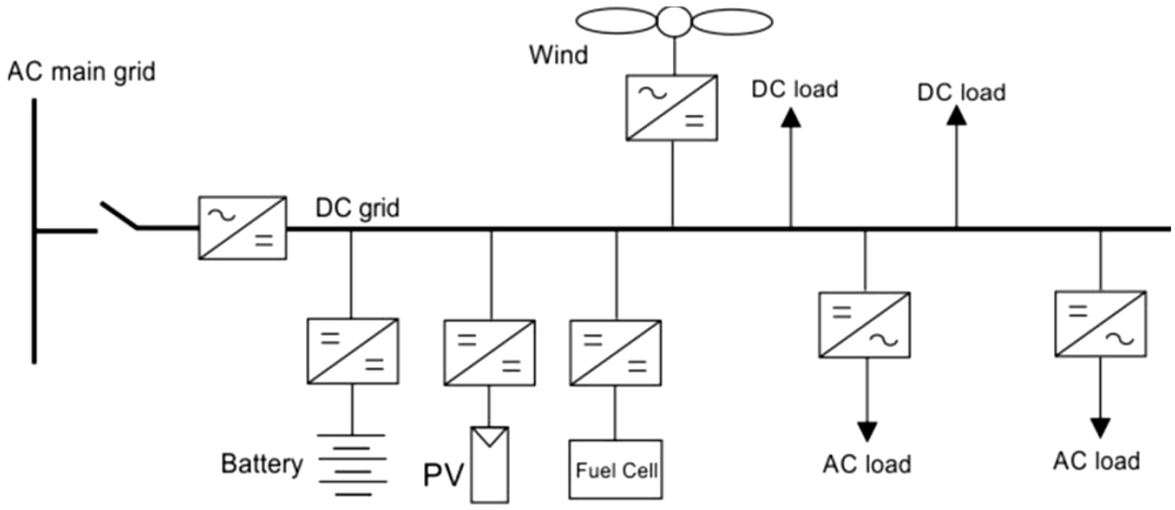

Fig. 4.3: Principle scheme of the DC Nano grid prototype [44]

Fig. 4.4 offers another configuration for a residential energy storage system (RESS) which uses a DC-DC converter to convert the solar panel voltage to a higher DC voltage level. This high voltage DC power can be converted to AC power via a bidirectional inverter or charge the battery bank via bidirectional DC-DC converter. [45]

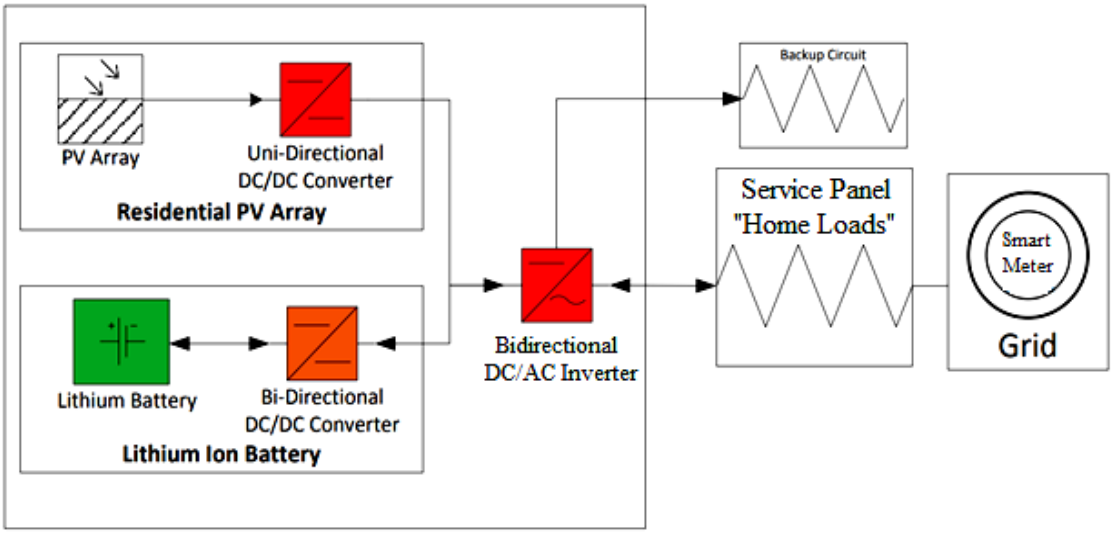

Fig. 4.4: schematic diagram of a directly connected RESS [45]

Fig 4.5 and Fig. 4.6 show two modes of operation for Tesla Powerwall 2 where it can work independently of the solar system or can provide power during a power outage. [46]

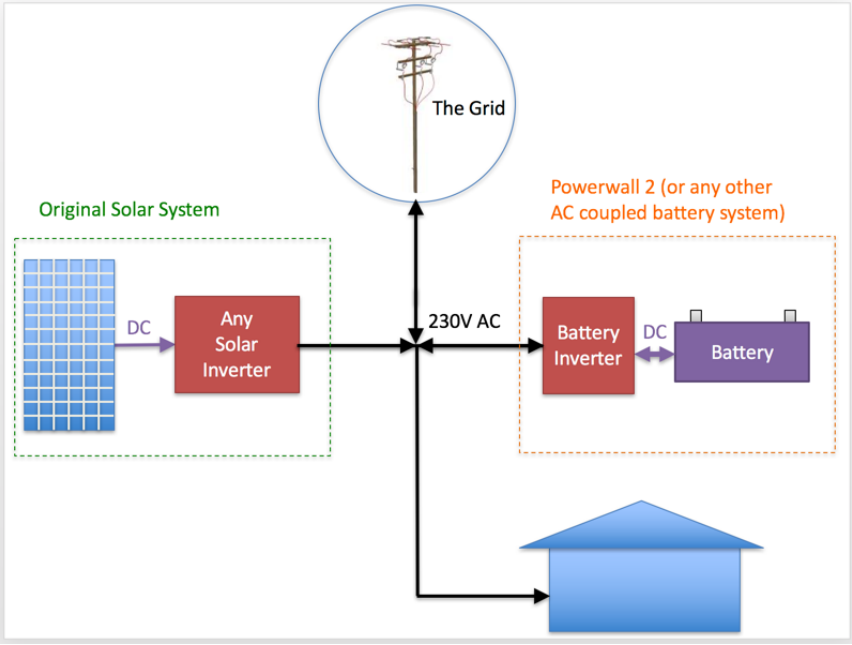

Fig. 4.5: Tesla Powerwall 2 diagram with grid power availability [46]

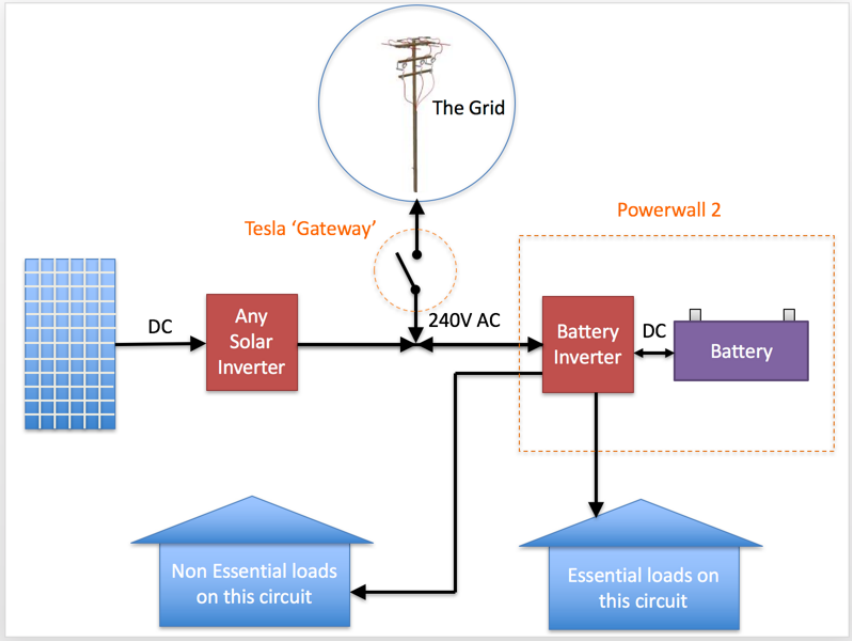

Fig. 4.6: Tesla Powerwall 2 diagram during power outage [46]

4.2 New HESS

After reviewing some of the existing ideas regarding home energy storage systems. A conventional energy storage is considered for this thesis. Fig 4.7 shows a conventional structure of renewable home energy storage system that consists of photovoltaic solar panels, maximum power point tracking (MPPT) solar charge controller, programmable battery charger, a single Li-ion battery bank, and grid-tie and off-grid inverters. The specification of each component for the new HESS is provided in chapter 5.

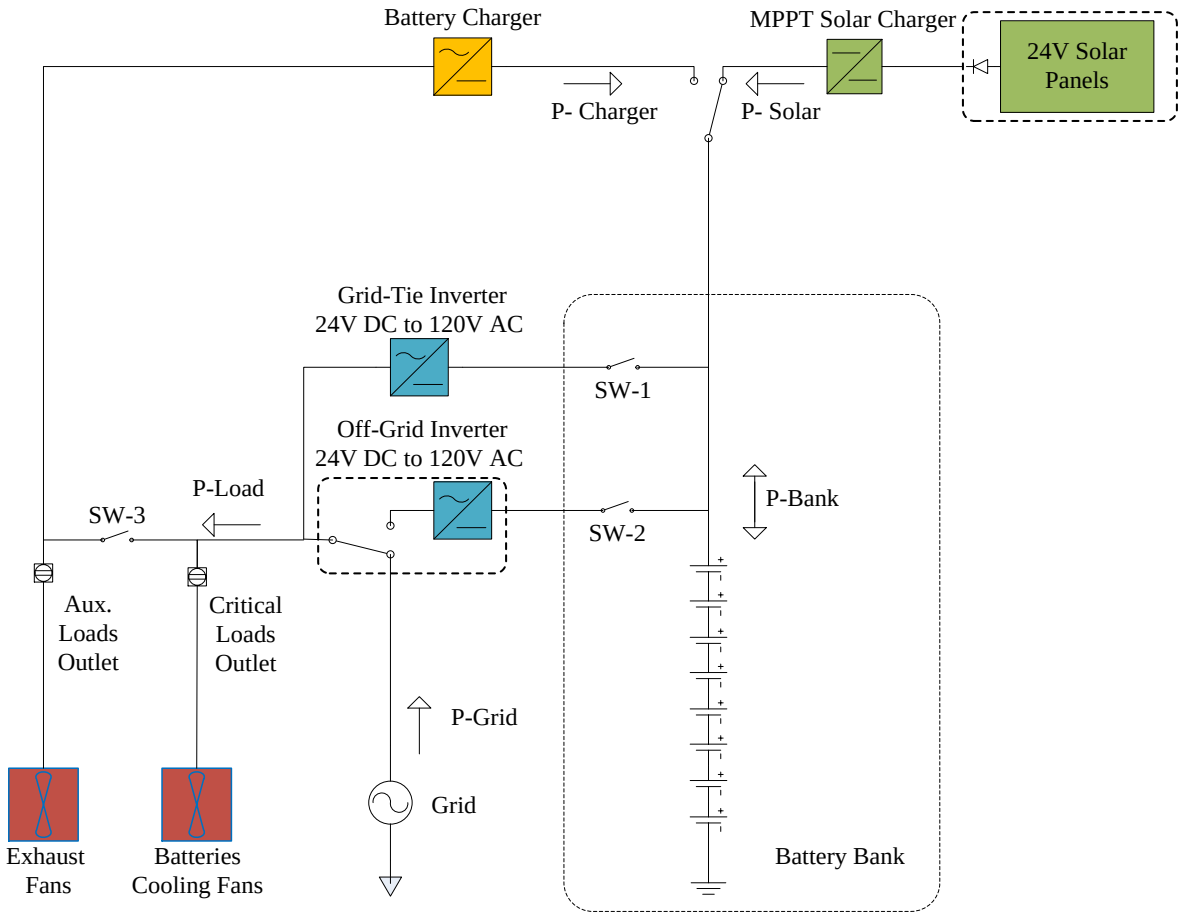

Fig. 4.7: Conventional HESS electrical diagram

In this system, the battery bank can be charged either by solar power or grid power during off-peak hours using continuous charging current (conventional) CCCV methods. The stored energy in the battery bank is used to provide most of the required power for household loads by the grid-tie inverter. This reduces the power consumption from power grid during peak hours. In other words, it reduces the household consumer's reliance to the grid system.

In addition, the stored energy can be used to provide backup power during the power outage by an off-grid inverter. Solar energy availability extends the power coverage capacity during the power outage.

If the pulsed method is used, half of the solar energy will be wasted. If conventional continuous charging is used, the battery lifetime cannot be improved. Therefore, there should be a compromise between the battery lifetime and the use of free energy.

In order to address this problem, the new HESS shown in Fig 4.8 introduces the split battery banks. In this approach, the battery bank is split in two equal sections to employ pulsed charge-discharge method. When the first battery bank is in charging mode the other one is in relaxing mode and vice versa. This method helps to increase the lifetime of the batteries while utilizing the total available free solar energy.

The HESS controller monitors the loads power, grid voltage and power continuously to determine the appropriate mode of operation according to the TOU schedule from the local electric utility. It should be noted that the split battery bank is more suitable for the applications in which free energy sources such as solar or wind energy is used.

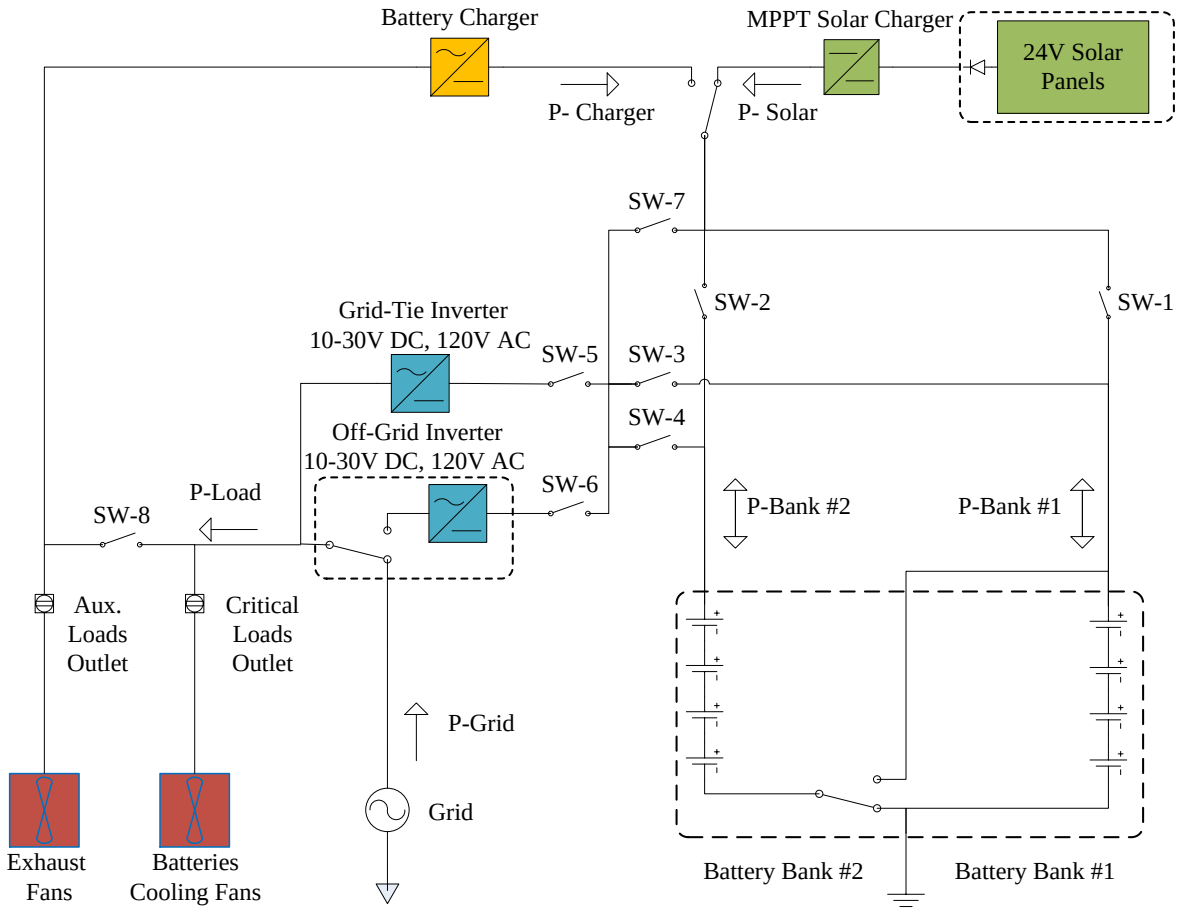

Fig. 4.8: New HESS electrical diagram

In this effort, each batter bank consists of Lithium-ion battery cells which are connected in series during charge and discharge operations. The SOC value of each battery bank is being estimated and used to adjust the pulsed charge and discharge duty cycle. So that both battery banks are charged or discharged equally. In other word, both battery banks would be balanced automatically.

Based on literatures [47] [48], temperature increase, over-charging and over-discharging reduce the lifetime of the batteries. Therefore, the Battery Management System monitors and controls the voltage of each cell to prevent overcharge or discharge of each battery cell at any time.

In order to maintain the battery temperature, the BMS measure the battery banks temperature and keep the battery banks temperature to room temperature by cooling fans.

It is very crucial to ensure that all battery cells have the same SOC value. Despite that the HESS balances the battery banks automatically, it does not promise that all battery cells are balanced at the end of each charge or discharge cycle. To overcome this issue, the HESS controller activates a cell balancing circuit to equalize all battery cells when the battery banks are not in service.

In this strategy, the total energy capacity remains the same as in the conventional method. However, the power capacity will be halved as only one battery bank is allowed to be in service at any time.

4.3 Modes of Operation

Figs 4.9 to 4.13 represent the new HESS in different modes of operation. Different modes of operation are available for the new HESS which they will be discussed in below.

In each mode of operation, Black wires represent no power flow in the circuit. The other colors show that there is some power flow in the related circuit based on the source of energy. Green and Red colors represent power from solar source and grid power source, respectively. Blue and Brown colors represent combinational ratios of energy source from both solar and grid.

4.3.1 Mode-1: Mid-peak hours

During mid-peak hours, due to moderate electricity cost, the benefit of charging or discharging the battery banks is not significant. In this mode, SW-1, SW-2, SW-3, SW-4 and SW-6 are all turned OFF. SW-5 and SW-7 will be turned ON to transfer the solar energy to the load

via the Grid-Tie inverter without involving the battery banks as it shows in Fig 4.9. The HESS enables the balancing circuit to equalize all battery cells.

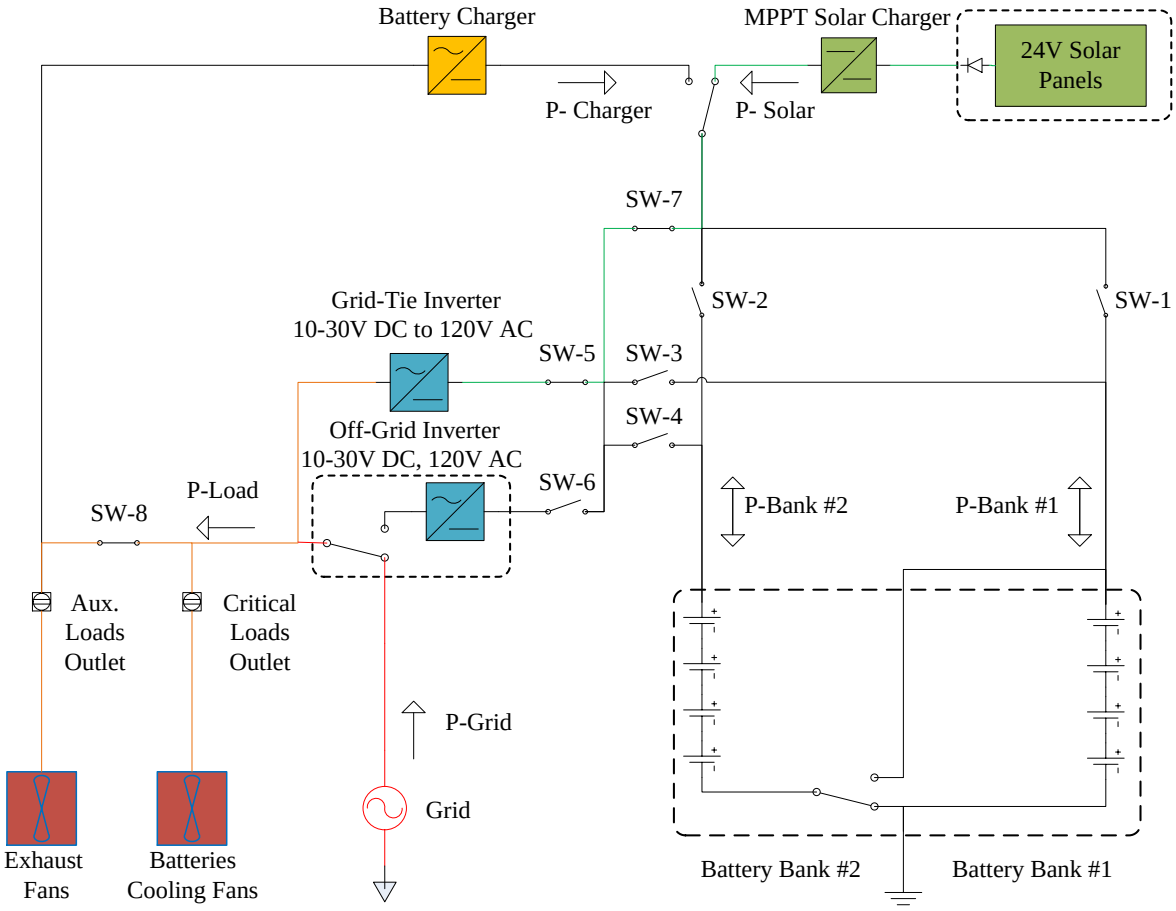

Fig. 4.9: Mode-1, HESS Operation during mid-peak hours

4.3.2 Mode-2: On-peak hours

During on-peak hours, HESS uses the stored energy in the battery banks to reduce the high electricity cost from the grid. In this mode, SW-1 and SW-3 or SW-2 and SW-4 are turned ON or OFF alternatively in order to employ pulsed charge-discharge method. SW-5 will be OFF and SW-6 and SW-7 are turned OFF as shown in Fig 4.10. When solar energy is available during on-peak hours, it charges the batteries partially when harvested solar energy is greater than the house hold

loads demand. It discharges the batteries partially to reduce high energy cost from the power grid when harvested solar energy is less that the loads demand.

The HESS controls the output power of the Grid-Tie inverter to minimize the grid power under any load condition.

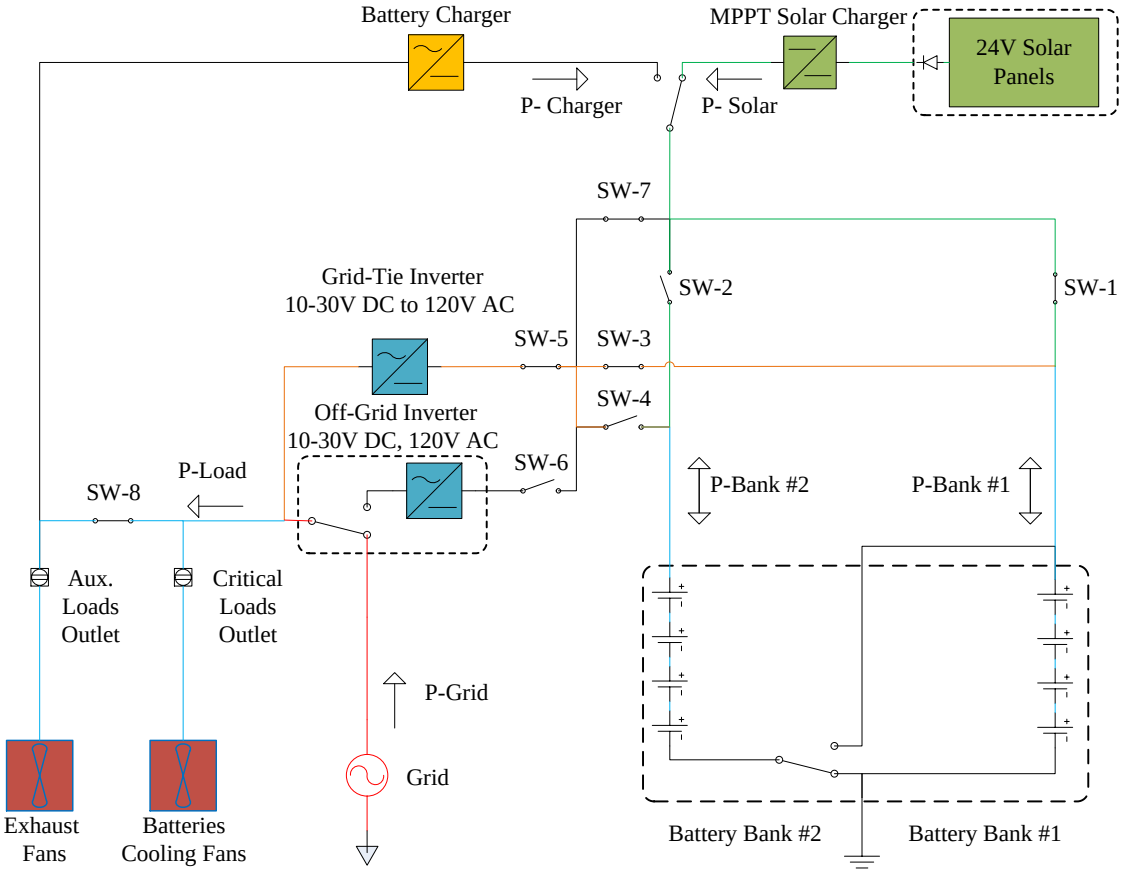

Fig. 4.10: Mode-2, HESS Operation during on-peak hours

4.3.3 Mode-3: Off-peak hours

Fig 4.11 shows the operating mode during off-peak hours when the electricity cost is at the lowest rate and there is no solar energy available. In this mode, the battery charger which it is fed from the grid charges the battery banks. SW-1 and SW-2 are turned ON or OFF alternatively. SW-3, SW-4, SW-5, SW-6 and SW-7 are turned OFF.

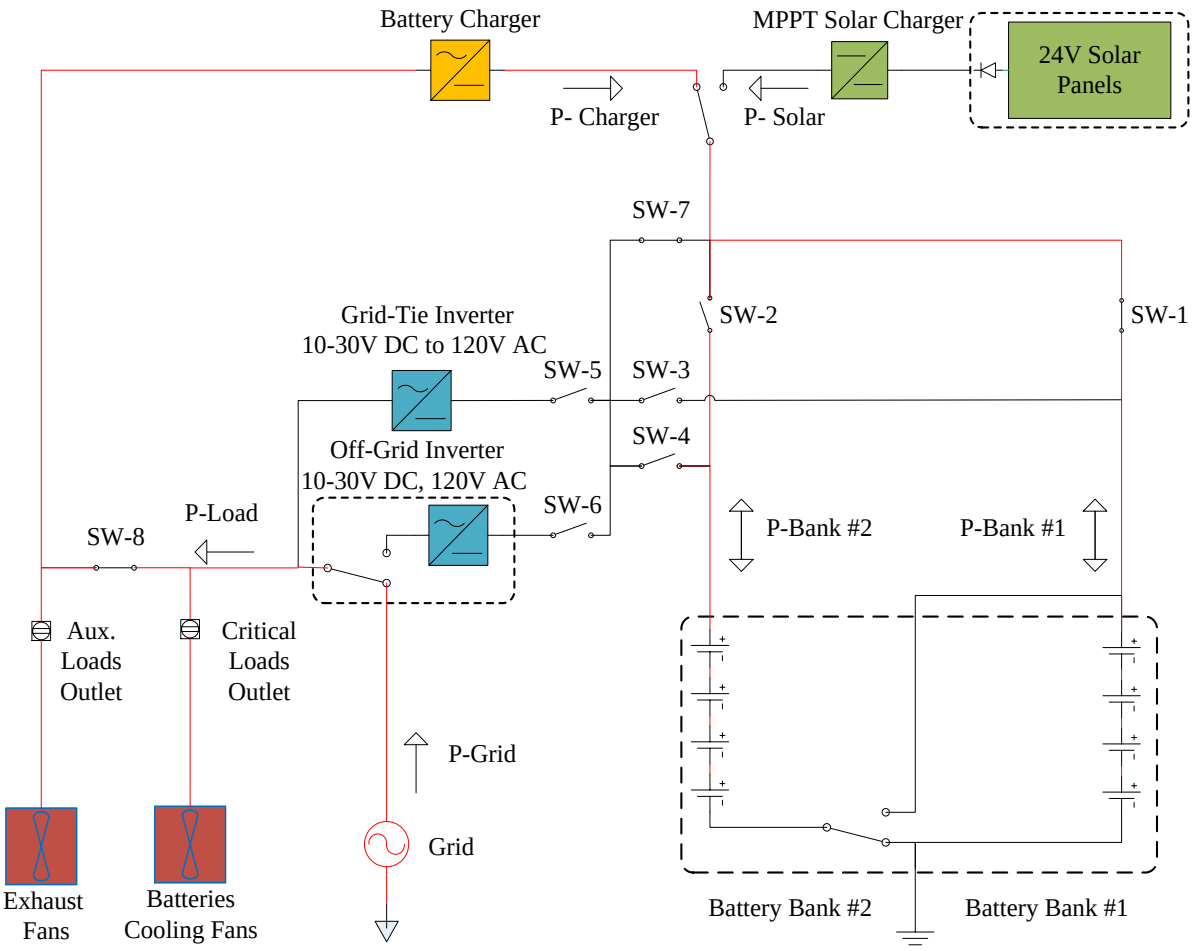

Fig. 4.11: Mode-3, HESS Operation during off-peak hours

4.3.4 Mode-4: Power Outage 12V DC Source

Fig 4.12 shows the operation during power outage, the Off-Grid inverter which has an embedded transfer switch isolates the power grid from home electrical circuits. In this mode, SW-1 and SW-3 or SW-2 and SW-4 are turned ON or OFF alternatively. SW-5, SW-7 and SW-8 are turned OFF. SW-6 is turned ON.

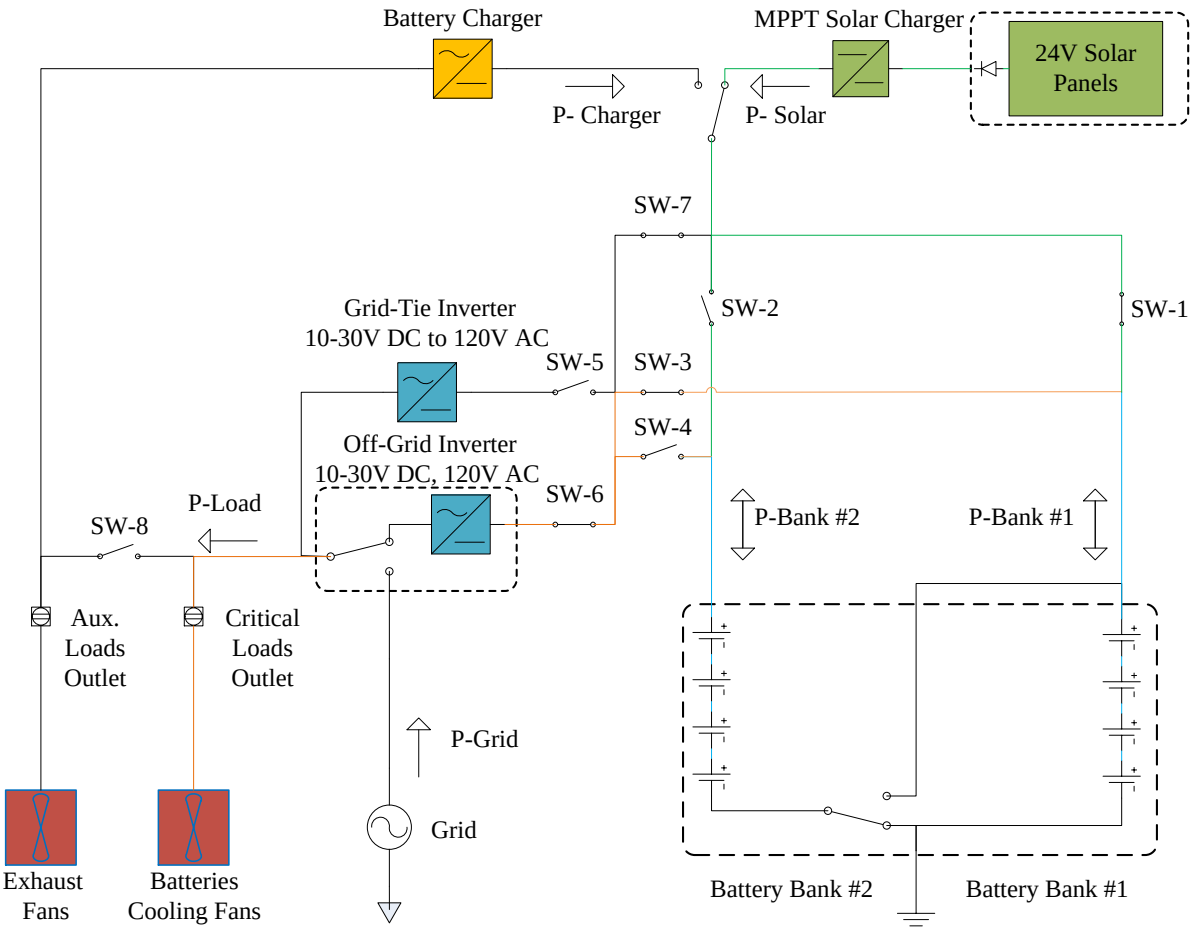

Fig. 4.12: Mode-4, HESS Operation during power outage

4.3.5 Mode-5: Power Outage 24V DC Source

Based on the specification of the existing Off-Grid inverter for this prototype system, the input voltage must be at 24V for normal operation. Therefore, the battery banks have to be connected in series to provide the nominal DC voltage. This may increase the system efficiency as the battery current is halved, therefore the copper loss on the internal resistance of batteries and circuits is reduced by four times as an advantage. However, pulse discharge method cannot be used in this mode which is the disadvantage of this mode. If solar energy is available during power outage it helps to extend the duration of power coverage time. In this mode, SW-2, SW-4 and SW-

6 are turned ON. SW-1, SW-3, SW-5, SW-7 and SW-28 are turned OFF. Fig 4.13 shows the power flow in this mode.

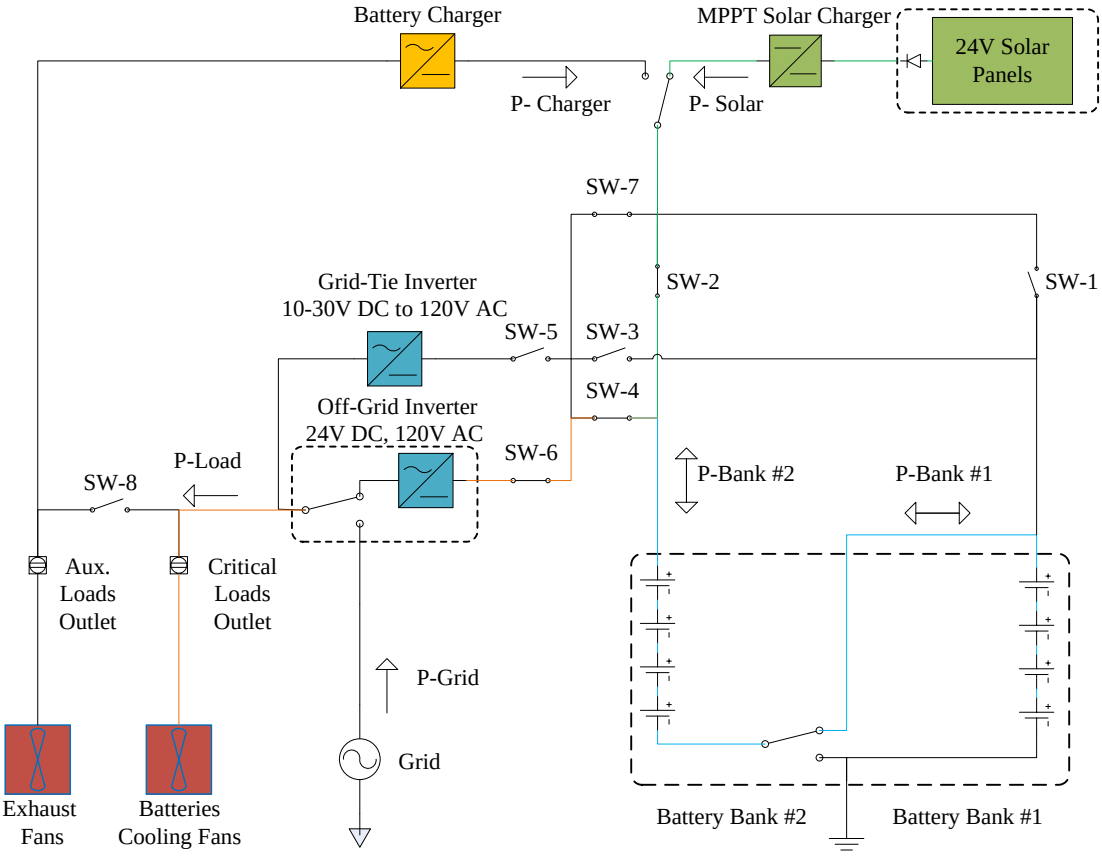

Fig. 4.13: Mode-5, HESS Operation during power outage-series banks

4.4 Simulation Studies

In order to study the performance of the new HESS configuration, a case study is developed in MATLAB/Simulink program. Fig 4.14 shows the Simulink block diagram of the new HESS.

In this study the following specifications are considered:

- Solar Panels can generate up to 1000 watts based on sun irradiance input.
- Battery Charger can charge the 12.8V battery banks at 500watts.
- Two 120V, 250watts resistive loads are used as main and auxiliary loads.
- A 120V, 500watts grid-tie inverter without MPPT capability is used to reduce the grid power to a minimum value during on-peak hours.
- A 120V, 250W pure sinewave inverter is added to provide power to the main loads during power outage.
- Two 12.8V and 40Ah Lithium-ion batteries banks are utilized.

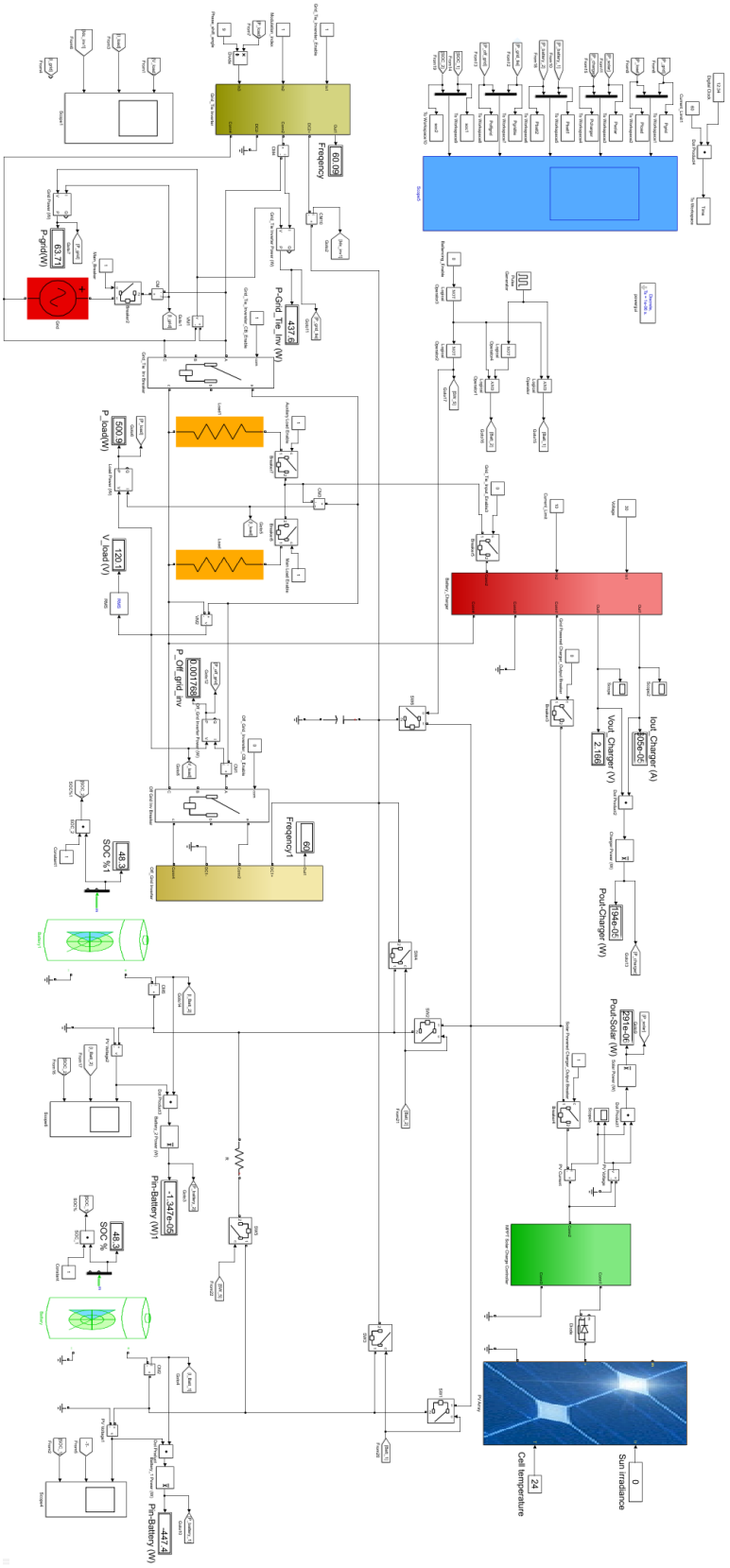

Fig. 4.14: Simulink diagram for the new HESS

Mode 1: Fig. 4.15 shows the simulation results during mid-peak hours. The HESS enables the balancing circuit to equalize all battery cells. However, if there is any solar energy available, the free energy is used to reduce the grid power without storing it. It can be seen that the SOC values stay constant.

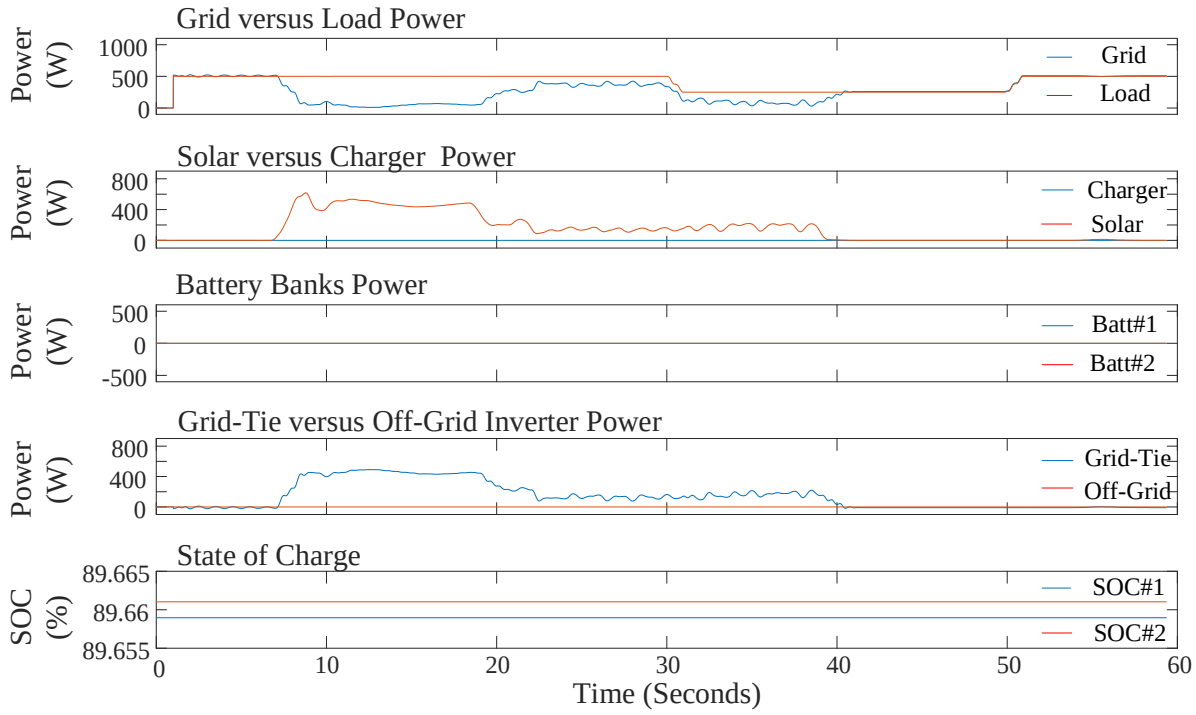

Fig. 4.15: Simulation result during Mode 1 (mid-peak hours)

In this study, the loads power is set to 500 watts at the beginning when there is no solar energy available. Hence, the grid power provides the same 500 watts plus the system power loss.

When solar panels generate about 400 watts, the incoming power from the grid is reduced to about 100 watts. Then, solar energy is reduced to about 150 watts. Consequently, the grid power is increased to about 350 watts. After 30 seconds, the load power is set to 250 watts when the solar power is still about 50 watts, the grid power is reduced to 100 watts accordingly. In this mode, the

SOC of both battery banks stay at the same level as the battery banks are disconnected from the charge or discharge equipment.

Mode 2: Fig 4.16 shows the simulation results during on-peak hours. At the beginning, the load is set to 250 watts, the grid–tie inverter generates about 240 watts to reduce the incoming power from the grid system to about 10 watts. The battery power charts show that one battery bank at a time provides the power to the grid-tie inverter. After increasing the load power to 500 watts the grid-tie inverter increases its output power automatically to reduce the grid power to about 50 watts. The battery power charts show higher discharge for each battery bank. The SOC charts demonstrate that both battery banks are discharged as it is expected.

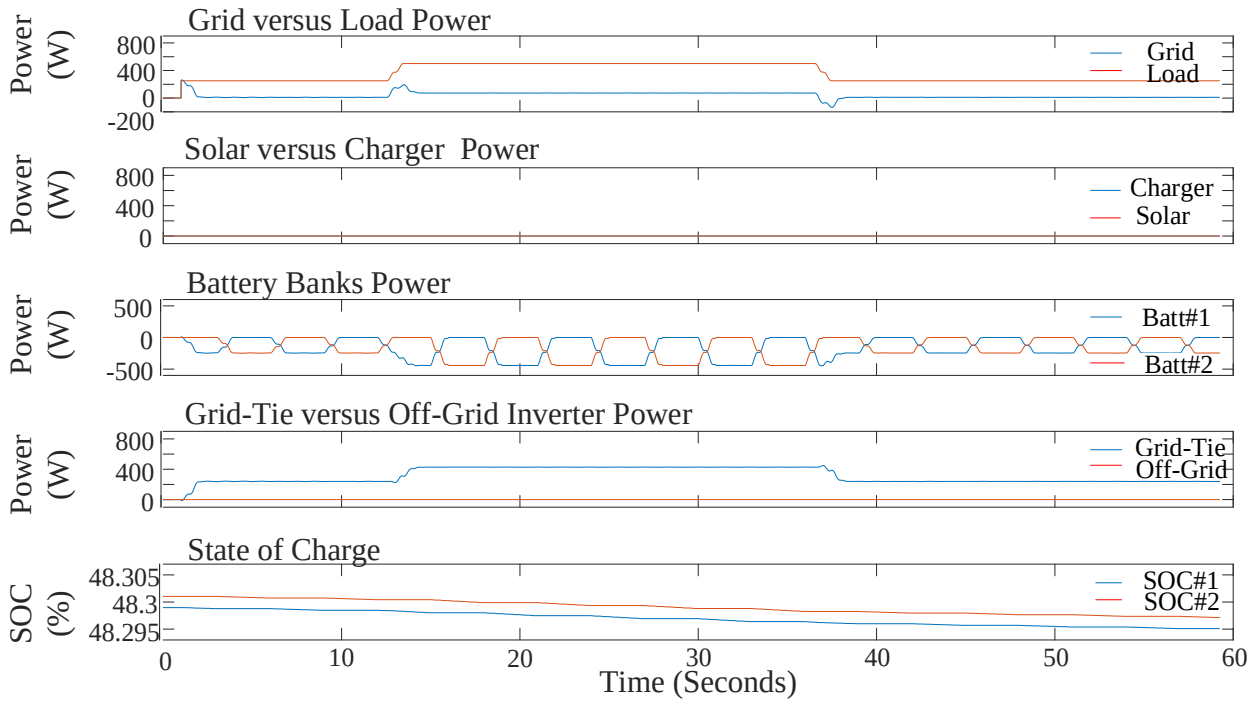

Fig. 4.16: Simulation result during Mode 2 (on-peak hours)

Fig 4.17 shows the simulation results during on-peak hours while solar energy is available. When solar panels generated about 1000 watts, 500 watts of the solar energy is consumed by the

load via grid-tie inverter and the excessive 500 watts solar power is used to charge the battery banks alternatively. When the solar power is less than the load demand, the battery banks provides the required power to ensure that the incoming power from the grid is as low as about 50 watts. The SOC charts demonstrate the charge and discharge cycles accordingly.

In Mode-2, the generated power by the Grid–Tie inverter is controlled to prevent power injection to the grid system.

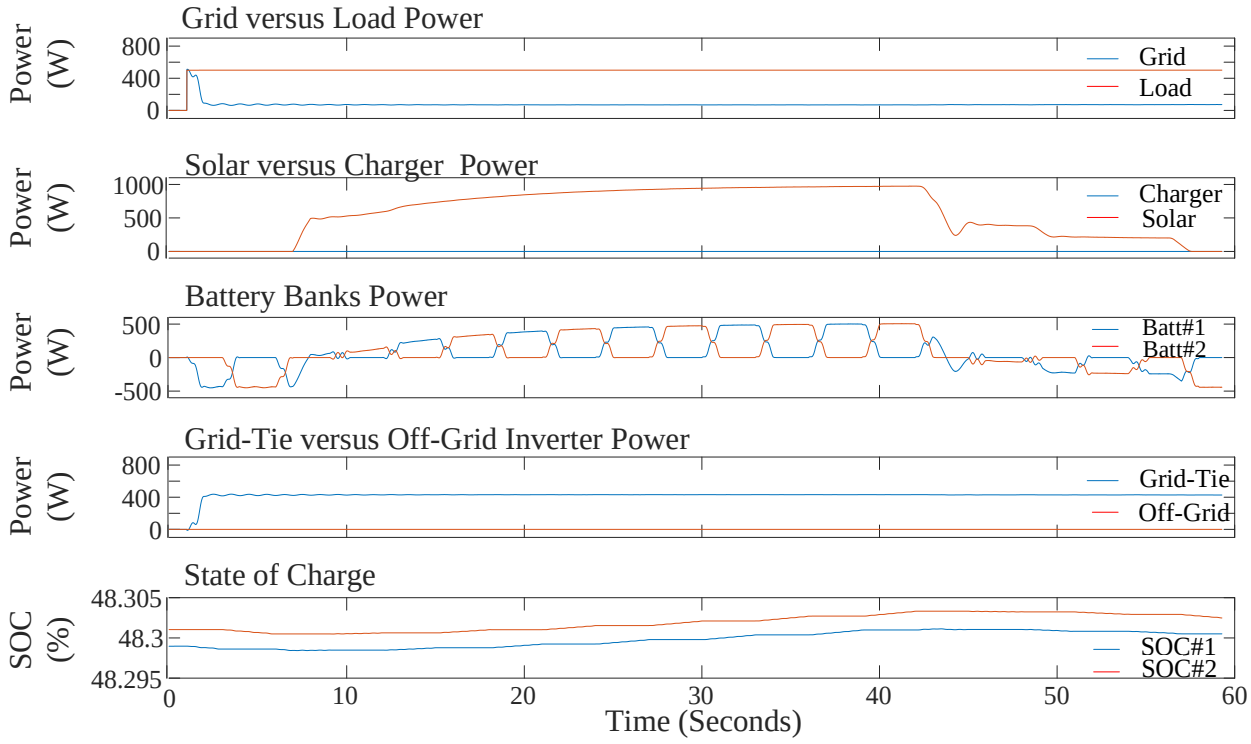

Fig. 4.17: Simulation result during Mode 2 with solar energy

Mode 3: Fig 4.18 shows the simulation results during off-peak hours. An adjustable battery charger uses the grid power to charge the battery banks alternatively. In this simulation example, the battery charger is adjusted to provide about 350 watts DC power continuously. The battery

charger and other loads consumes about 850 watts from the grid. The SOC charts demonstrates the increase on SOC value due to charging cycle.

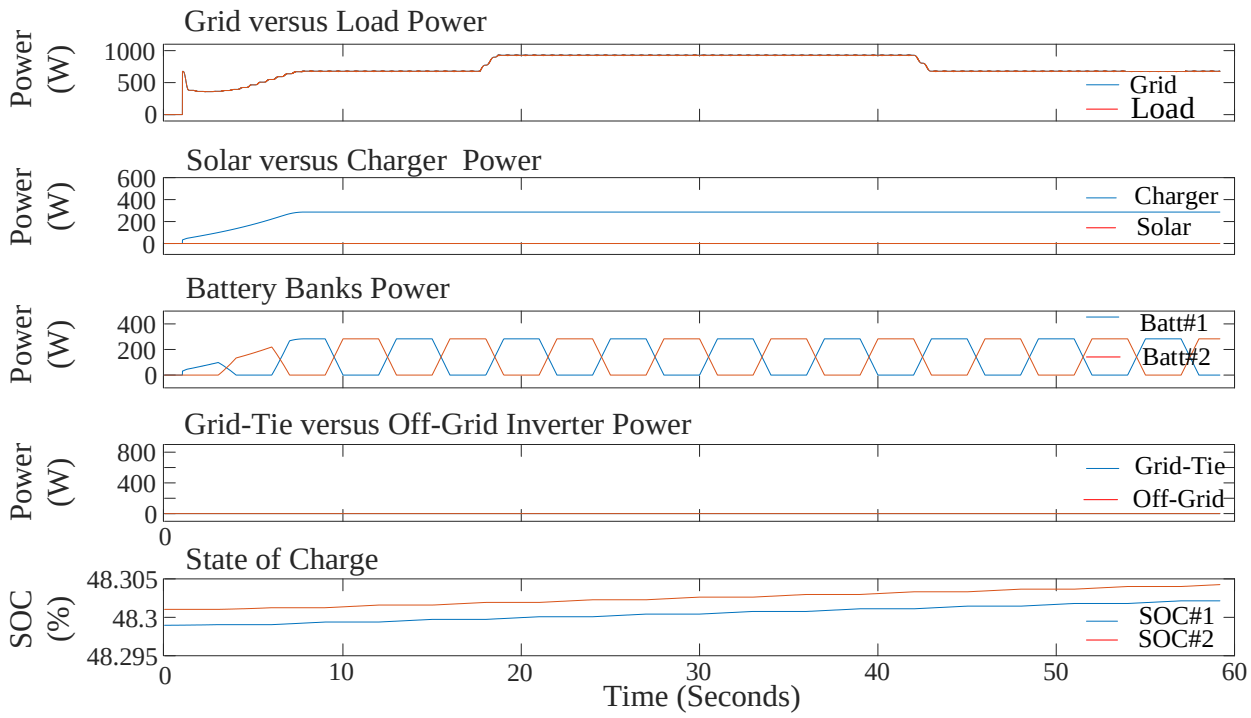

Fig. 4.18: Simulation result during Mode 3 (off-peak hours)

Mode 4: Fig. 4.19 shows the simulation results during a power outage. The off-grid inverter generates AC power to feed only the critical loads by discharging the battery banks alternatively when there is no solar energy available. The off-grid inverter discharges the battery banks to generate about 250 watts to supply the critical loads.

When solar panels generates from 400 to 600 watts, the excessive 150 to 350 watts power is utilized to charge the battery banks alternatively. This can be observed from the battery banks power charts. Therefore, the solar energy will be extended the coverage time during a power

outage. The SOC charts show increase and decrease in SOC values during charge and discharge cycles.

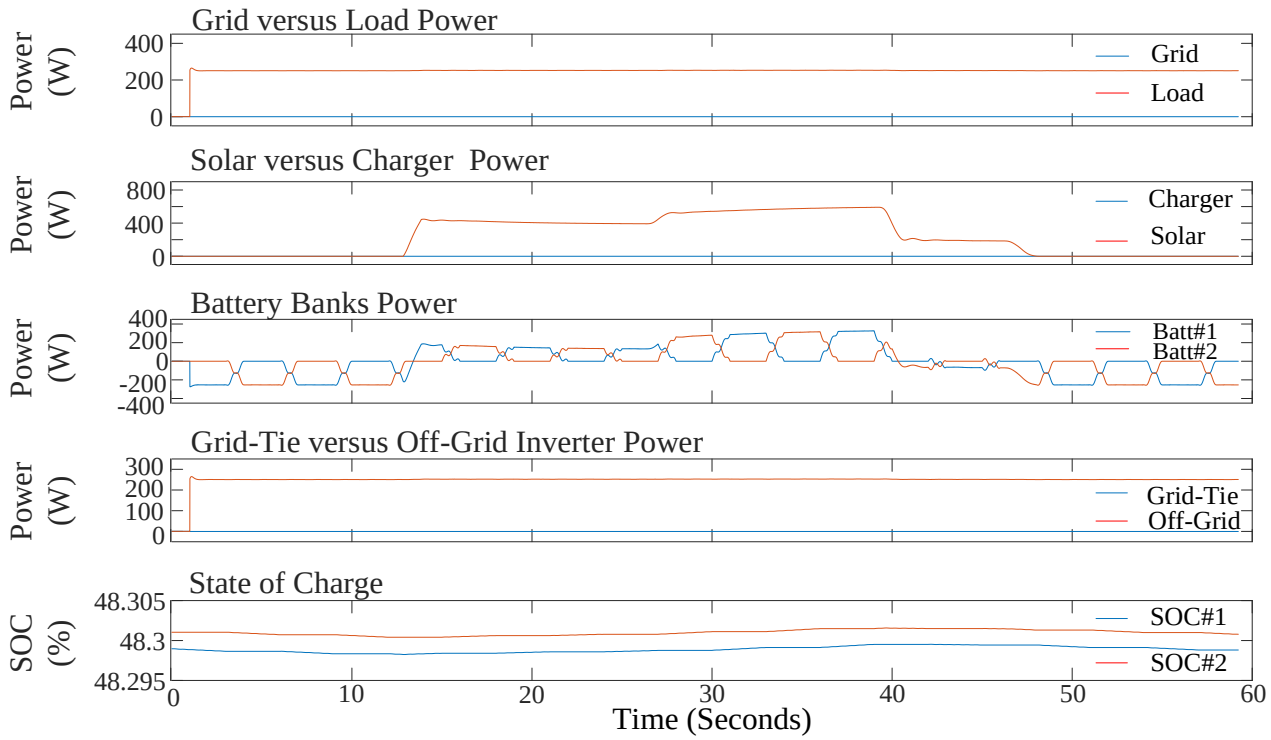

Fig. 4.19: Simulation result during Mode 4 (during power outage)

4.5 Flowchart for automatic operation

Now that all modes of operation are reviewed and simulated, the HESS can be controlled automatically by monitoring the current time versus the TOU schedule. Fig. 4.20 shows the flowchart that will be considered to control the HESS automatically.

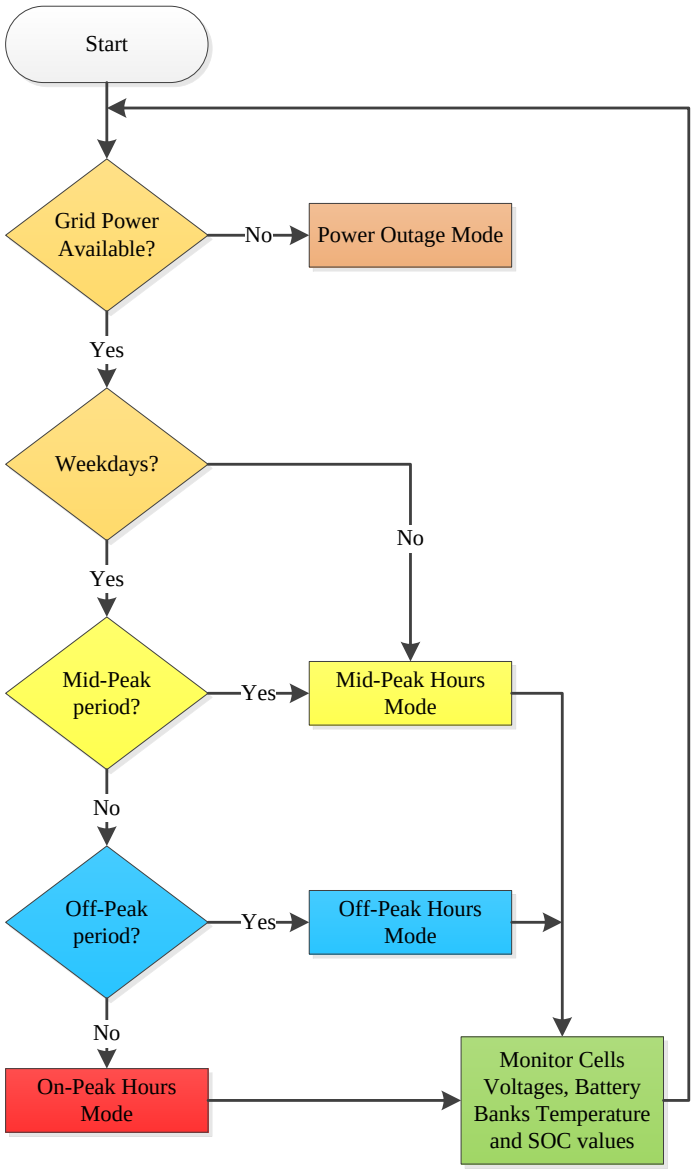

Fig. 4.20: Flowchart of automatic operation for new HESS

Chapter 5 : Implementation of the Prototype HESS

In order to evaluate the performance of the new HESS, a prototype of the new configuration is developed:

5.1 Hardware

The prototype HESS consists of solar panels, MPPT solar charge controller, battery charger, measuring boards, relay boards, data acquisition system, Lithium-ion battery cells, Grid-Tie and Off- Grid inverters. Fig. 5.1 shows the implemented prototype of the new Home Energy Storage System. In the next section, the hardware components of the prototype system will be reviewed.

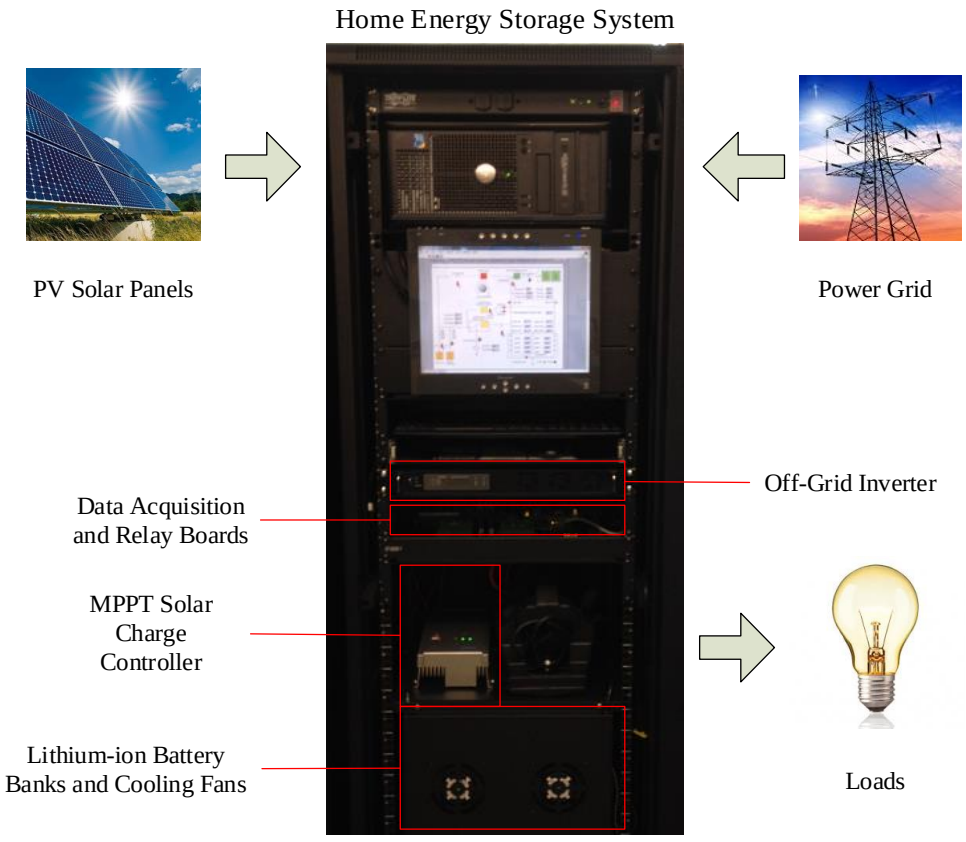

Fig. 5.1: Implemented Home Energy Storage System (HESS)

5.1.1 Battery Banks

Two battery banks is considered for this system which consists of eight Lithium-ion battery cells (LiFeMnPO4, 40Ah). Table 5.1 provides the specification of the battery cells which are used as the energy storage device for the prototype home energy storage system. [49]

Table 5.1: Specification of the Lithium-ion battery used in HESS

Cell Nominal Voltage	3.2V
Max cell voltage	4.00V (Recommend not to exceed 3.80V)
Min cell voltage	2.50V (Recommend not to drop below 2.80V)
Capacity	40Ah
Operating temperature	Charge: 0ºC to 65 ºC (32F to 149F) Discharge: -20ºC to 65 ºC (-4F to 149F)
Current range	Up to 3C (120A) continuous current for charging and discharging Up to 10C (400A) impulse (≤10 seconds) discharge current Recommended charging and discharging current: 0.5C (20A)
Internal Resistance	≤2.5mΩ
Energy Density	91.4 Wh/kg
Cycle life	Cell: ≥2000 cycles at 80% DOD at room temperature Pack: ≥1500 cycles at 80% DOD at room temperature
Self-discharge	Max 3% per month
Weight	Cell: 1.4Kg (3.1LB) 4-cell pack: 6.6Kg (14.55LB)

Each battery bank or pack includes four battery cells connected in series to have a 12.8 Volt battery bank. Fig. 5.2 shows the pictures of the cell and one battery bank/pack.

3.2V cell **12.8V pack**

Fig. 5.2: Lithium-ion battery cell and pack used in HESS [49]

The first step to use a battery cell for any system is to find the charge and discharge curves of the battery cell at a very low C rate. Fig. 5.3 shows the circuit diagram that is used for this step. A 1.35Ω resistive load (1Ω resistor plus 0.35Ω resistance of wires) was use to discharge the battery cell at 2.365A. Since the battery cell capacity is 40Ah, the discharge rate is about C/17. The DC power supply voltage is set to 3.8V and the current limit to 2.365A for charging cycle. The battery cell is discharged completely until the terminal voltage of the battery reaches to it 2.8V volte at very low C rate.

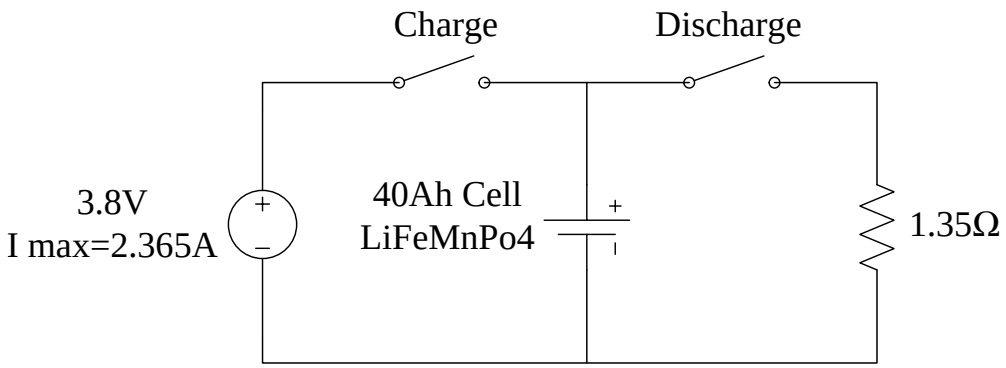

Fig. 5.3: 40Ah cell Charge and Discharge circuit

Then, the charge switch is closed to start charging the battery cell at 2.365A (0.059C) while recording the cell terminal voltage continuously (one sample per second) by a KEYSIGHT Digital Multimeter model# U1233A. All the measured data is exported to Excel for creating the Charging Curve. Fig. 5.4 represents the Charging Curve of the battery cell.

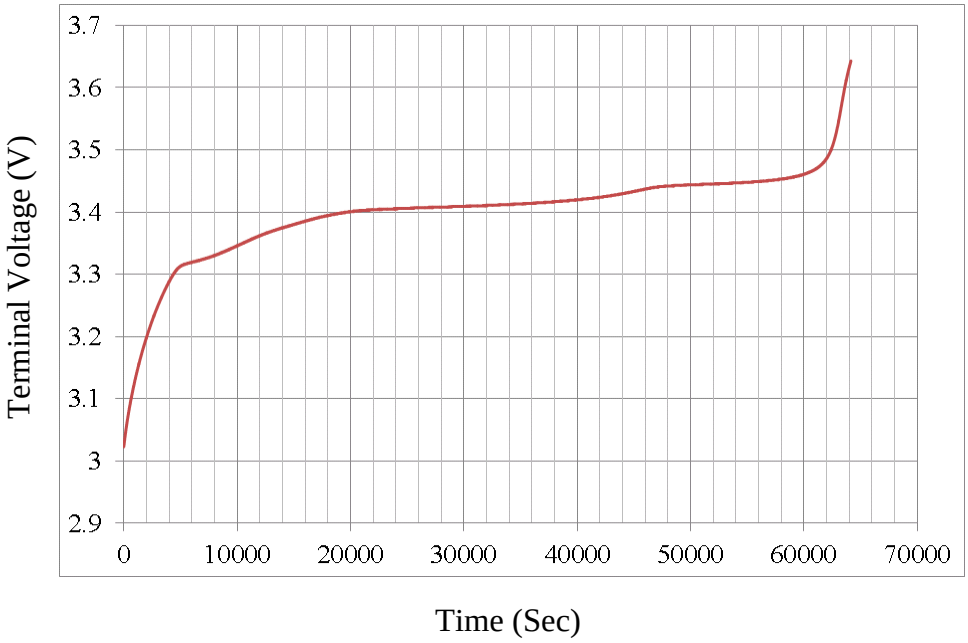

Fig. 5.4: Charging Curve at 0.059C at 0.059C for the 40Ah Lithium-ion battery cell

After completing the charge cycle, the charge switch is turned off. The voltage of the cell starts to decrease very slowly until it settles to fixed value. This means that the cell is relaxed and is ready for discharge cycle. The cell relaxation takes a few hours for the cell.

Now the discharge switch is closed to discharge the battery cell at the same 0.059C rate until it gets discharged completely when the cell voltage reaches to 2.8V. Fig. 5.5 represents the discharge curve of the battery cell. The next step is to generate the OCV-SOC curve by using the data from charging and discharging curves.

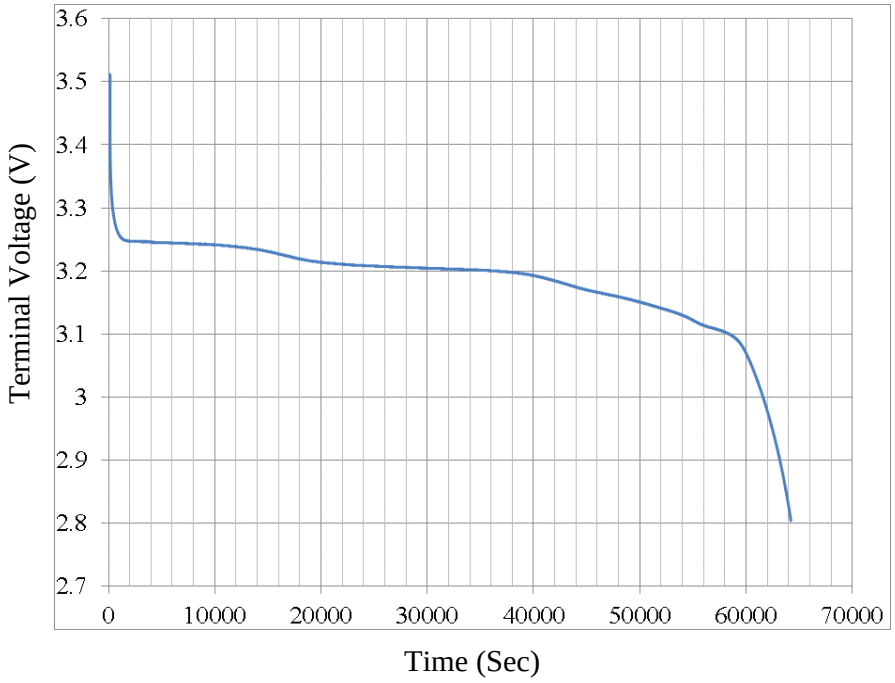

Fig. 5.5: Discharging curve at 0.059C for the 40Ah Lithium-ion battery cell

The OCV-SOC curve is very crucial to estimate the SOC value of the battery banks. Fig. 5.6 demonstrations the OCV-SOC Curve (Green) which is the average voltage of the terminal voltage of Charge (Red) and Discharge (Blue) curves versus SOC.

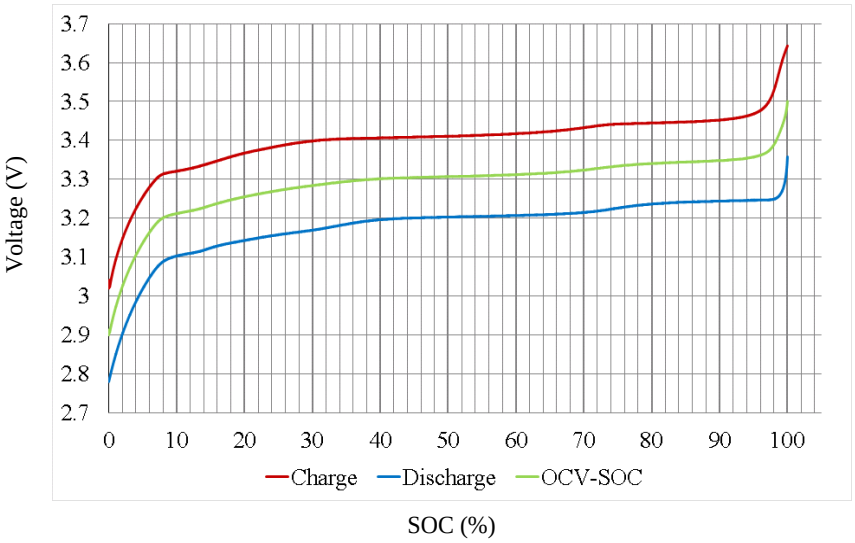

Fig. 5.6: OCV-SOC versus Charge and Discharge Curves

5.1.2 Battery Bank Configuration Circuit

A battery configuration circuitry was designed and implemented to provide the appropriate DC voltage for the modes of operation that were discussed in chapter 4. The following battery configuration cases are:

5.1.2.1 Series Battery Banks

In series configuration, all battery cells are connected in series as shown in fig. 5.7. The HESS controller enables the K_7 and K_s relays to provide a 24VDC battery bank at V_8 terminal. The series mode is suitable during the power outage and also to operate the prototype system as a Conventional HESS if is needed. The blue lines show the current flow paths.

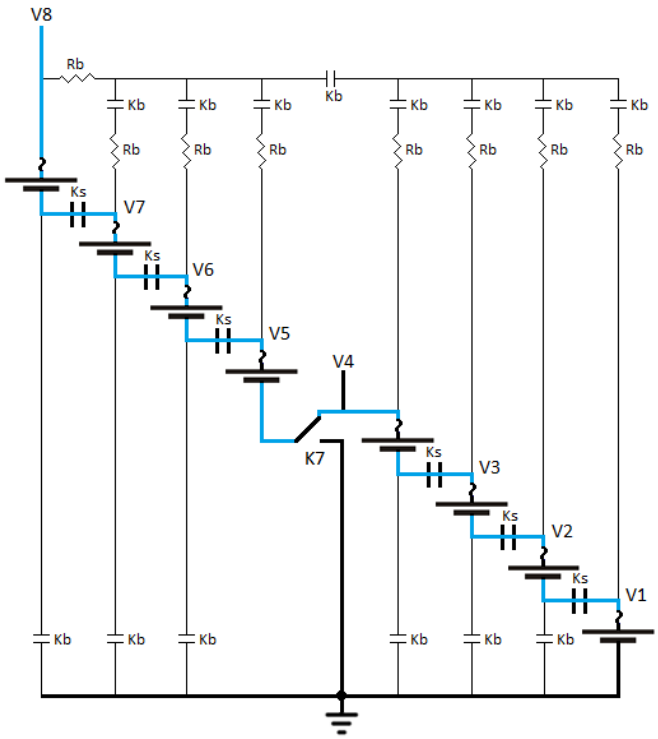

Fig. 5.7: Series battery configuration mode

5.1.2.2 Split Battery Banks

In split battery configuration, two battery banks are connected in a way to create to split battery banks as shown in Fig. 5.8. The HESS controller enables only K_s contacts to provide two split 12V DC battery banks as it was discussed in Chapter 4. This battery configuration mode is suitable for the modes of operations which the pulsed charge-discharge method is used (new HESS). V_4 and V_8 terminals are the positive terminals of battery bank #1 and bank #2, respectively.

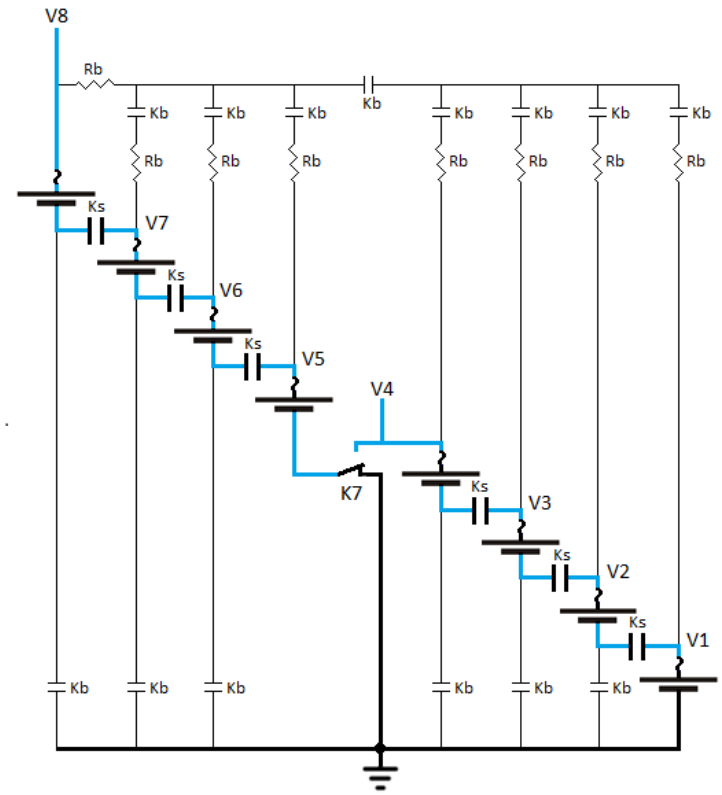

Fig. 5.8: Split battery configuration mode

5.1.2.3 Cells Balancing (Equalizing)

Although all battery cells are connected in series and assumed identical, however in practice the battery cells do not behave exactly the same during charge or discharge cycles. In other word, the battery cell voltages will not be the same even they were charged or discharged equally and this voltage variance causes unbalancing the battery cells.

As it was explained in Chapter 3, Lithium-ion batteries should not be overcharged at any time. An unbalanced situation can cause overcharging at least one of the battery cells in each series branch. To prevent overcharging the cells, the BMS monitors all battery cell voltages continuously to ensure that each battery cell voltage never exceeds the maximum voltage limit.

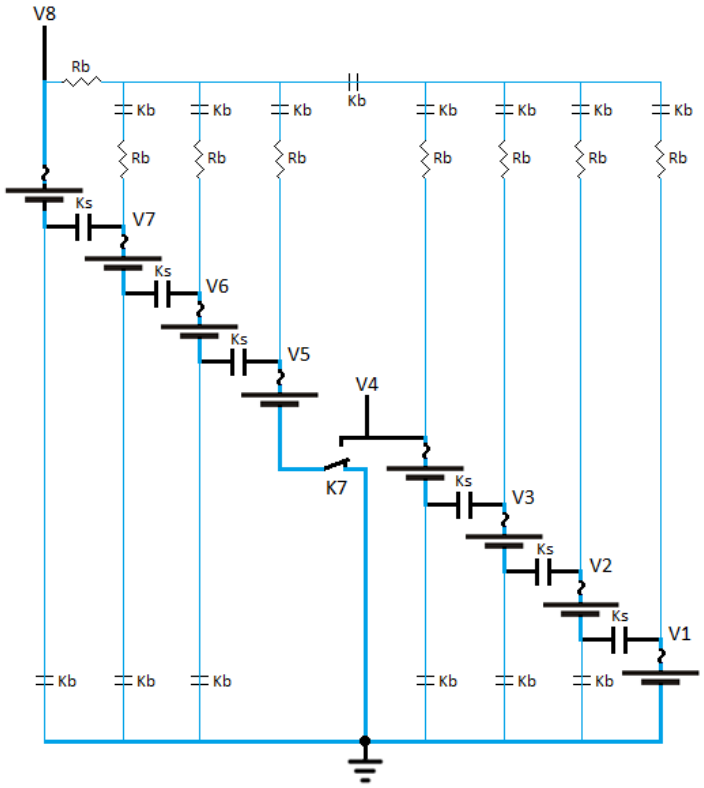

Fig. 5.9: Balancing battery configuration mode

In order to improve the HESS operation and also utilize the maximum capacity of the battery bank, the HESS Controller enables K_b and K_7 relays.

As it is shown in Fig 5.9, all battery cells are connected in parallel where each Battery cell has a pair of series current limiting resistor and protection fuse. This will provide the paths to equalize the battery cells when the battery banks are isolated from the rest of the system. Fig. 5.10 shows the banks arrangement along with the cell balancing board. More pictures of battery banks can be found in Appendix A.

Fig. 5.10: Battery banks arrangement

5.1.3 Battery Balancing Circuit

Fig. 5.11 and Fig. 5.12 show the schematic circuit diagram, the printed circuit board for the battery cells balancing or equalizing mode of operation.

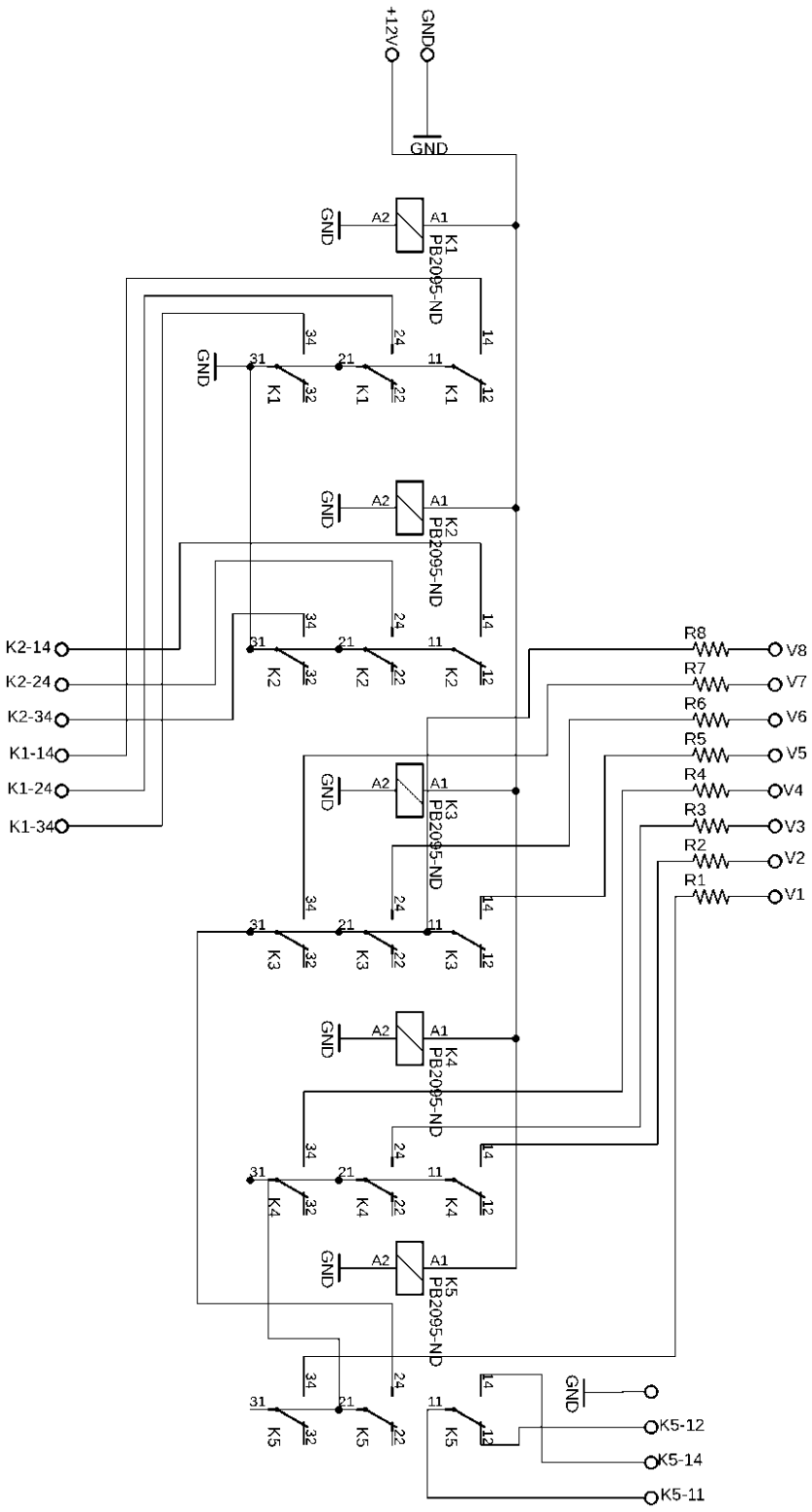

Fig. 5.11: Cells balancing schematic circuit diagram

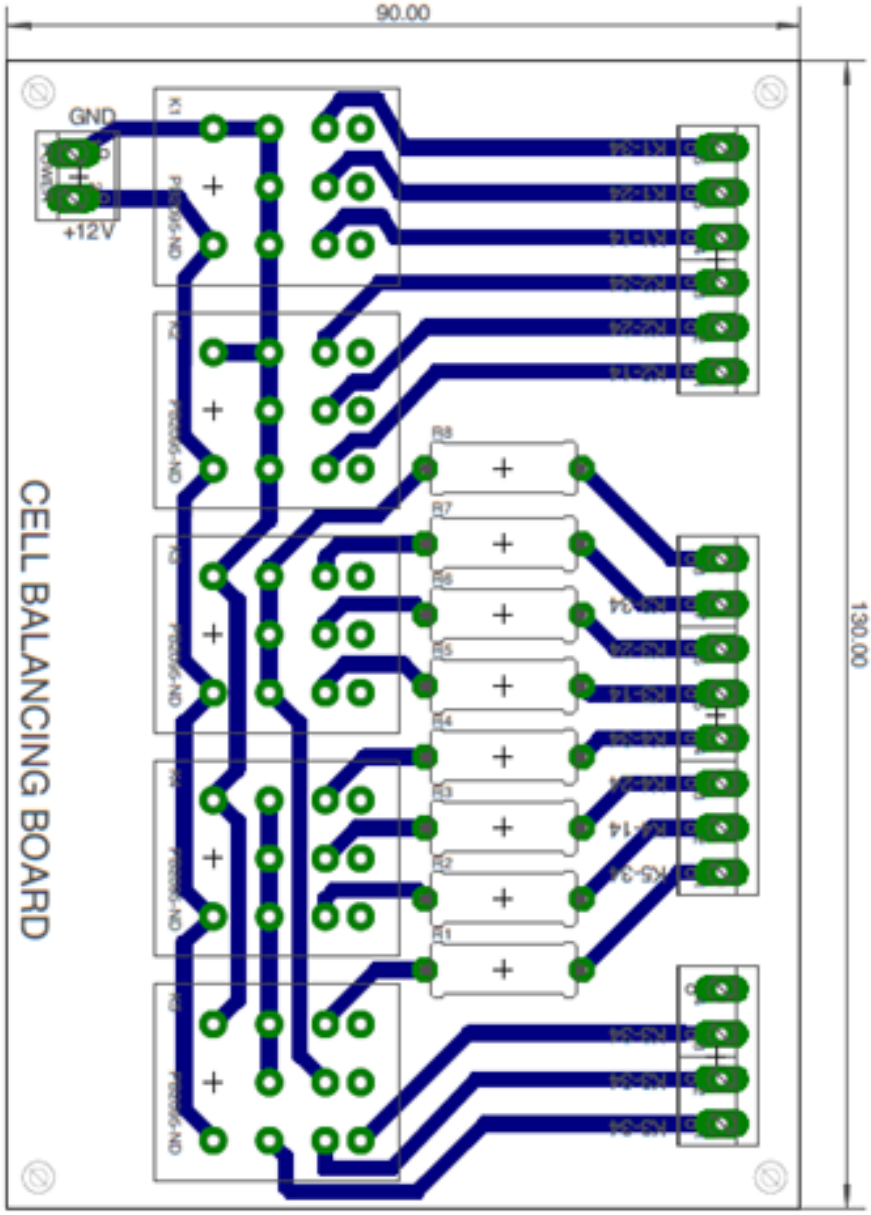

Fig. 5.12: Cells balancing printed circuit board

5.1.4 Relay Control Board Circuit

The schematic circuit diagram of the relay control board is shown in Fig. 5.15. The relay board basically is the interface circuit that isolates the high voltage or current circuits and low voltage control devices by using Opto–isolators and Electromechanical relays. The digital output signals of the data acquisition are at TTL level and isolated by opto-coupler devices (i.e. 4N25M). Since the electromechanical relays in this circuit have 12V DC coils, a relay driver (ULN 2803, a Darlington Transistor Arrays) was used to control the relays. The TTL signals are generated by a data acquisition system via its digital output ports. An example of a relay driver circuit with isolation is shown in Fig. 5.13.

Fig. 5.14 shows the schematic diagram of the relay board. Each relay board consists of eight 12VDC electromechanical relays. The normally open contact of the relays are rated at 30A.

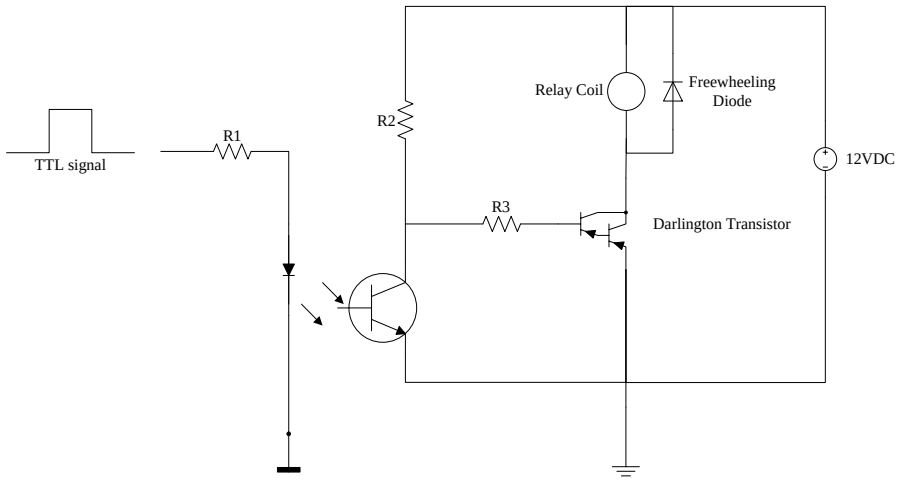

Fig. 5.13: An example of a Relay driver circuit

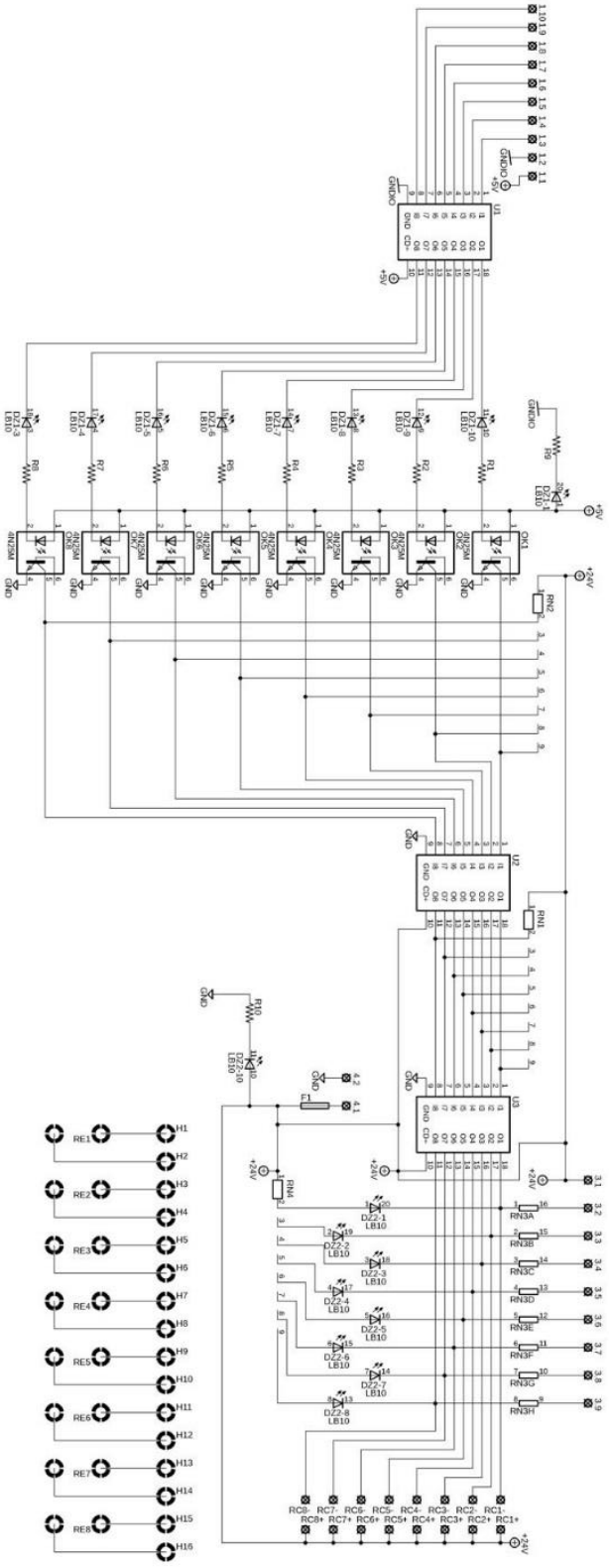

Fig. 5.14: Relay control board Schematic Diagram

Fig. 5.15 shows the printed circuit board of the relay board which two of them were implemented to provide the requirement of the new HESS.

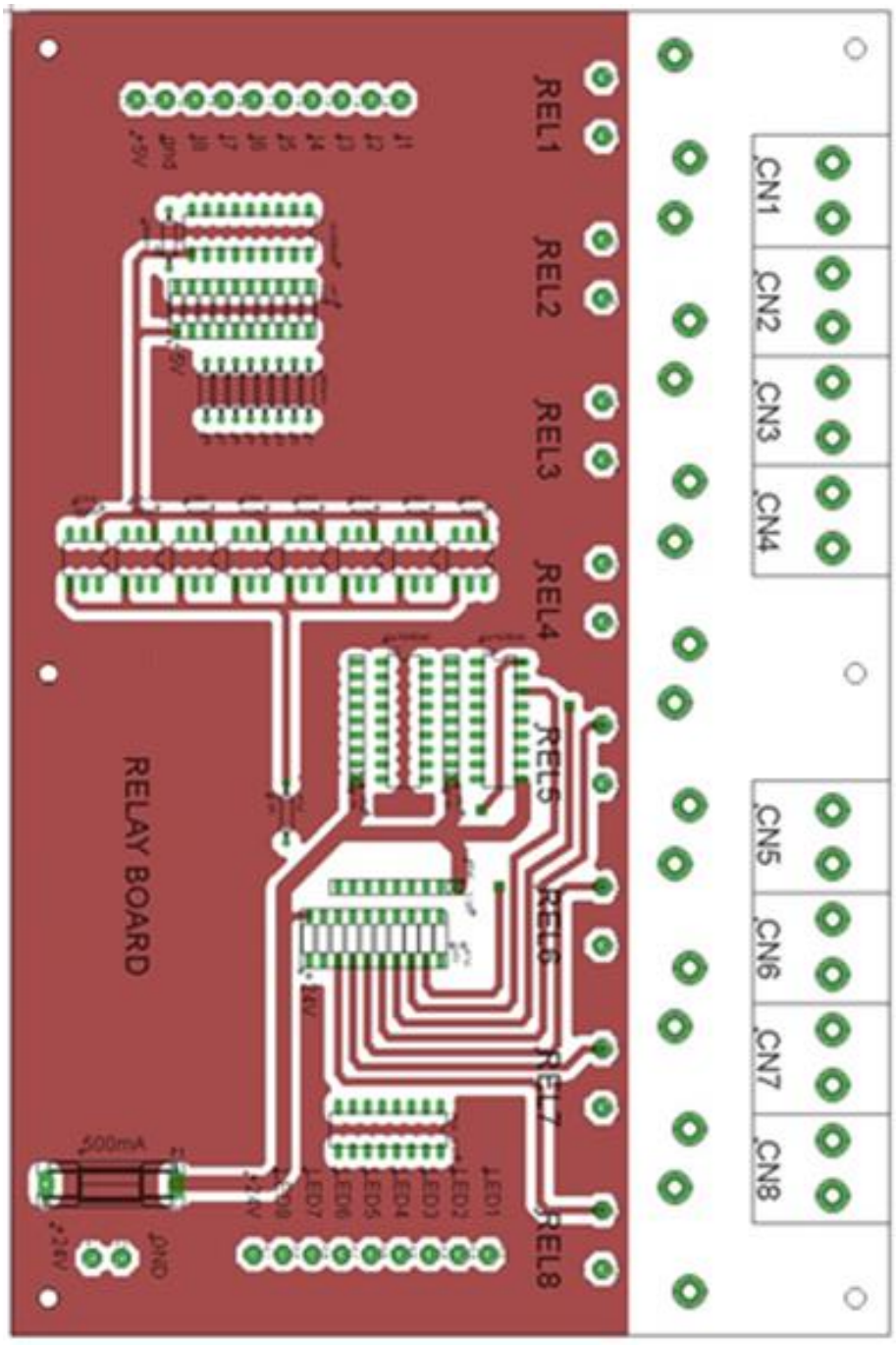

Fig. 5.15: Printed circuit board of the Relay board

5.1.5 Measuring Board

The measuring board contains different signal conditioning circuits which generally prepare the signals for the data acquisition system. The following signal conditioning circuits are the components of the HESS measuring board.

5.1.5.1 AC Voltage Measurement

Since the load voltage is in AC form, a potential transformer (PT) is required to measure the Load/Grid voltage. Fig. 5.16 shows the AC voltage measurement circuit. The potential transformer 3FD-310 is used to convert high voltage (120V) to low voltage signal (up to 5V).

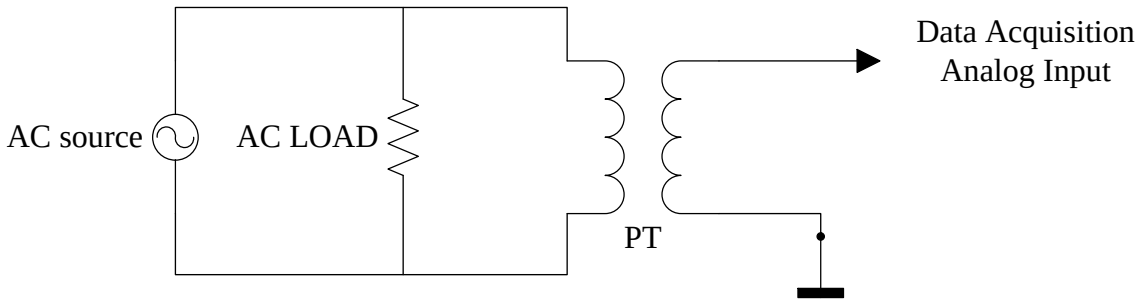

Fig. 5.16: AC voltage conditioning circuit

5.1.5.2 AC Current Measurement

As the load and grid currents are in AC form, a current transformer (CT) is required for each current. Fig. 5.17 shows the AC current measurement circuit. The current transformer CSE187L is used to convert high current (up to 30A) to low current signal (up to 60mA). The burden resistor R_1 converts the current to voltage which is within the range of ±10V suitable for the data

acquisition analog input port. Resistor R_2, Zener diodes D_1 and D_2 are considered for the purpose or high voltage protection.

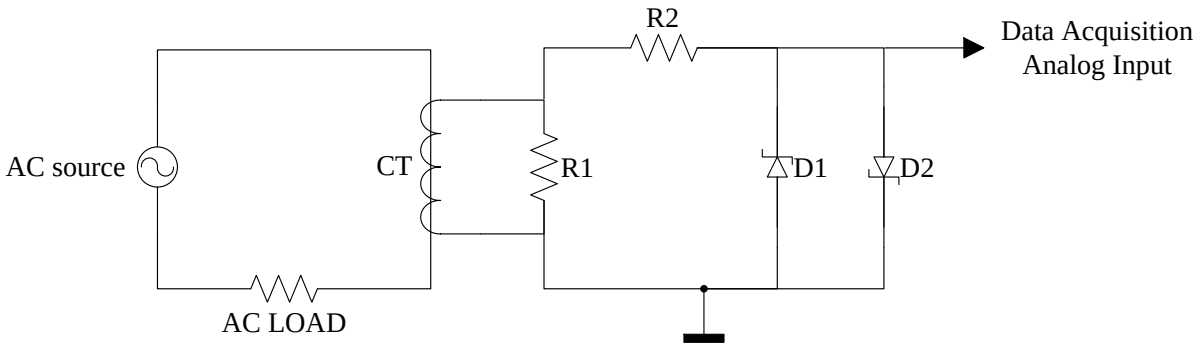

Fig. 5.17: AC current conditioning circuit

5.1.5.3 DC Voltage Measurement

In order to measure the DC voltages that exceed the acceptable voltage range of the data acquisition analog input port, a simple voltage divider circuit is needed to scale down the high voltage signals (i.e. PV voltage ≈38V). Fig. 5.18 shows the voltage divider circuit along with a Zener diode for the purpose of high voltage protection.

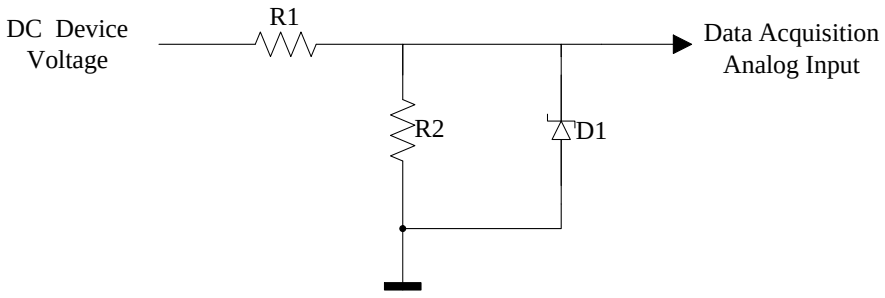

Fig. 5.18: DC voltage conditioning circuit

5.1.5.4 DC Current Measurement

Direct-current current-transducer (DCCT) is a good solution to measure high DC currents. Current transducer LTS 15-NP was used to measure DC current up to 48A and convert it to a DC voltage signal. This signal is sent to data acquisition system. Fig. 5.19 shows the signal conditioning circuit for DC current measurement. The measuring board contains four of these circuits to measure the batteries currents and the Charger and Solar Charge controller currents.

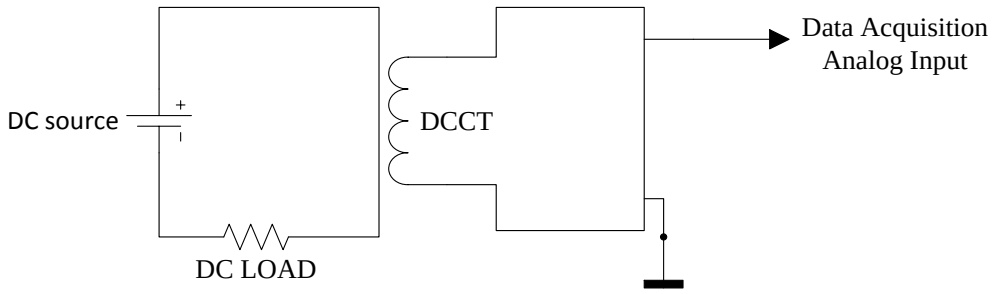

Fig. 5.19: DC current conditioning circuit

Fig. 5.20 and Fig. 5.21 show the Schematic diagram and the printed circuit board of the conditioning circuits.

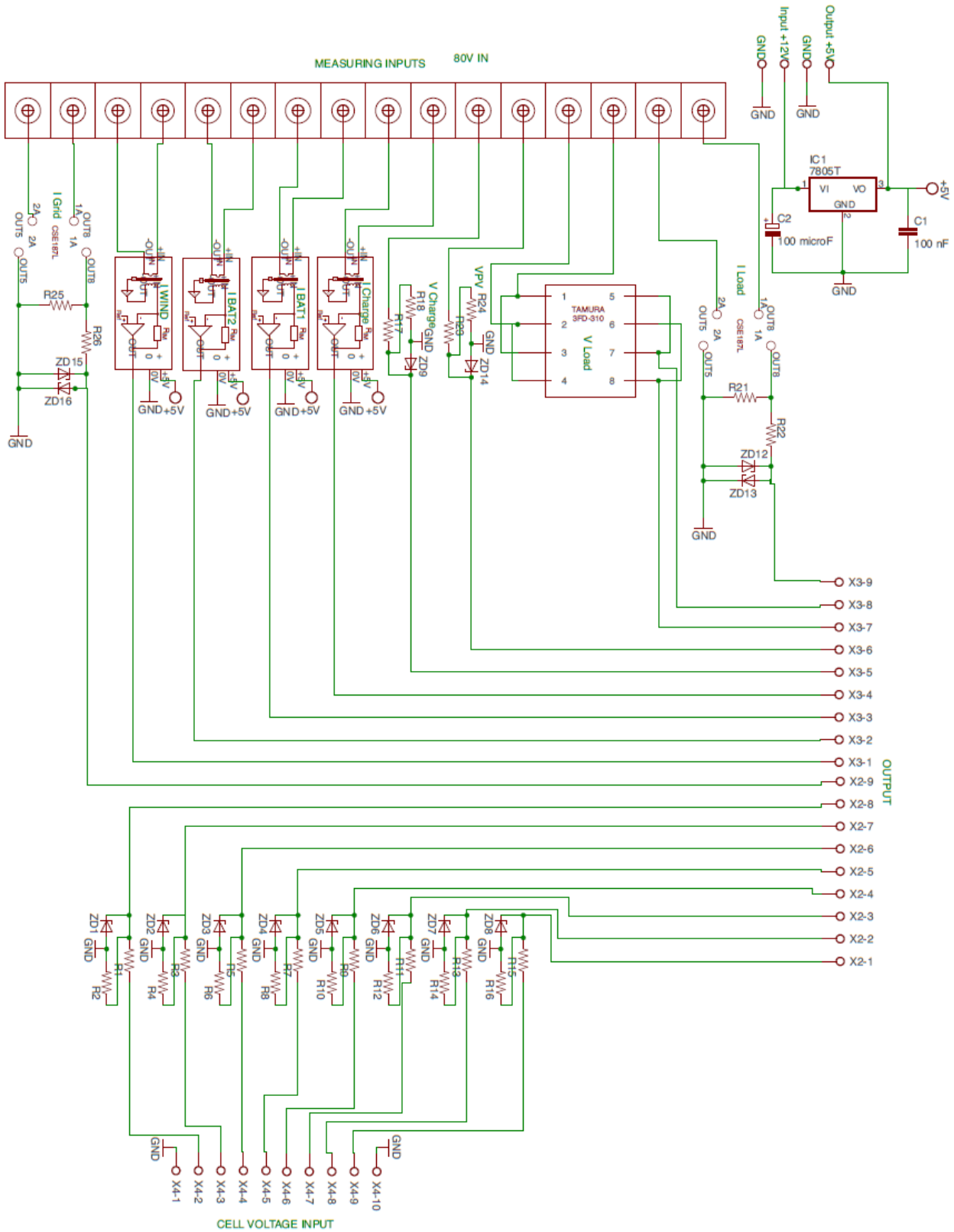

Fig. 5.20: Measuring board schematic diagram

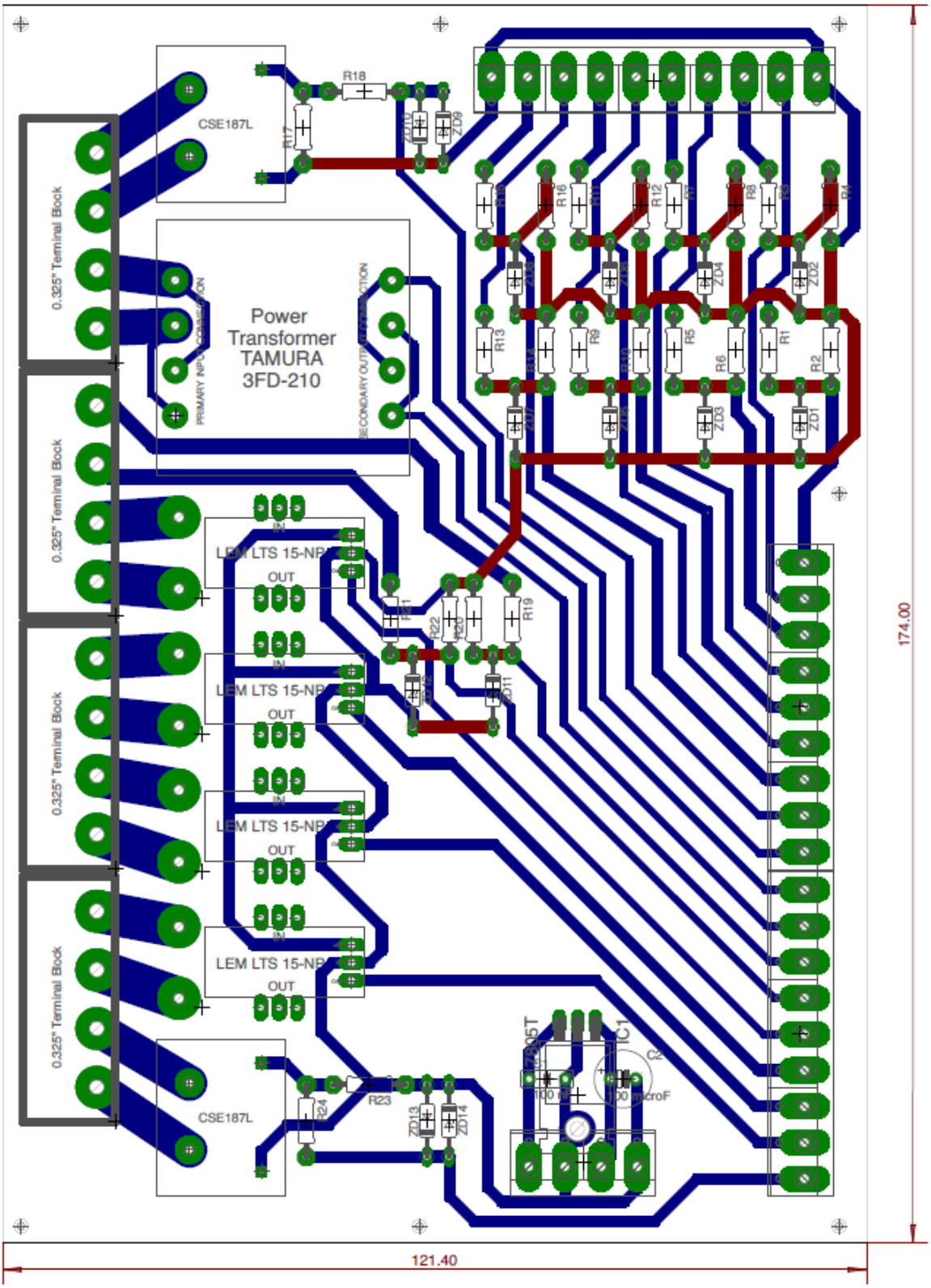

Fig. 5.21: Measuring circuits' printed circuit board

Fig. 5.22 shows the implemented measuring and relay boards in service.

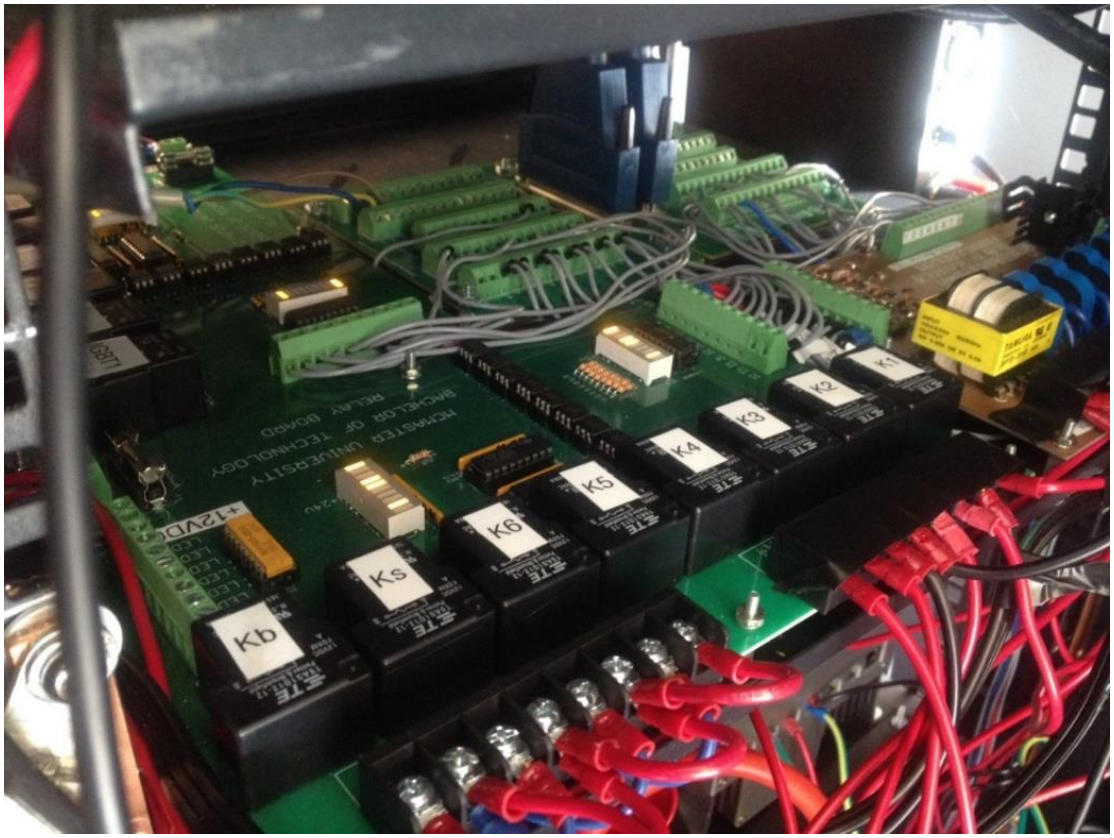

Fig. 5.22: Implemented Measuring and Relay boards

5.1.6 Solar Panels

Eight Renogy High Quality Premium solar panels (100Watts, 12Volts) are used to convert solar energy to electrical energy for the prototype system. Two solar panels are connected in series to create a 24V DC solar source and four of these branches are connected in parallel to generate maximum 800 Watts.

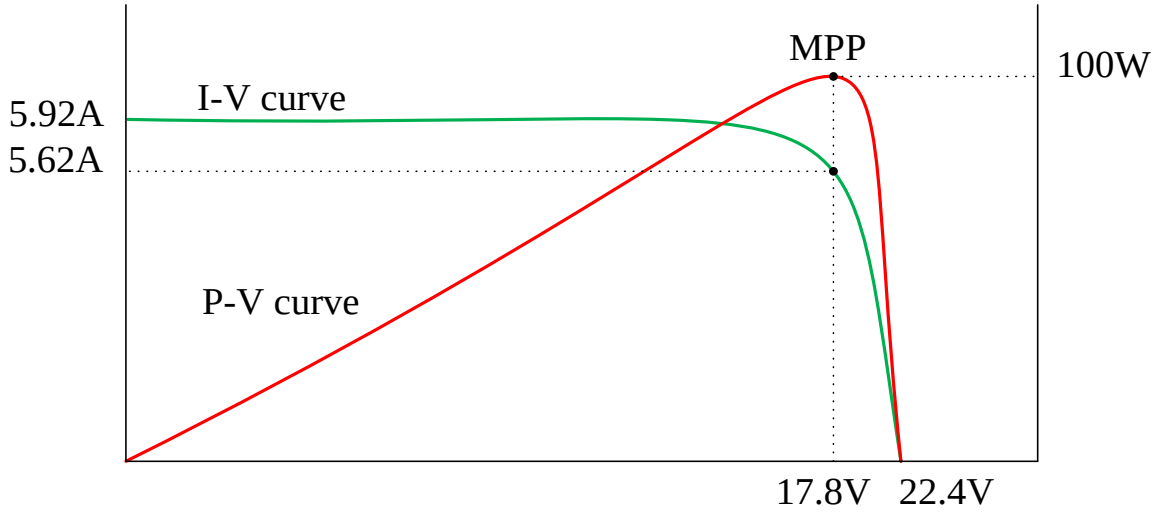

Fig. 5.23: I-V and P-V curves for the Renogy Solar Panel RNG_100P

Based on the specification of the Renogy solar panel from fig. 5.23 and based on equation 3.1, the Filling Factor of the solar panel is equal to:

$$FF = \frac{5.62 \times 17.8}{5.92 \times 22.4} = 0.7543$$

5.1.7 MPPT Solar Charge Controller

As it was discussed in Chapter 3, we need to use a Maximum Power Point Tracking controller in order to extract the maximum solar energy as efficient as possible. Fig. 5.24 shows a Renogy 40Amp MPPT Solar Charge Controller (Model# CTRL-MPPT40) which is used in the HESS prototype. The MPPT solar charge controller can be used for 12V or 24V deep cycle sealed Lead-acid, Gel or Flooded Battery banks.

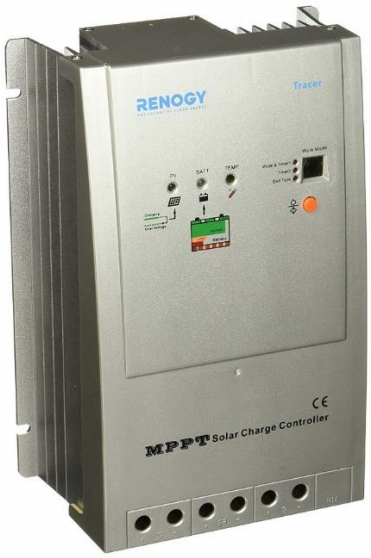

Fig. 5.24: Renogy MPPT solar charge controller [50] - *Courtesy of RENOGY*

5.1.8 Battery Charger

A switching mode DC power supply, BK Precision Model #1687B is utilized to work as the battery charger during off-peak hours. This unit is equipped with a remote control option which allows the user to control the output voltage and current via two 0 to 5V analog signals. The output voltage and current can be changed from 0 to 36V and 0 to 10A by the HESS data acquisition system, respectively. The HESS controller sends the appropriate reference signals to the Remote Control port to set the output voltage suitable for split (12V) or series (24V) configurations automatically. Fig. 5.25 shows the front and rear view of the DC power supply.

Fig. 5.25: Front and Rear view of the DC power supply BK Precision Model #1687B [51]- *Courtesy of BK PRECISION*

5.1.9 Grid-Tie Inverter

A 300W Grid-Tie Inverter, model # GTI-300W is used to convert 10.5 to 30 VDC to 120 Volt AC at 60Hz and inject the electric power to grid. The total harmonic distortion (THD) of the output is less than 5%. Fig. 5.26 represents the grid-tie inverter that is used in the new HESS.

Fig. 5.26: 300W Grid-Tie Inverter [52]

5.1.10 Off-Grid Inverter

A 1000W Off-Grid Pure Sinewave inverter, COTEK model # SR1000-124 is used to convert the 24VDC to 120 Volt AC at 60Hz . The total harmonic distortion (THD) of the output is less than 2% which represents very good power quality of the generated AC power. The off-grid inverter contains a transfer switch (bypass relay) to isolate the power grid and the DC to AC inverter during automatically a power outage. Fig. 5.27 and Fig. 5.28 show the unit and its block diagram.

Fig. 5.27: 1000W Off-Grid Pure Sinewave Inverter- *Courtesy of COTEK*

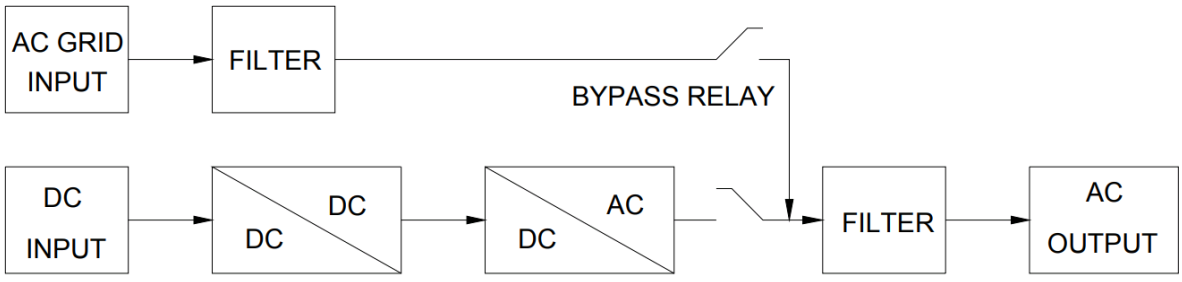

Fig. 5.28: Block diagram of the Off-Grid Inverter [53]- *Courtesy of COTEK*

5.1.11 Battery Management System

The battery management system (BMS) mainly monitors the terminal voltage and the current of battery cells continuously to estimate OCV and SOC values. Then it can avoid the cells from over-charging and over-discharging situations by interrupting the charge and discharge cycles.

BMS is also responsible to manage the battery cells temperature and uses cooling fans or other means to reduce the battery bank temperature toward the ambient temperature about 25 °C. This is so important for safety and good performance of the energy storage system. [54]

As it was discussed before, there are different methods to estimate the OCV and SOC values for batteries. To estimate these values of the prototype system, BMS employs Coulomb Counting method. The initial SOC value is needed to be recognized generally for all methods including Coulomb Counting. So that the cell terminal voltage at the end of balancing mode when the cells are completely relaxed, is measured to determine the initial SOC value of the battery cell based on OCV-SOC curve. Fig. 5.29 represents the OCV-SOC curve of the Li-ion cell that is used for the new HESS.

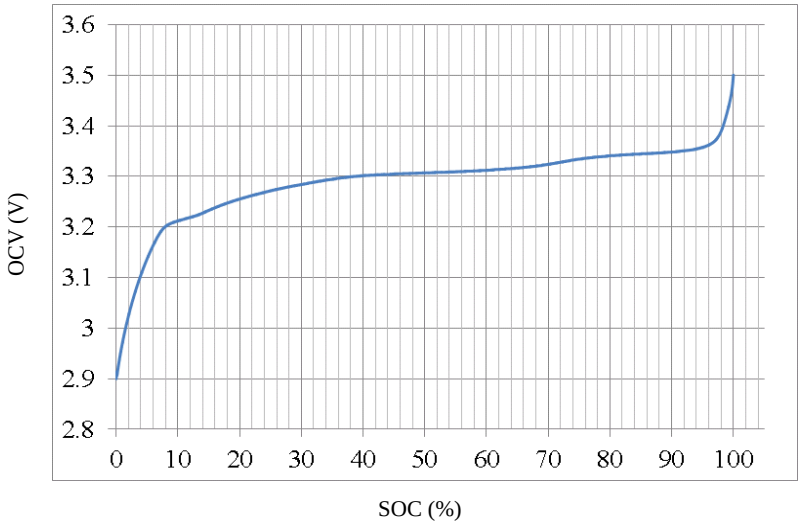

Fig. 5.29: OCV-SOC curve for the 40Ah Li-ion Cell

In order to measure the voltage of individual battery cells, the voltage at positive terminal of each battery cell is measured. When the battery banks are connected in series, the voltage of each battery cell can be determined by subtracting the voltages of positive and negative terminals when the reference voltage is ground.

The same strategy is used for split battery banks to measure the cell voltages. However, as it is shown in Fig. 5.30, the voltage for cell#5 will be the same as V_5 and in balancing configuration, V_1 will be the voltage of Cell#1, V_2 for Cell#2 voltage and so on.

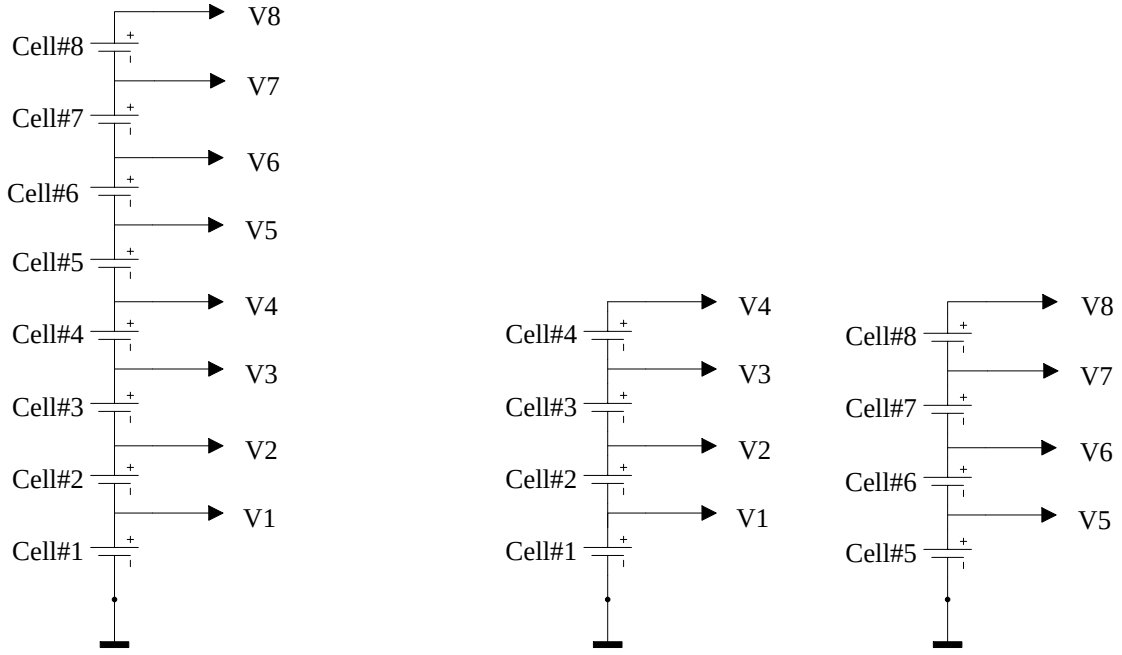

Series Configuration Split Configuration

Fig. 5.30: Cells voltage measuring

5.2 Software

Fig. 5.31 represents the simplified block diagram of the prototype HESS. As it was discussed before the measuring board is responsible to convert the high level voltages and currents to low level values suitable for the data acquisition system.

The Relay boards receive the control signals from the data acquisition system to activate the desired devices for each mode of operation accordingly. The energy storage system (ESS) controller and battery management system (BMS) blocks are the two programs that are linked together to monitor and control the entire HESS. LabVIEW (Laboratory Virtual Instrument Engineering Workbench) program was employed which is a graphical programing language from National Instruments.

Each LabVIEW program is called a VI (virtual instrument) which contains a Front Panel and a Function Block windows. The Front Panel is an interface window between the user and the Function Block which consists of Controls and Indicators. The Function Block contains all the required graphical functions. Fig.5.32 to Fig. 5.38 show the Virtual Front Panel views of the HESS when batteries are being charged during off-peak hours.

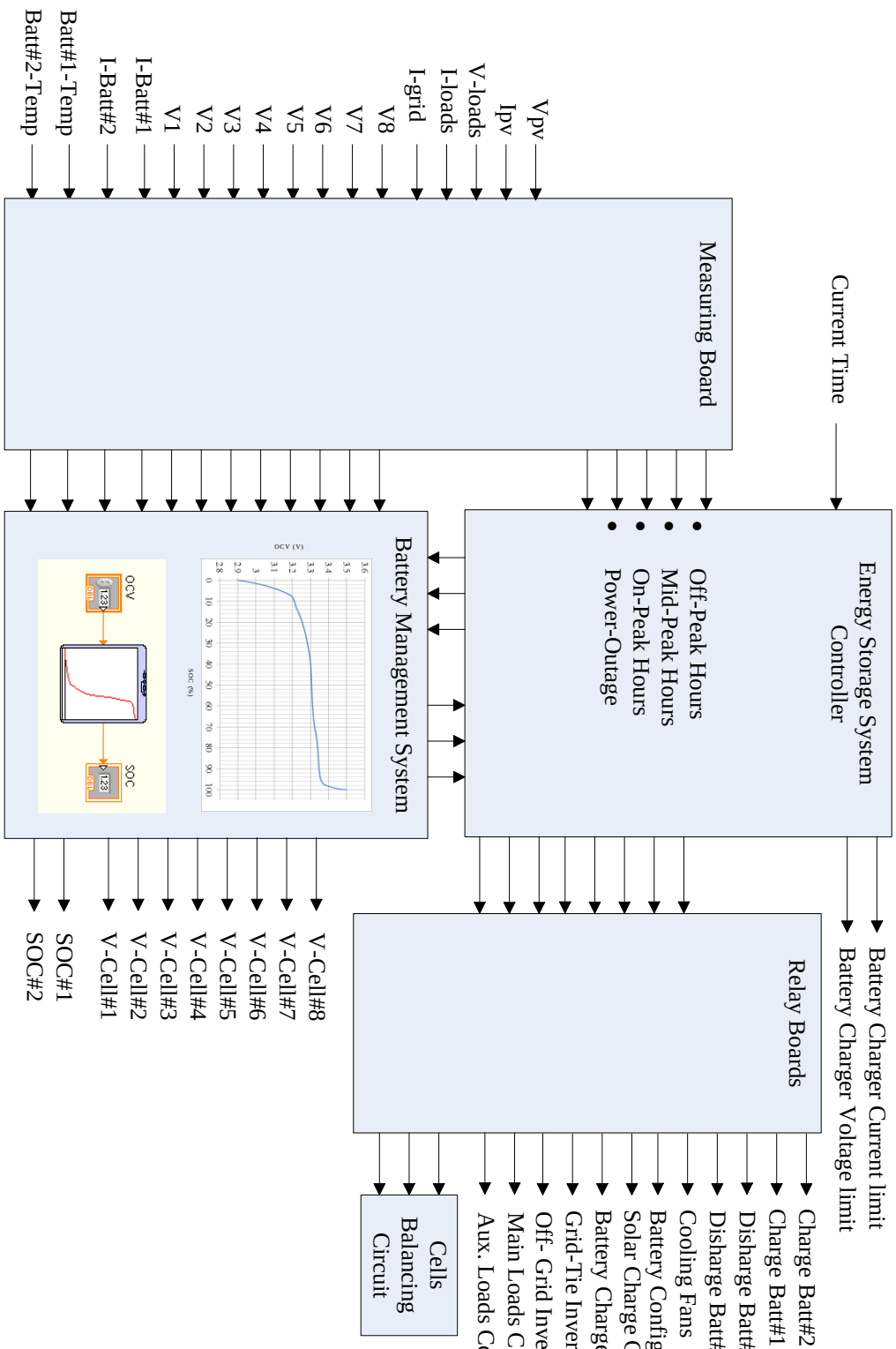

Fig. 5.31: HESS simplified block diagram

Fig. 5.32 shows the simplified diagram of the HESS that displays the real time value of incoming or outgoing power and also SOC of the battery banks.

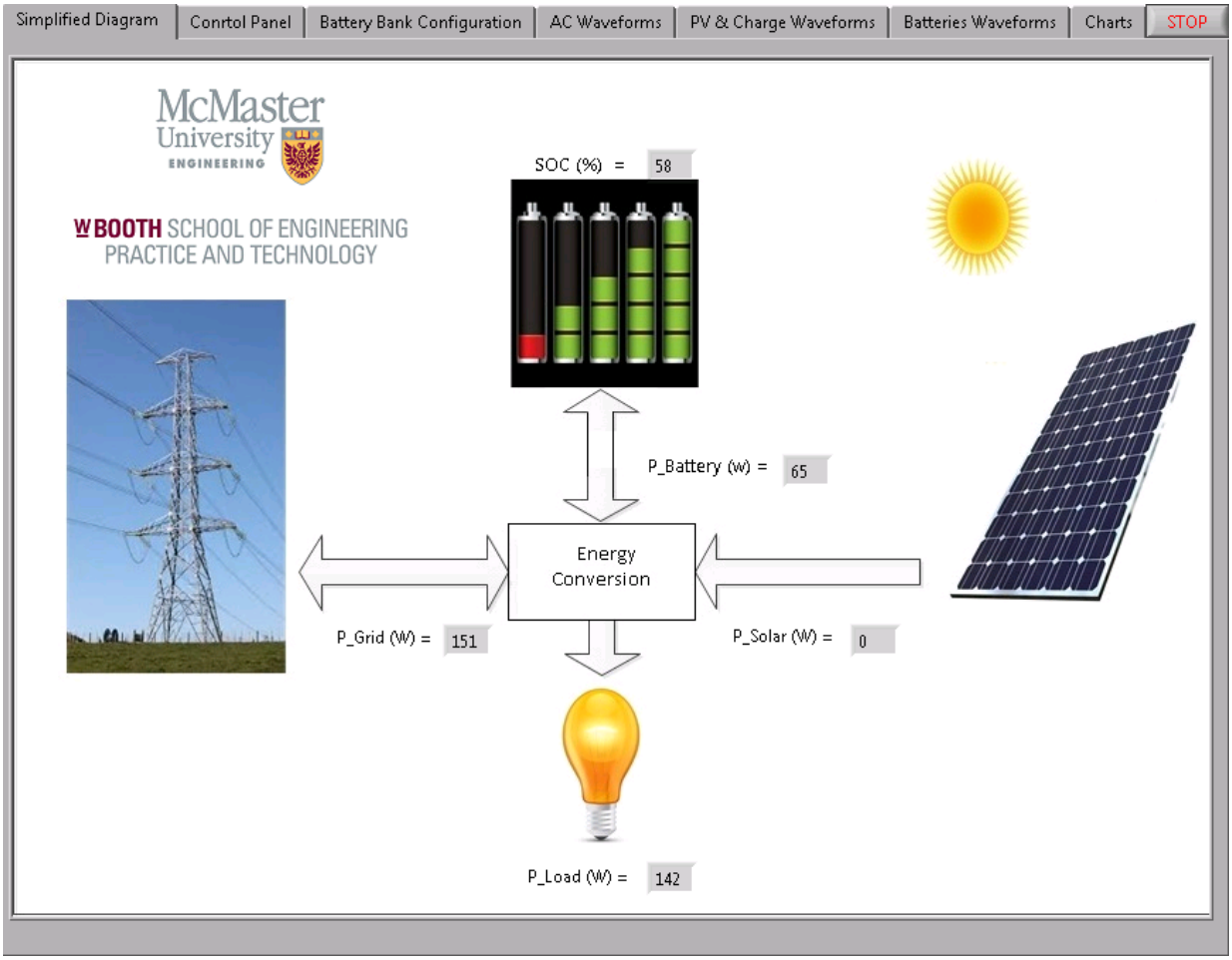

Fig. 5.32: HESS Front Panel simplified diagram tab

Fig. 5.33 shows the Control Panel tab of the HESS that allows the user to control the HESS manually. In this tab, the user may monitor the status of all digital or analog variables and control the entire HESS system by changing the switches accordingly. For example, switches K_1, K_3 and K_5 are closed to provide DC power to be sent to the battery banks through K_9 or K_{10} alternatively.

The current limit knob of the Battery Charger is set to about 4A to charge each battery bank alternatively.

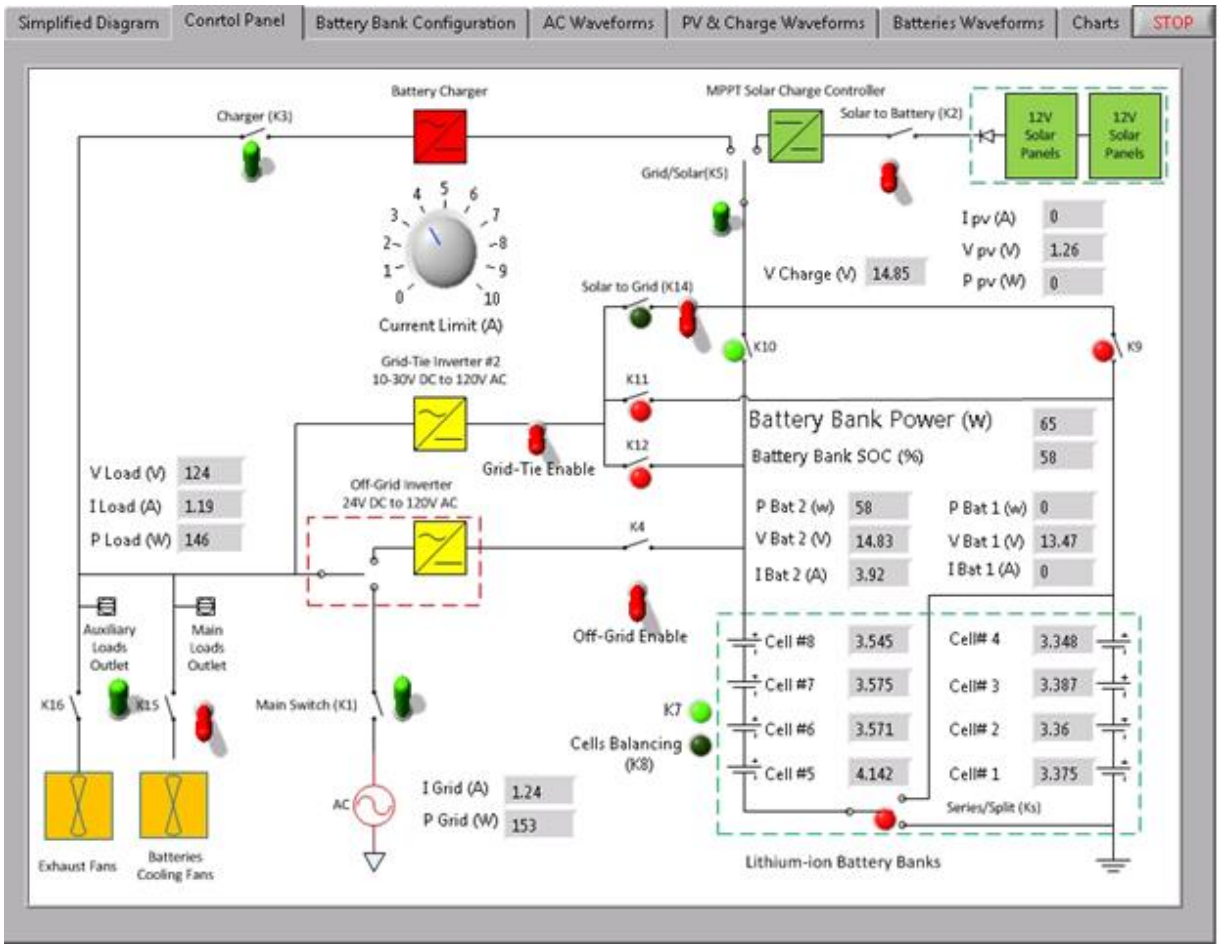

Fig. 5.33: HESS Front Panel Control Panel Tab

Fig. 5.34 shows the Battery Configuration tab that displays how battery cells are connected. In Split bank configuration four battery cells are connected to series to create a 12.8 volt battery bank.

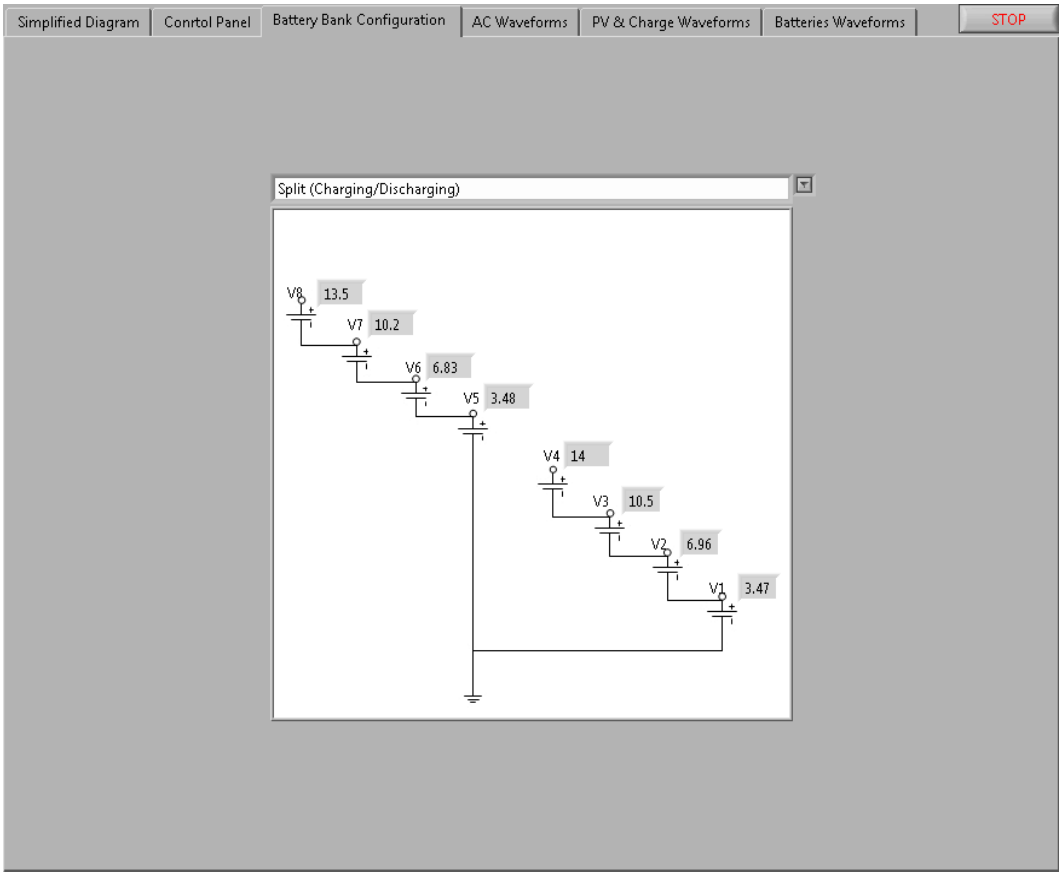

Fig. 5.34: HESS Front Panel Battery Bank Configuration Tab

Fig. 5.35 shows the AC waveforms tab that displays the AC voltage waveform at the Load or Grid. It also displays the AC current waveforms of the Grid and Load.

Fig. 5.36 shows the Solar Panel and Charge waveforms tab which includes the voltage and current waveforms at the inputs of the MPPT Solar Charge Controller and the waveforms of the voltage and current coming out of the common contact of switch K_5.

Fig. 5.37 shows the Batteries waveforms tab that displays the voltage and current waveforms of each battery bank.

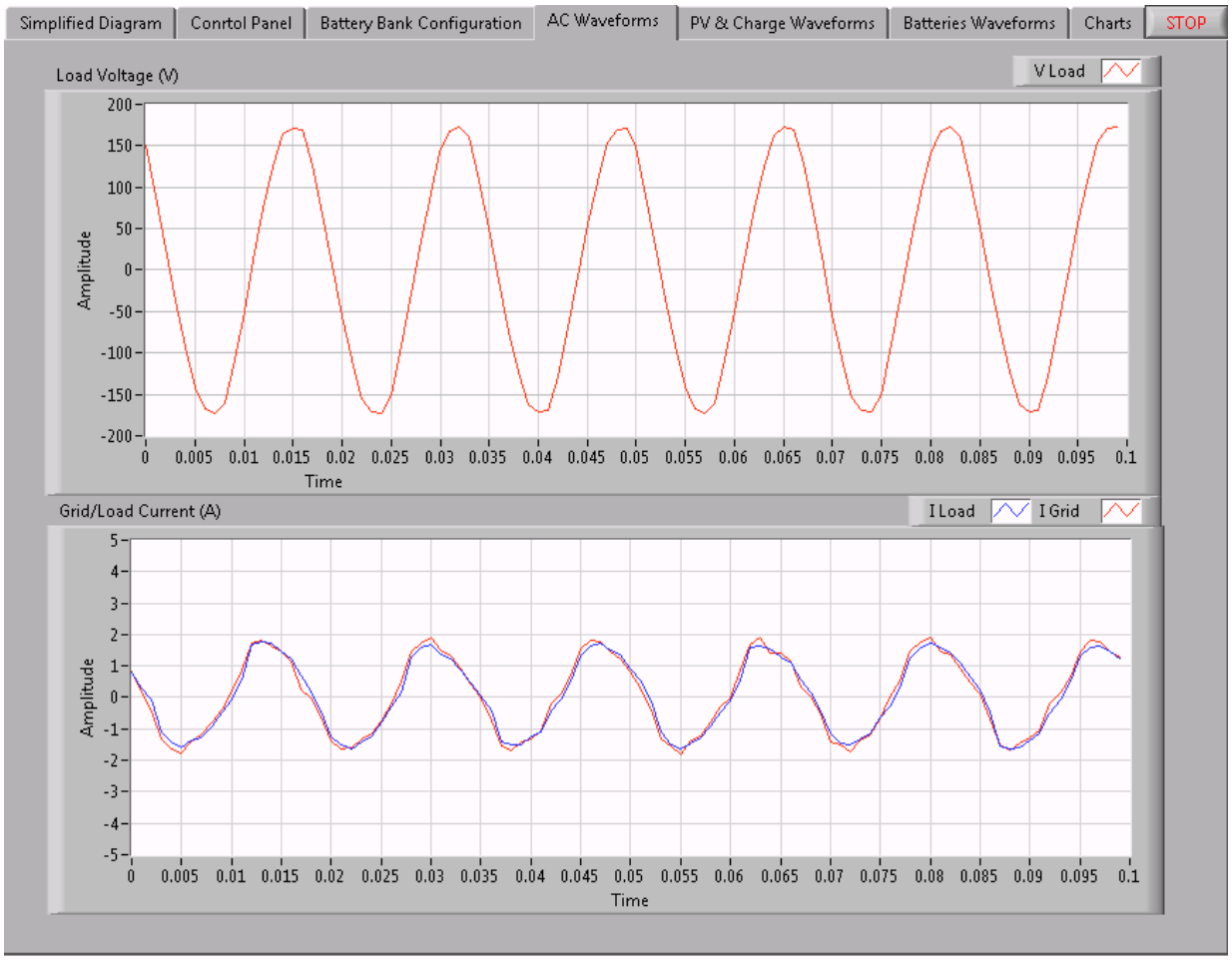

Fig. 5.35: HESS Front Panel AC Waveforms Tab

Fig. 5.36 shows the PV and Charge Waveforms tab that displays the voltage and current waveforms of the solar Panels and the battery charger.

Fig. 5.37 shows the Batteries waveforms tab which they display the voltage and current waveforms of the battery banks.

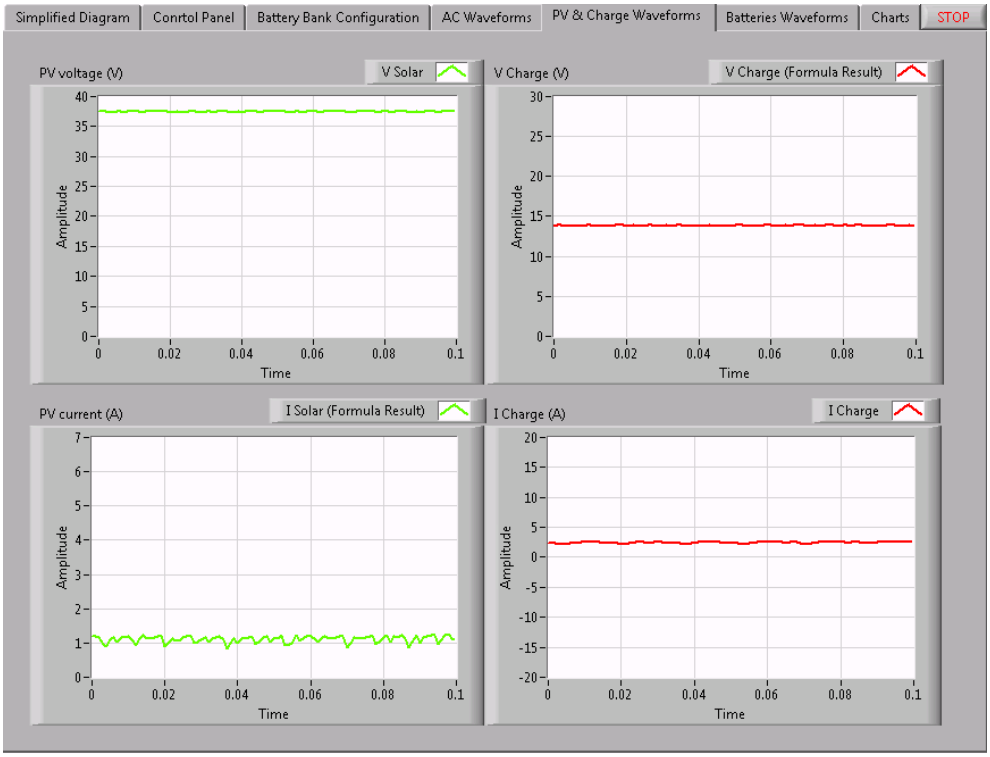

Fig. 5.36: HESS Front Panel PV and Charge Waveforms Tab

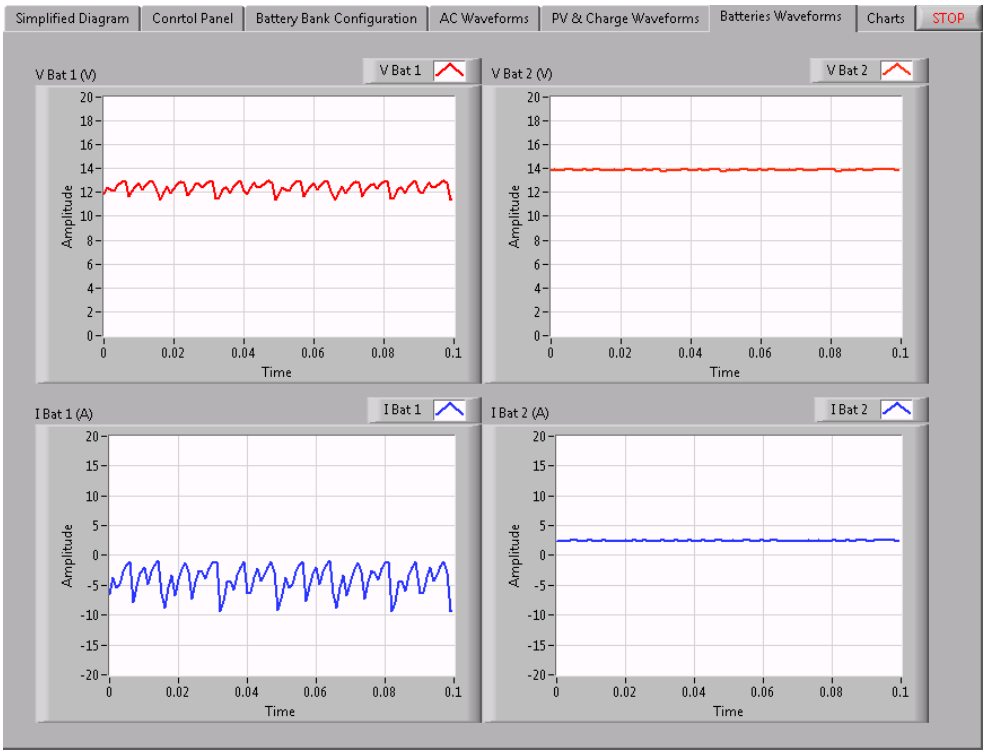

Fig. 5.37: HESS Front Panel Batteries Waveforms Tab

Fig. 5.38 to Fig. 5.42 shows the Charts tab which it displays the Power charts for the Loads, Grid, Solar, battery Charger, battery banks, Inverters and the SOC chart for the battery banks.

Mode 1: In this mode, the battery banks are isolated from the rest of HESS circuit in for equalizing the battery cells during mid-peak hours. As it is shown in Fig 5.38, the load value is about 20watts at the beginning. Then, the load changes to 60, 140, 60 and 20 watts sequentially. The SOC#1 and SOC#2 value will be equal when all battery cells are equalized. However, due to unwanted noise in the system, there are some disturbances in the terminal voltages measurement. This issue needs to be looked after in the future work. It can be seen that the battery banks power stay at zero as the battery banks are isolated.

Fig. 5.38: HESS Front Panel Charts during mid-peak hours (Mode-1)

Mode 2: In this mode of operation when there is no solar power available, the battery banks are set to split configuration during on-peak hours so that they can be charged or discharged alternatively. Fig. 5.39 shows a case in this mode where the load value is set to zero watts then changed to 150watts. The grid–tie inverter generates about 50 watts to reduce the grid power from 150 to 100 watts. The batteries are discharged alternatively to provide the DC power to the grid-tie inverter. Since the SOC values are not exactly the same, the discharging duty cycle of the battery bank#1 is higher than SOC of Bank#2. This feature balances the battery banks automatically by the controller system. The SOC charts demonstrate gradual SOC reduction for both battery banks.

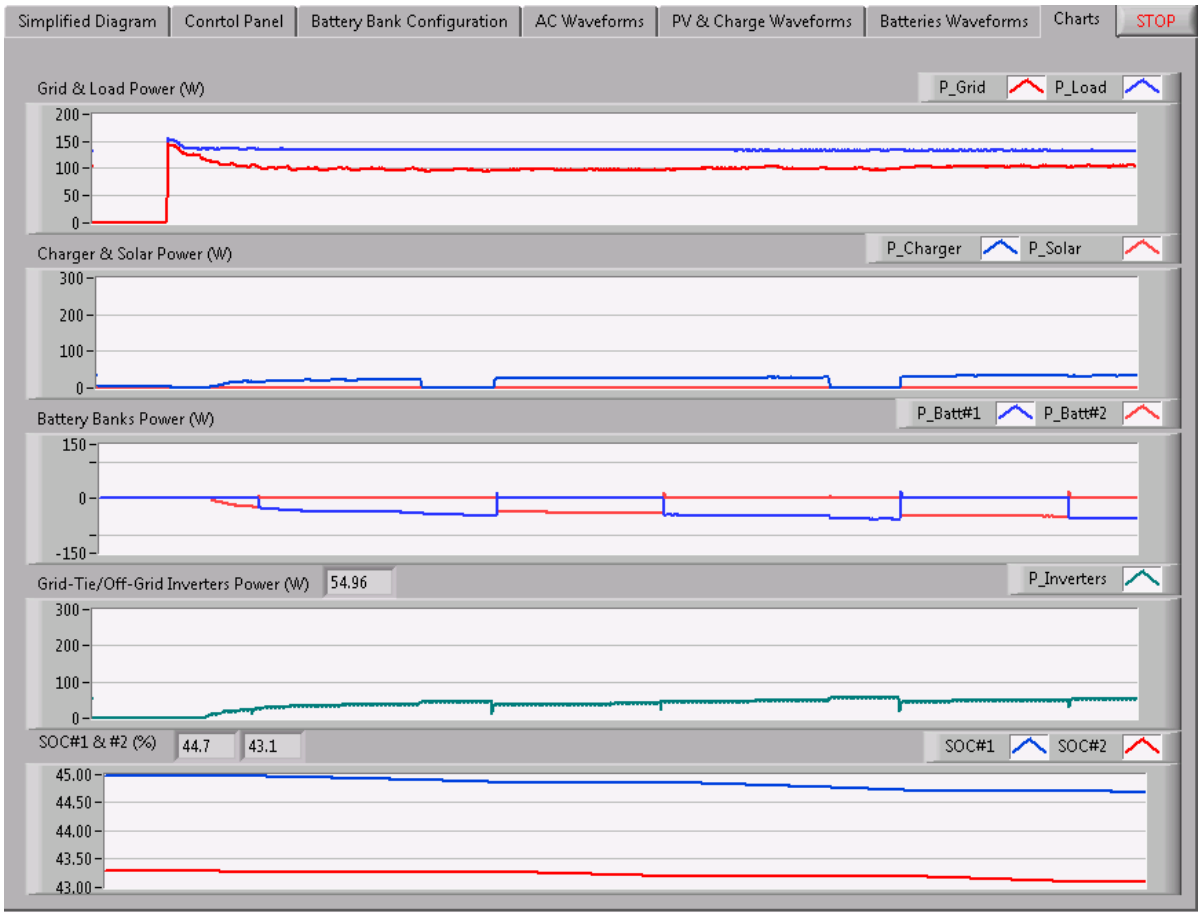

Fig. 5.39: HESS Front Panel Charts during on-peak hours (Mode-2) without solar

Fig. 5.40 shows a case in mode-2 when there is solar power available. The load value is set to zero watts then changed to 150watts. The grid–tie inverter generates variable power to reduce the grid power depending on the generated solar power. The batteries are charged or discharged based on the amount of harvested solar power. Since the SOC value of the battery banks are not exactly the same, the discharging duty cycle and charging duty cycle vary accordingly to balance the battery banks automatically. The SOC charts demonstrate gradual SOC changes for both battery banks.

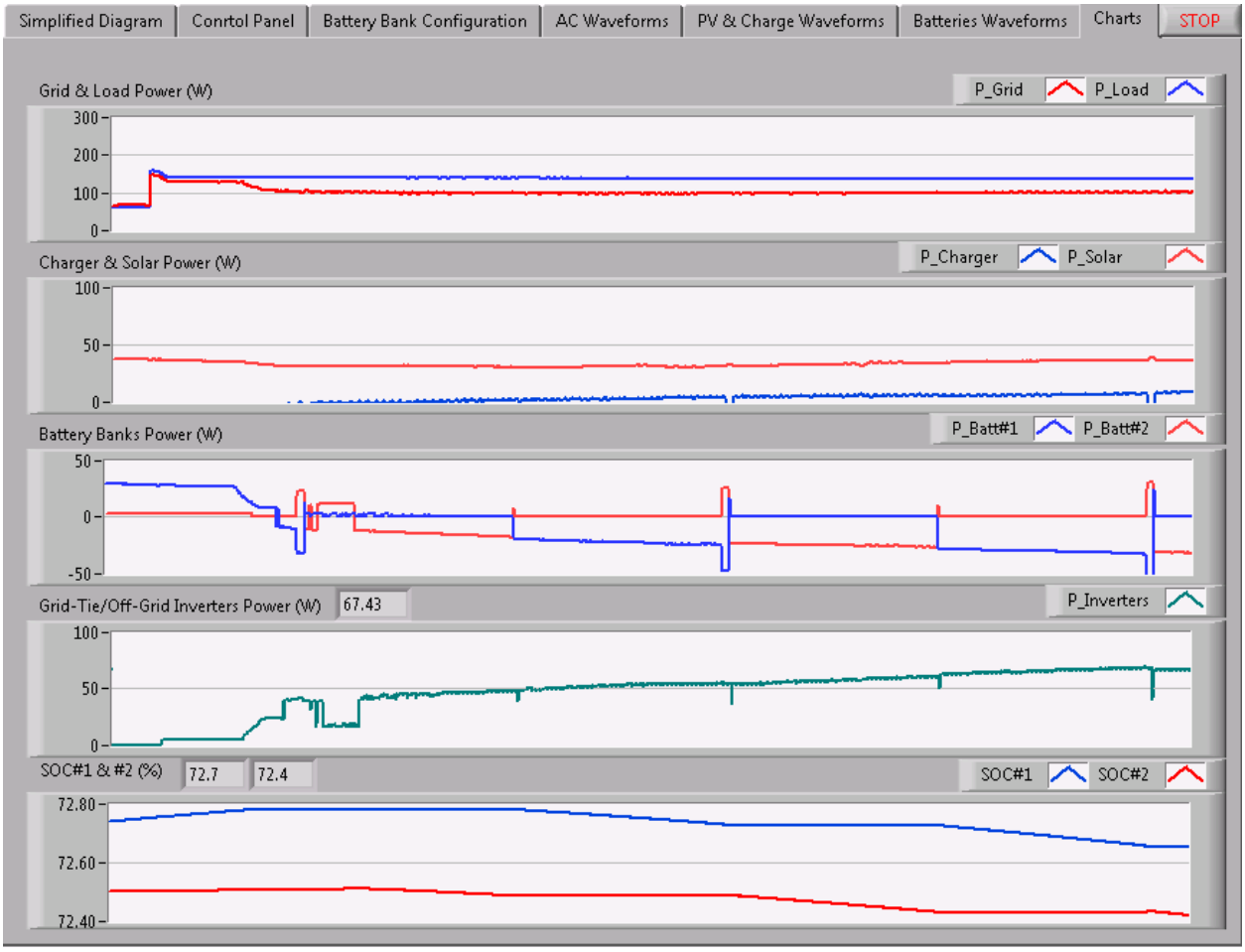

Fig. 5.40: HESS Front Panel Charts during on-peak hours (Mode-2) with solar energy

Mode-3: During off-peak hours when the electricity price is at its lowest rate, the battery charger which is fed from the grid, charges the battery banks alternatively. Fig. 5.41 shows a case in mode-3 when the load power is set to 60watts at the beginning and then the battery charger generates about 90watts. As it can be seen from the battery power charts, the duty cycle for the battery bank #1 is smaller than battery bank#2 to equalize the battery banks during charge cycles automatically. SOC charts show gradual rise in SOC value of both battery banks,

Fig. 5.41: HESS Front Panel Charts during off-peak hours (Mode-3)

Mode-4: During a power outage, due to the off-grid inverter specification, the battery banks are set to Series configuration s to provide 24VDC input voltage. The main load is set to 90Watts. The off-grid inverter generated the load power by discharging the battery banks continuously

which each battery bank provides 45Watts to satisfy the load demand. The SOC charts show continuous discharge on both battery banks.

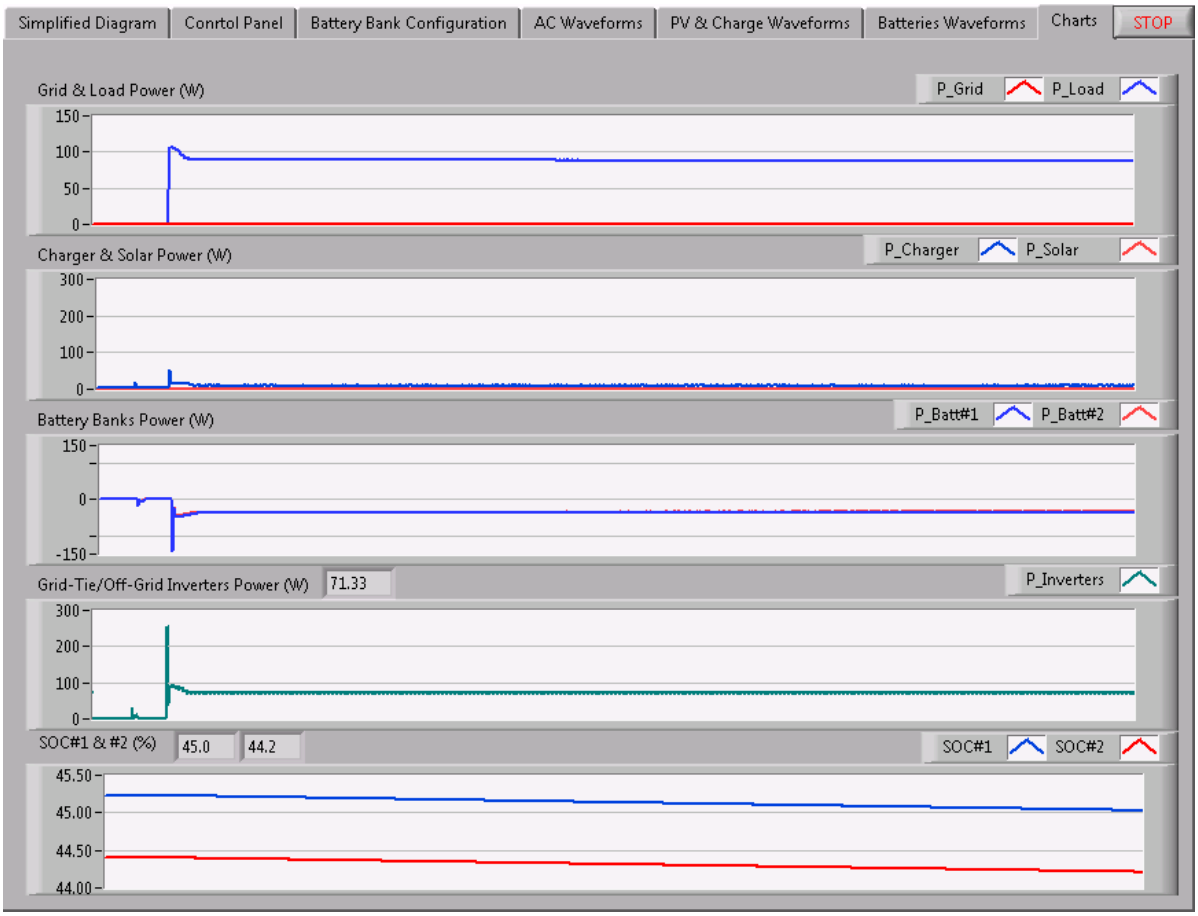

Fig. 5.42: HESS Front Panel Charts during Power outage hours (Mode-4)

The function block window of the HESS is shown in Fig. 5.43 which contains the Battery Management System and Energy Storage System controller.

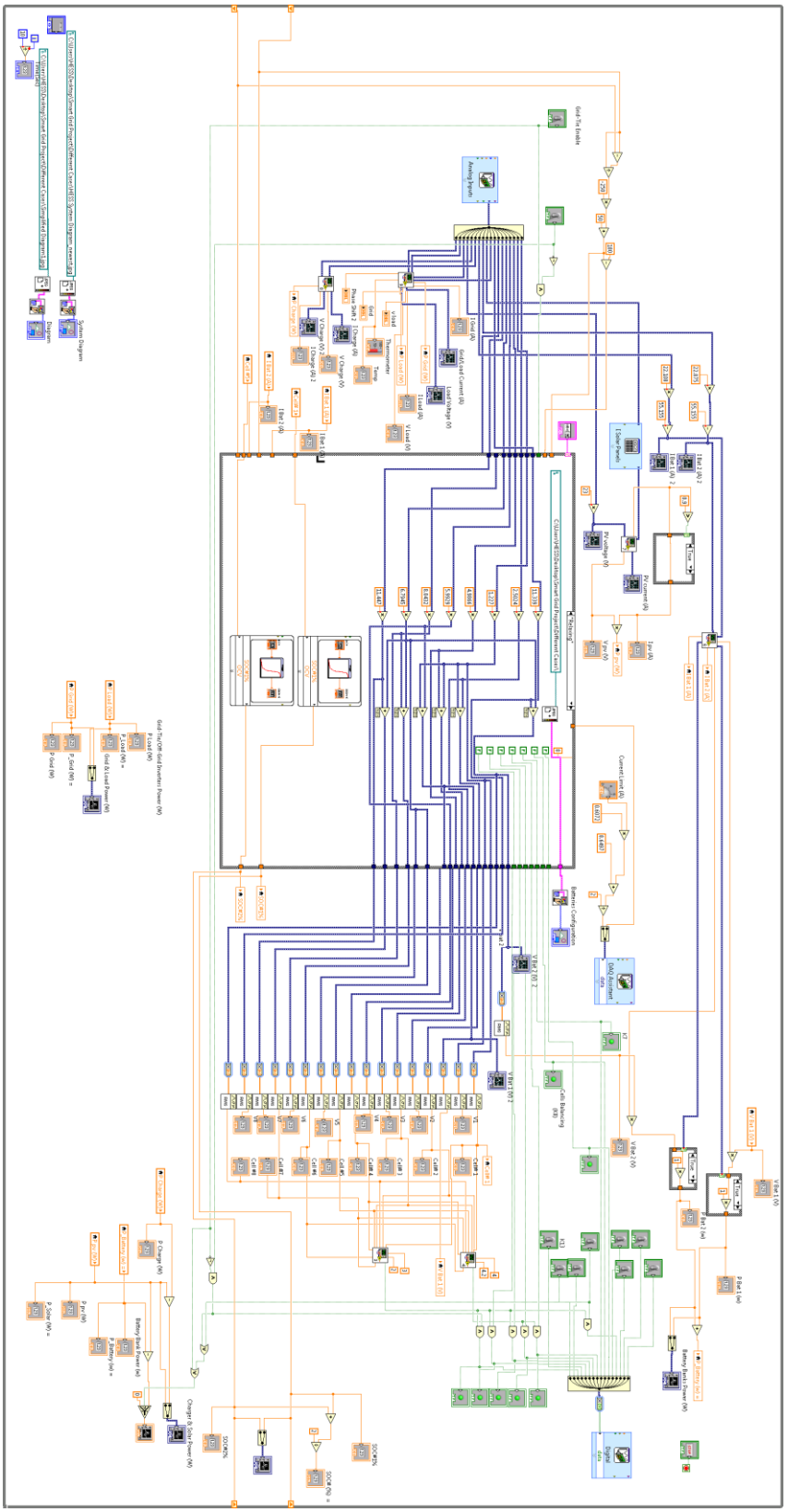

Fig. 5.43: LABVIEW Function Block of HESS

Fig. 5.44 shows the signal acquiring section for all analog signals (voltage) from the measuring board which are converted to digital signal via DAC modules embedded in the National Instrument PCI Card. Fig. 5.45 represents the signal generating module that converts all Boolean signals to TTL signals in order to control the electromechanical relays. Fig. 5.46 shows the module that generates two 0 to 5Vdc signals to control the Battery Charger output voltage and current according to the requirements for each mode of operation.

Fig. 5.47 represents the function that generates the duty cycle values for Charging and Discharging devices based on the present SOC value of the battery banks. When both banks have the same SOC value, the duty cycle will be 50% for both charging and discharging devices. When SOC#1 is greater than SOC#2, battery banks #1, will receive Duty cycle less than 50% to be charged slower than battery banks#2. However, the discharging duty cycle value for battery banks #1 will be higher than 50% to allow faster discharge.

Fig. 5.48 represents the case structure section of the Function Block for the Split bank strategy. Two square wave signal generators are added to control the current flow of the battery banks alternatingly while equalizing the charge and discharge duty cycles based on the SOC values of each battery banks. Fig. 5.49 shows the case structure section of the Function Block during balancing mode where the SOC-OCV curve is used in lookup table functions in order to determine the SOC value of each battery bank.

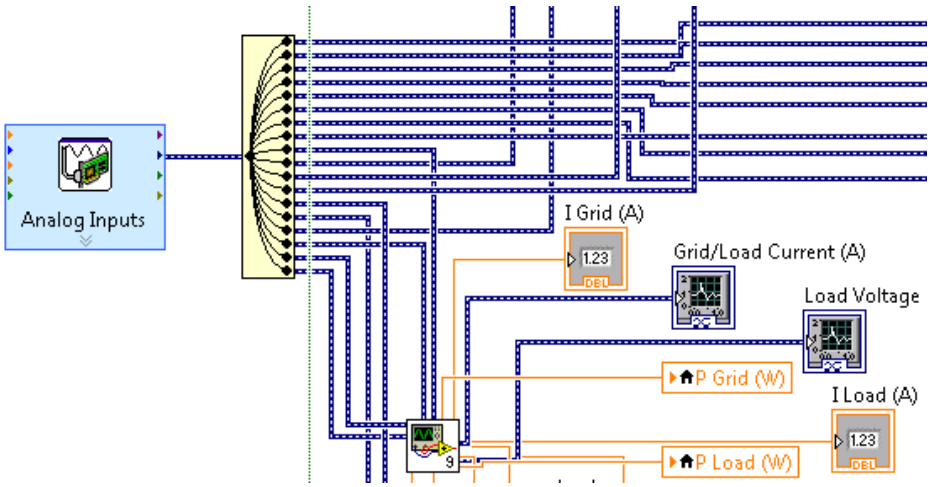

Fig. 5.44: Signal acquiring section of LabVIEW program

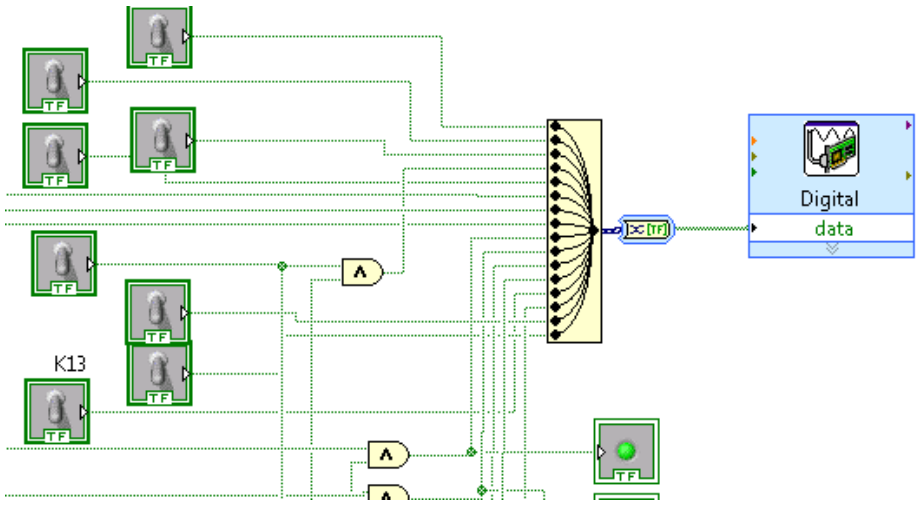

Fig. 5.45: Signal generating section of LabVIEW program

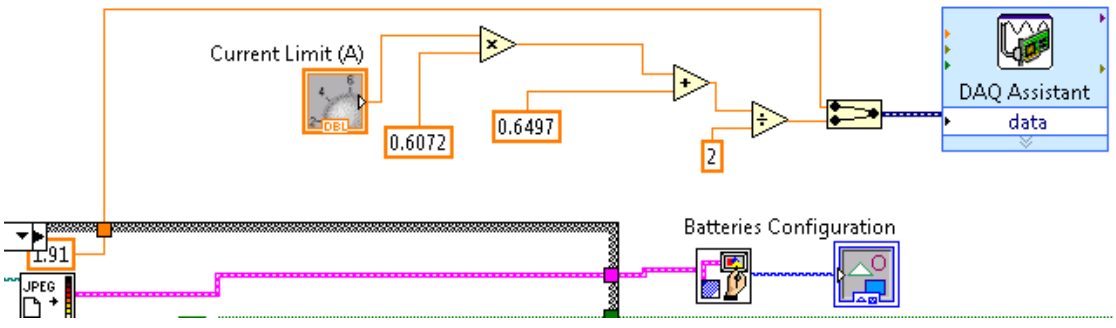

Fig. 5.46: Current limit and Voltage adjustment module for the Battery Charger

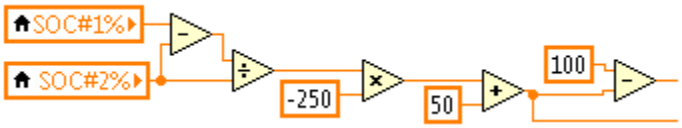

Fig. 5.47: Duty cycles function for battery bank balancing

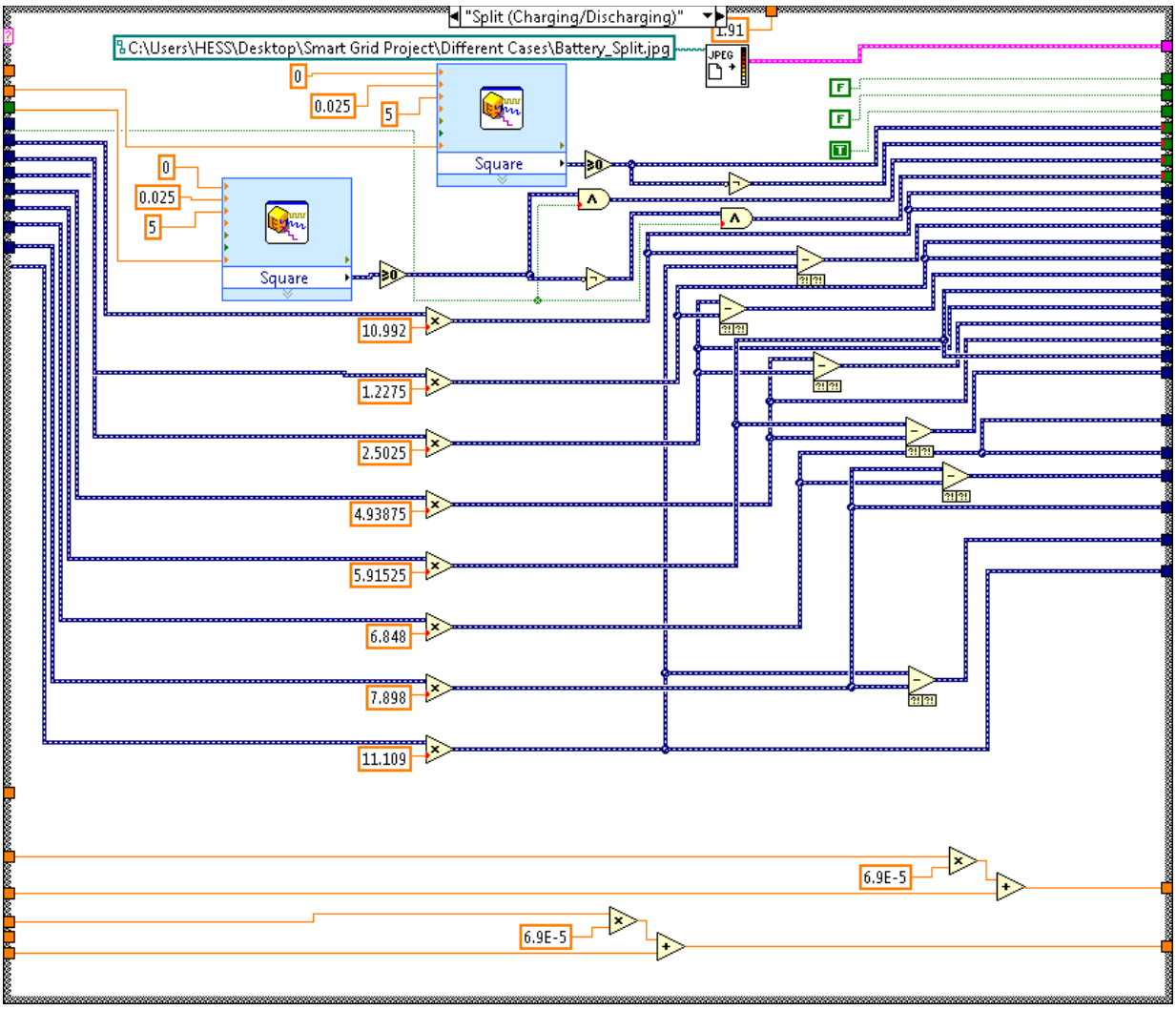

Fig. 5.48: Split bank case structure of the LABVIEW Function Block diagram

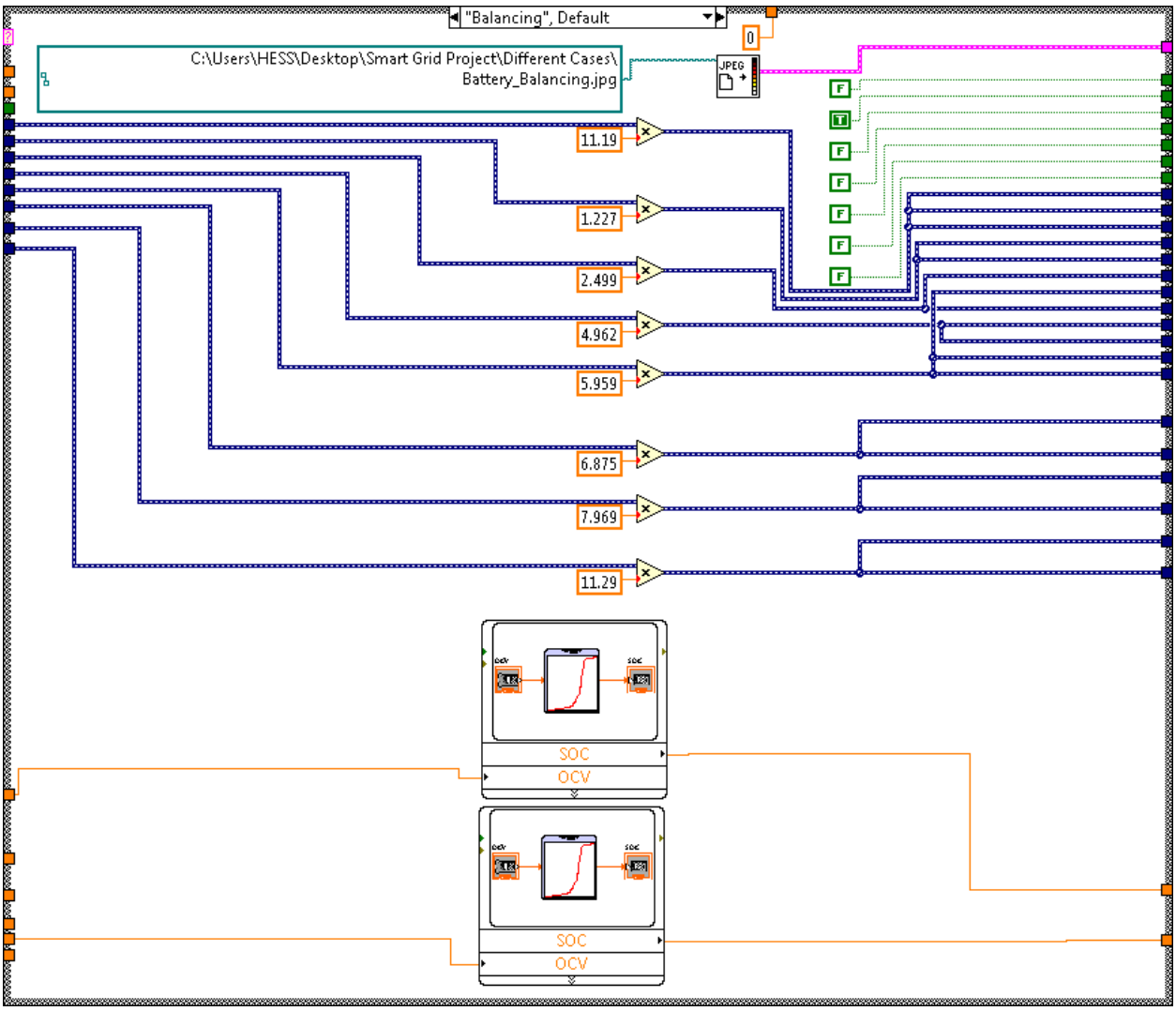

Fig. 5.49: Balancing case structure of the LABVIEW Function Block diagram

Chapter 6 : Experimental Results

6.1 Stress test with extreme over discharging

As it was discussed before, the pulse charging-discharging method increases the longevity of the batteries. In order to verify this claim, the following tests were performed.

First, two identical fresh Lithium-ion battery cells with a 3300mAh capacity were utilized and a capacity test was completed for one of them in order to generate the reference capacity curve as benchmark.

In this test, the battery cell was fully charged and then was disconnected from the charger. A fixed resistive load (20 ohm) was connected to discharge the battery cell at C/20 rate as it shown in fig. 6.1. The terminal voltage versus time was reordered to generate a capacity curve for the fresh battery cell.

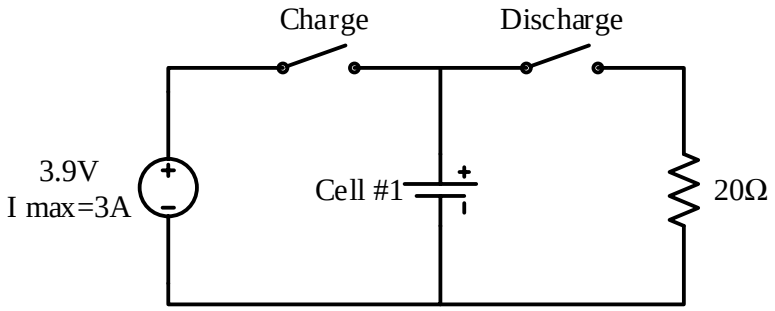

Fig. 6.1: Capacity Test Circuit Diagram

Second, both battery cells were put under a stress test in which both cells were charged fully and then discharged completely for about 225 times. The stress test for both batteries was done under the same ambient temperature and same charge and discharge currents. In order to reduce the stress test duration while making sure that both battery cells were being tested under the same

source and load conditions, fig. 6.2 shows the circuit diagram for the stress test, was designed and implemented.

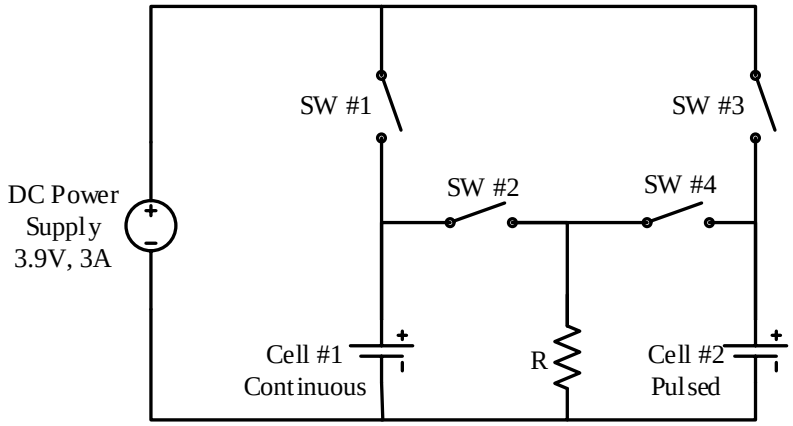

Fig. 6.2: Stress test circuit diagram

The switches were controlled by a data acquisition module accordingly to Table 6.1 sequence order. The first battery cell (Cell#1) was charged using continuous Constant-Current Constant-Voltage (CCCV) method at 1C rate and discharged through a power resistor at about 1.25C rate.

Sequence	SW #1	SW #2	SW #3	SW #4
1	OFF	OFF	OFF	OFF
2	OFF	OFF	OFF	Pulse
3	ON	OFF	OFF	Pulse
4	OFF	Pulse	ON	OFF
5	OFF	Pulse	OFF	OFF
6	OFF	Pulse	OFF	OFF
7	OFF	Pulse	ON	OFF
8	ON	OFF	OFF	Pulse
9	OFF	OFF	OFF	Pulse

Table 6.1: Stress test cycle sequence

Fig 6.3 shows the LabVIEW program block diagram to control the switches (relays).

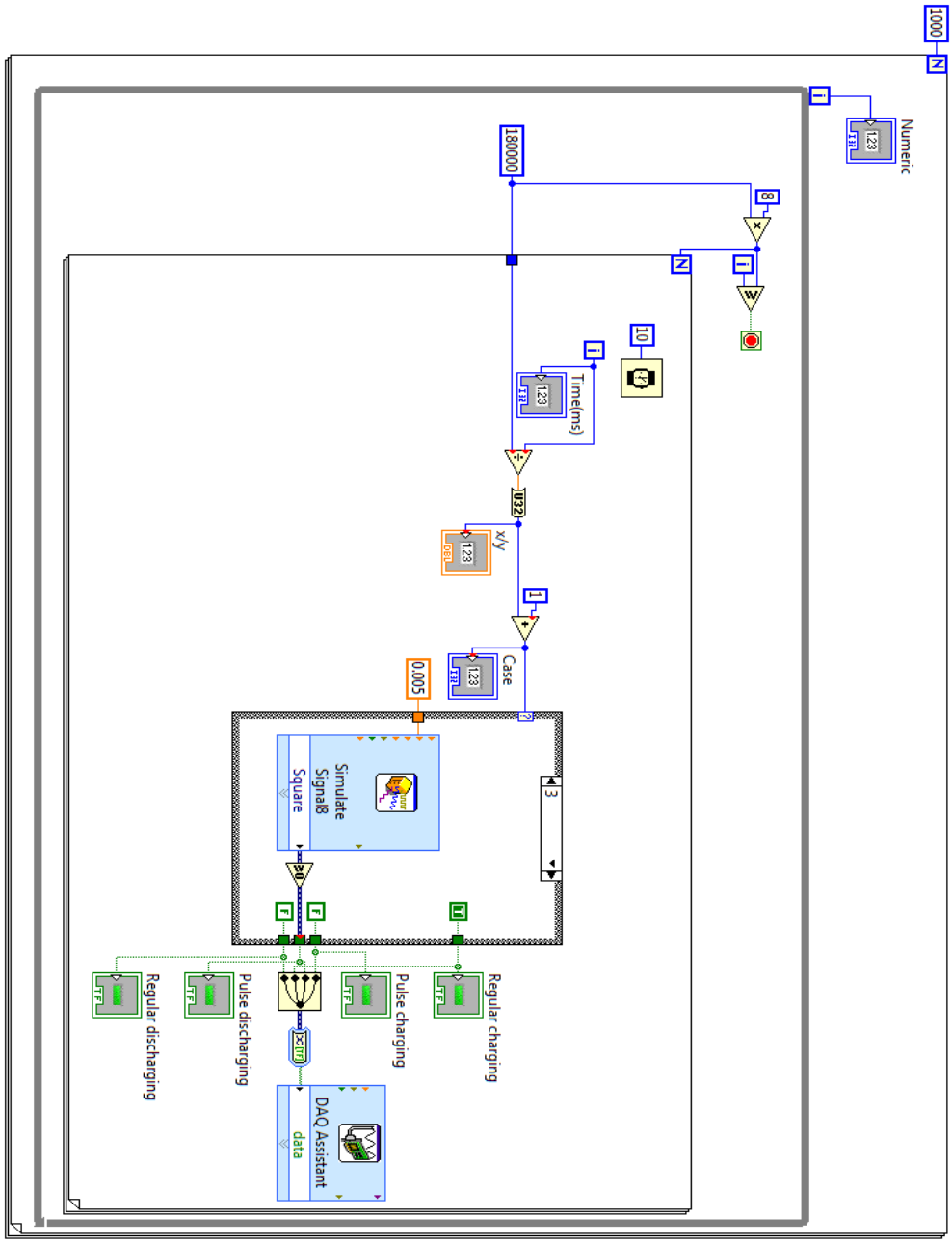

Fig. 6.3: LabVIEW program Block Diagram for the batteries Stress Test

The second battery cell (Cell#2) was charged and discharged under the same charging and discharging C rates as for Cell#1 under the same ambient temperature. But the charging and discharging currents were interrupted every 10 seconds to relax the battery cell for 10 seconds.

Fig. 6.4 shows the stress test cycle for cell#1 in 24 hours that it was charged and extremely over discharged continuously.

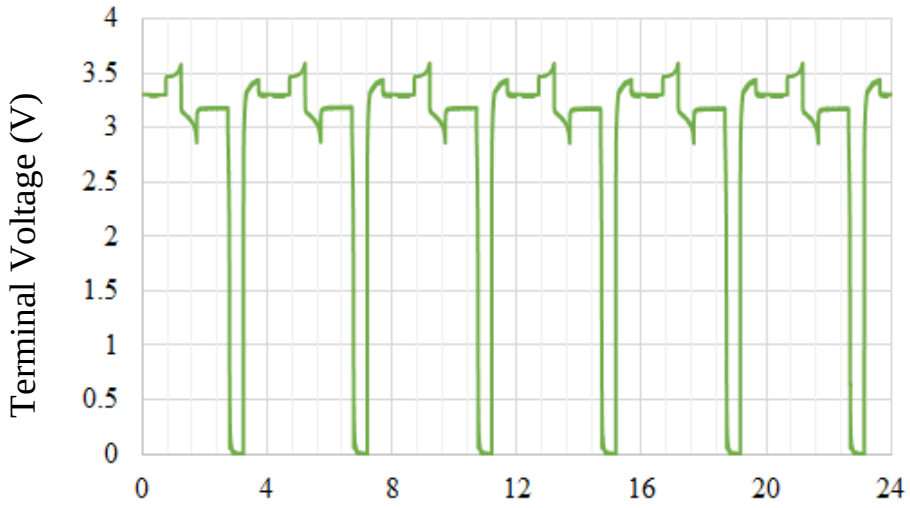

Fig. 6.4: Stress test for Cell#1 (Continuous) in a day

Fig. 6.5 shows the stress test cycle for cell#2 in 24 hours that it was charged and extremely over discharged by adding relaxation time. Fig 6.6 and Fig 6.7 show the Capacity-Fading curves of the battery cells after 200 cycles of the stress test.

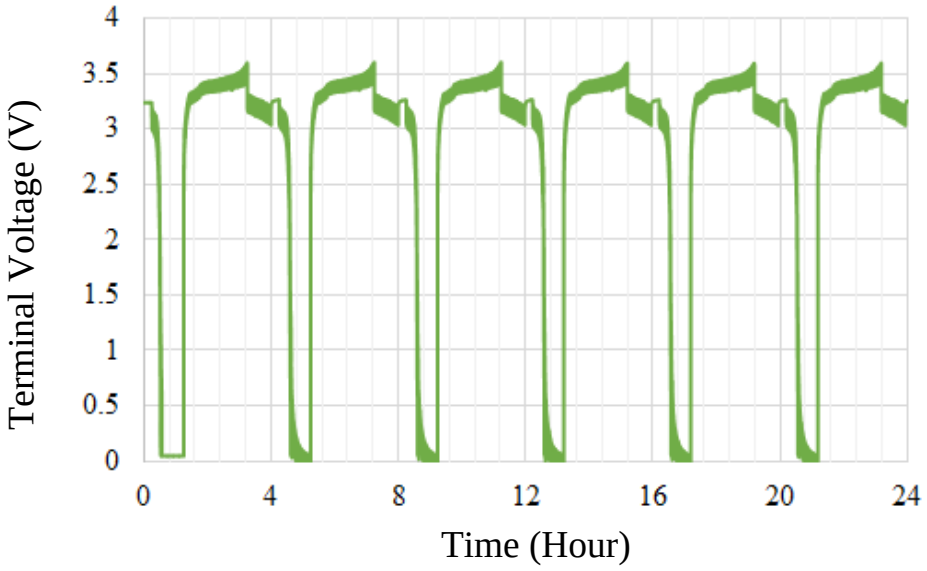

Fig. 6.5: Stress test for Cell#2 (Pulse) in a day

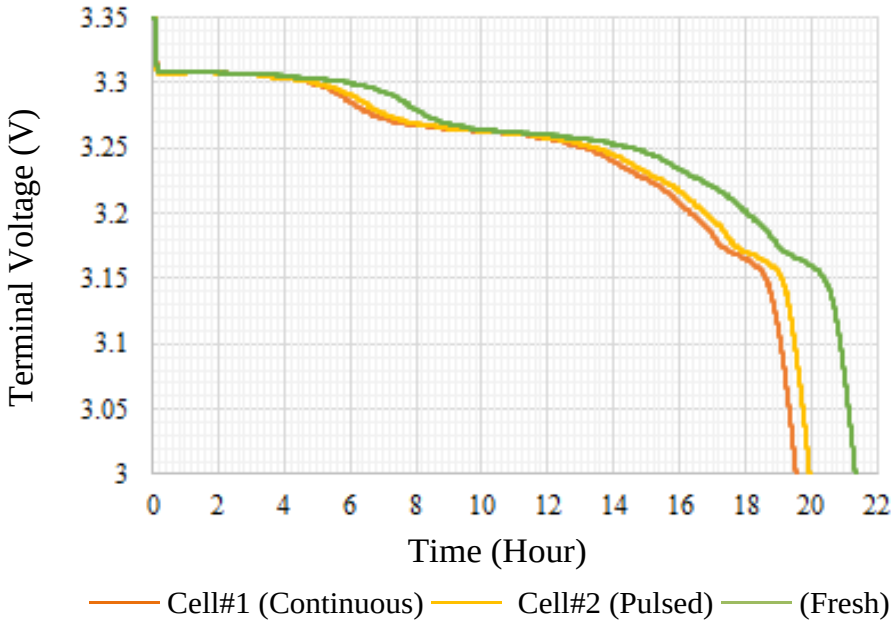

Fig. 6.6: Discharge curves for aged batteries after 200 cycles of stress test versus fresh battery

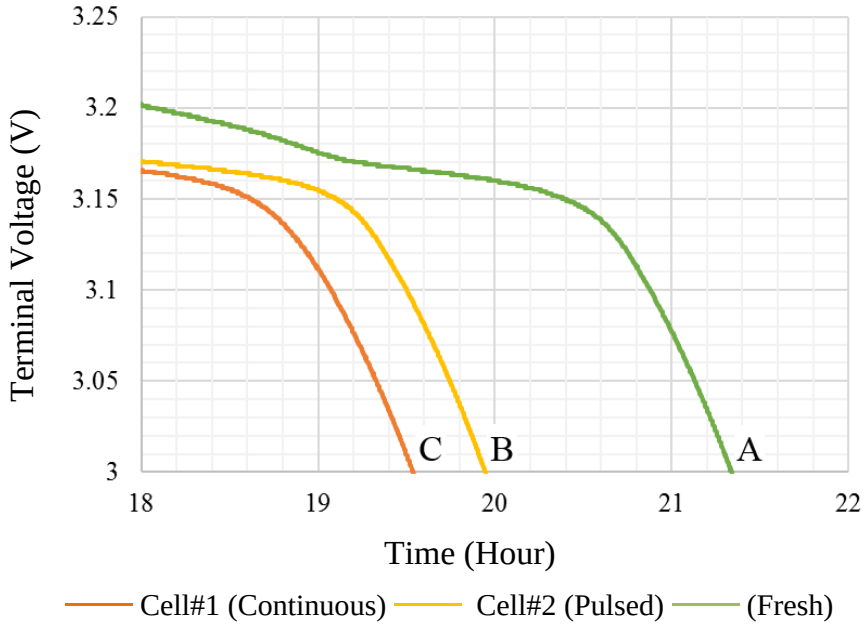

Fig. 6.7: Zoomed discharge curves for aged batteries after 200 cycles of stress test versus fresh battery

In order to determine the amount of capacity loss of each battery, the elapsed time for each battery cell was used when it reached to 3.0Volt [55]. The time value for points A, B and C were used for the Fresh, Cell#2 and Cell#1 batteries, respectively.

To calculate the approximate capacity loss of the aged battery cells, the capacity improvement was calculated using equation-1. Battery capacity improvement percentage is approximately equal to [55]:

$$\approx \frac{(t_B - t_C)}{(t_A - t_C)} \times 100 \qquad (7\text{-}1)$$

Therefore:

$$(20\text{-}19.52) / (21.5\text{-}19.52) \times 100 \approx \mathbf{20\%}$$

In addition, the stress test was continued until both battery cells failed. The battery Cell #1 and Cell#2 failed after 325 and 381 cycles, respectively. This result shows that the lifetime of the battery was extended about 17% by splitting the battery bank.

6.2 Stress Test without Extreme Over-discharging

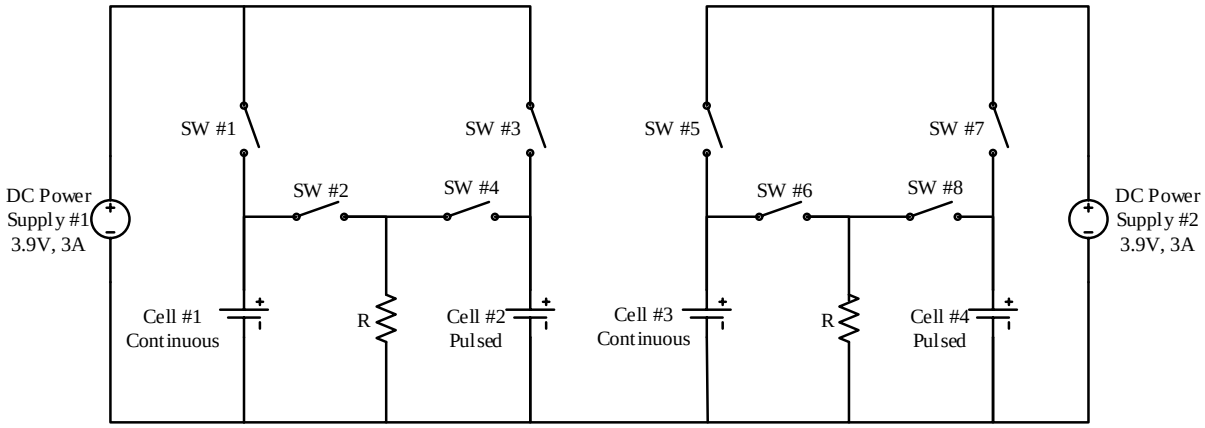

Fig. 6.8: Stress test circuit diagram for two sets

The switches were controlled by a data acquisition module accordingly to Table 6.2 sequence order. The battery cells (Cell#1& #3) were charged using continuous Constant-Current Constant-Voltage (CCCV) method at 1C rate and discharged through a power resistor at about 0.8C rate.

Fig. 6.9 shows the experimental setup, consists of a National Instrument data acquisition USB module, Li-ion cells, relay board and KEYSIGHT Digital Multi-Meter (for capacity-fading measurement).

Table 6.2: Stress test cycle sequence for two sets

Seq.	Duration (Min)	Charge	Discharge	Charge	Discharge	Charge	Discharge	Charge	Discharge
		SW #1	SW #2	SW #3	SW #4	SW #5	SW #6	SW #7	SW #8
1	15	OFF	OFF	OFF	OFF	OFF	OFF	OFF	OFF

2	30	OFF	OFF	OFF	Pulse	OFF	OFF	OFF	Pulse
3	30	OFF	OFF	OFF	Pulse	OFF	OFF	OFF	Pulse
4	30	OFF	OFF	OFF	Pulse	OFF	OFF	OFF	Pulse
5	30	ON	OFF	OFF	Pulse	ON	OFF	OFF	Pulse
6	30	OFF	ON	Pulse	OFF	OFF	ON	Pulse	OFF
7	30	OFF	ON	Pulse	OFF	OFF	ON	Pulse	OFF
8	30	OFF	ON	Pulse	OFF	OFF	ON	Pulse	OFF
9	30	OFF	ON	Pulse	OFF	OFF	ON	Pulse	OFF
10	30	ON	OFF	OFF	Pulse	ON	OFF	OFF	Pulse
11	30	OFF	OFF	OFF	Pulse	OFF	OFF	OFF	Pulse
12	30	OFF	OFF	OFF	Pulse	OFF	OFF	OFF	Pulse

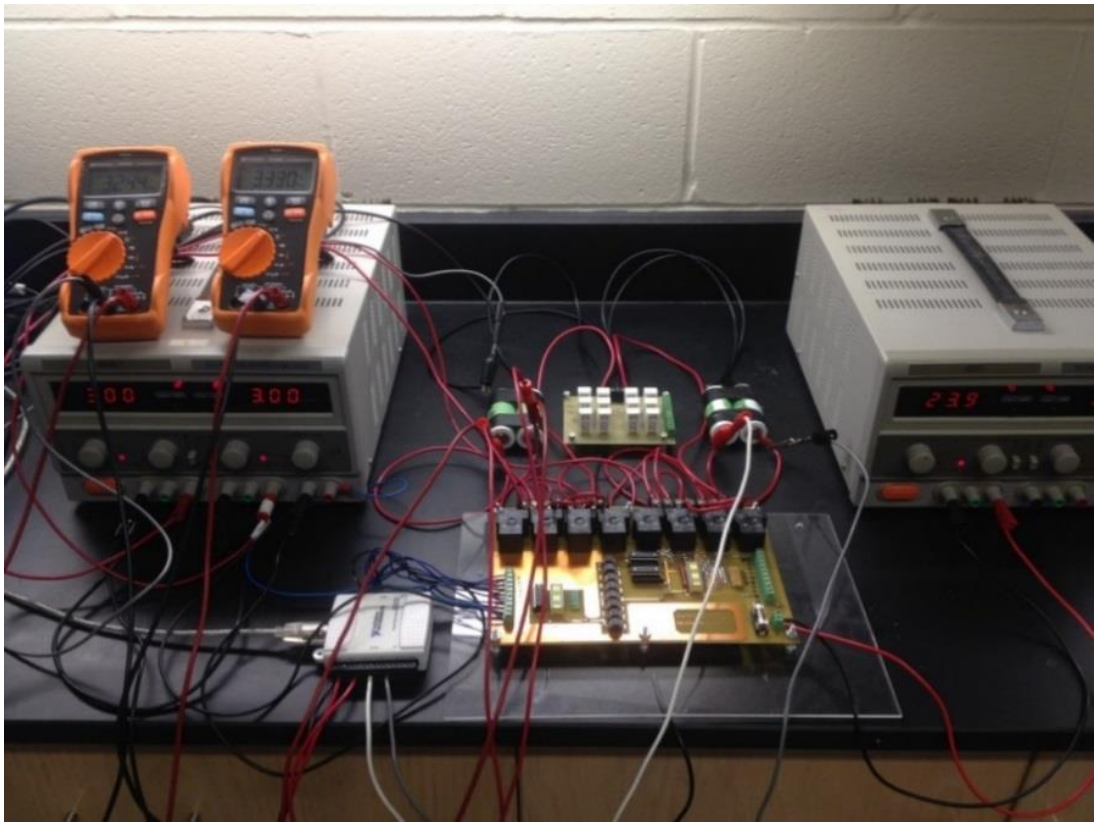

Fig. 6.9: Stress Test experimental setup

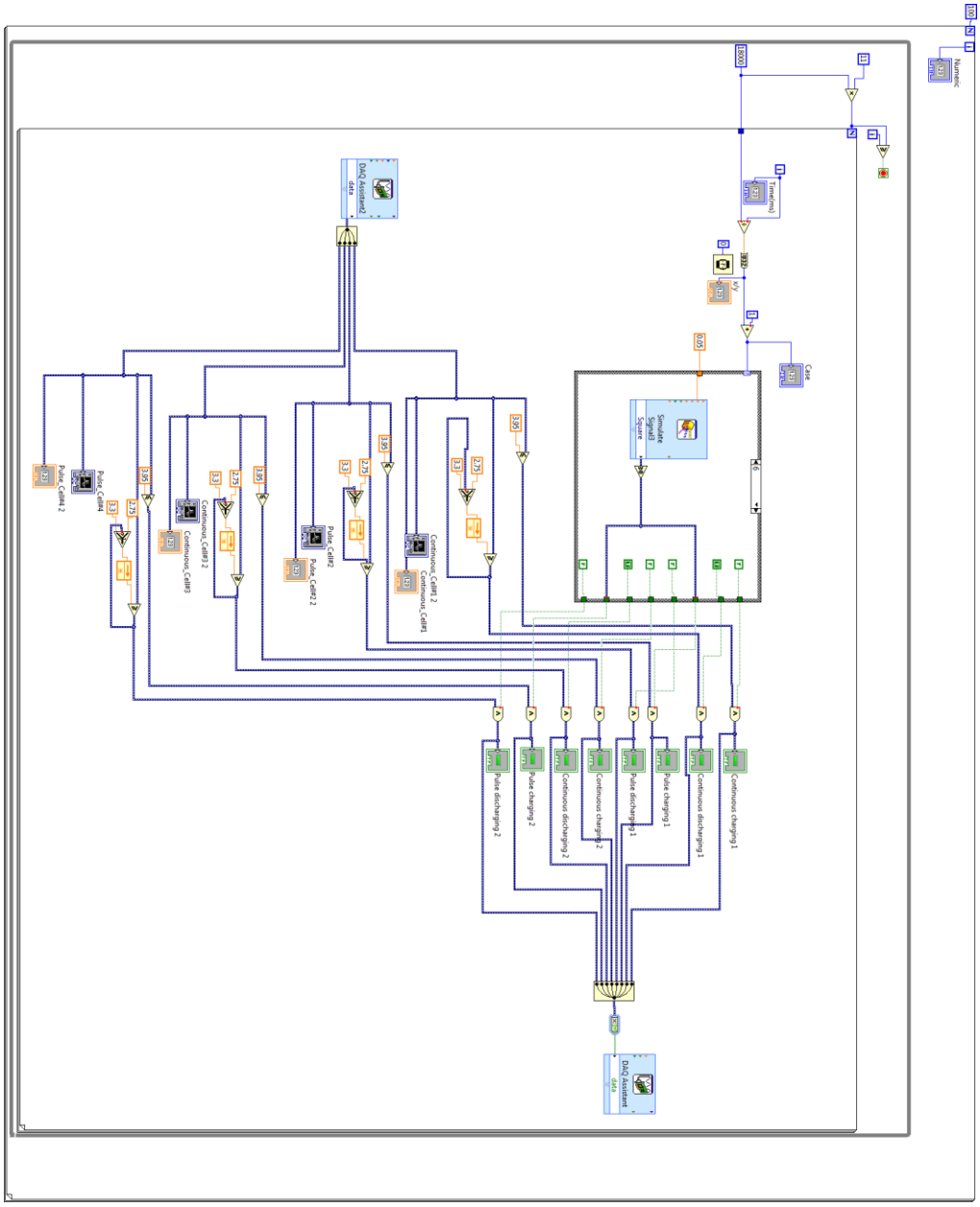

Fig. 6.10: Function Block diagram of the experimental setup

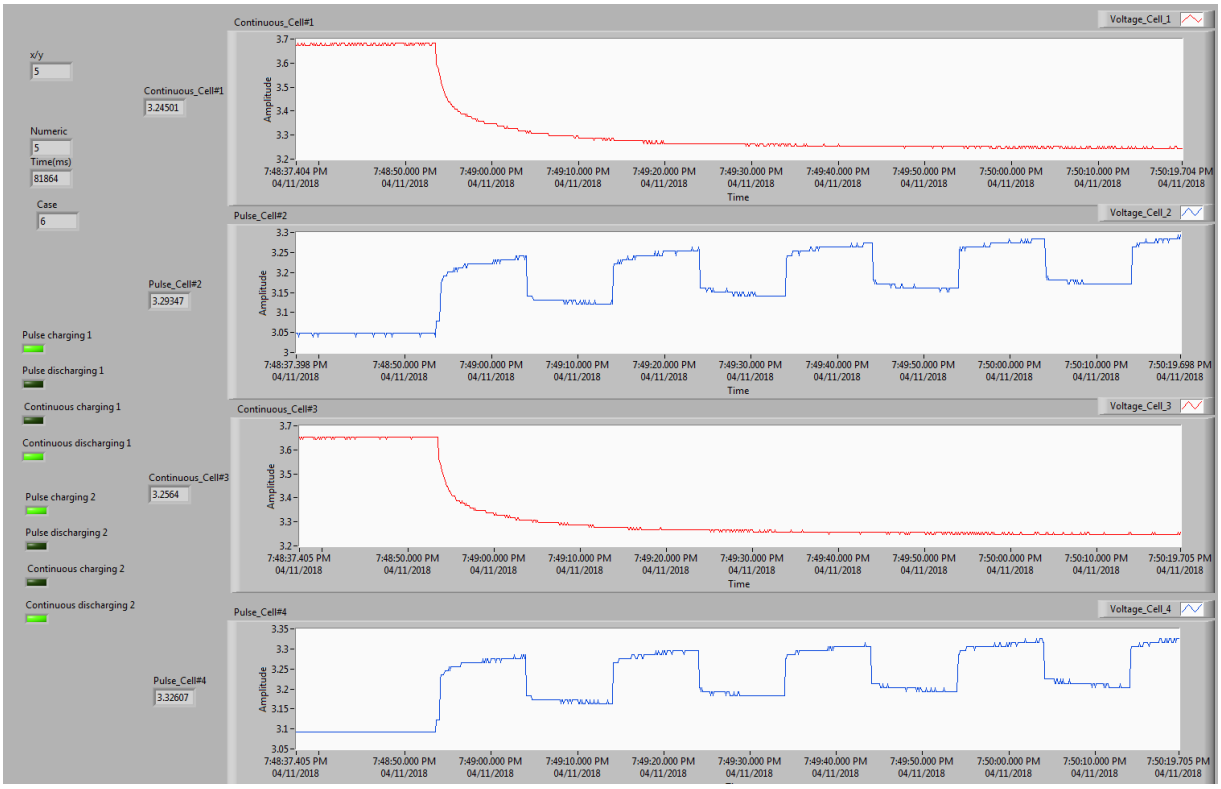

Fig. 6.11: Front Panel diagram of the experimental setup

Fig. 6.10 and Fig. 6.11 show the Function Block and the Front Panel diagrams which were used to run the stress test on the two battery sets.

Fig. 6.12 shows the stress test cycle for cell#1and cell#3 in 24 hours which they were charged and discharged continuously. Fig. 6.13 shows the stress test cycle for cell#2 and cell#4 in 24 hours that they were charged and discharged by adding relaxation time.

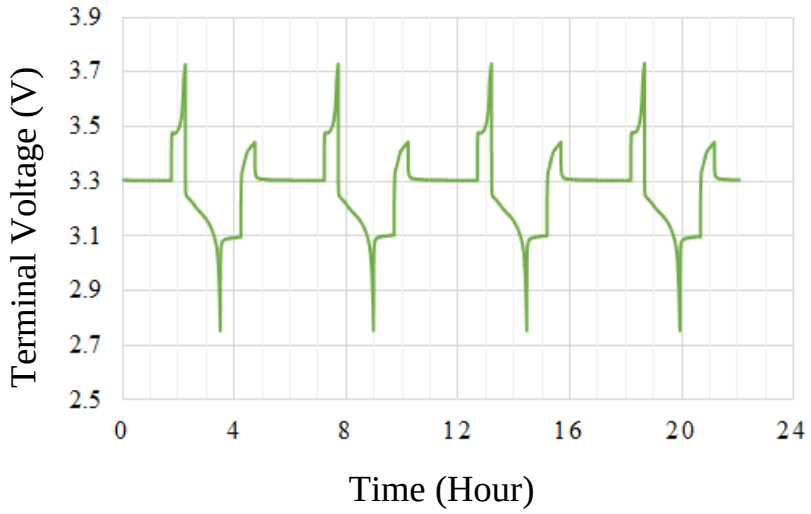

Fig. 6.12: Stress test for Cell#1and Cell#3 (Continuous) in a day

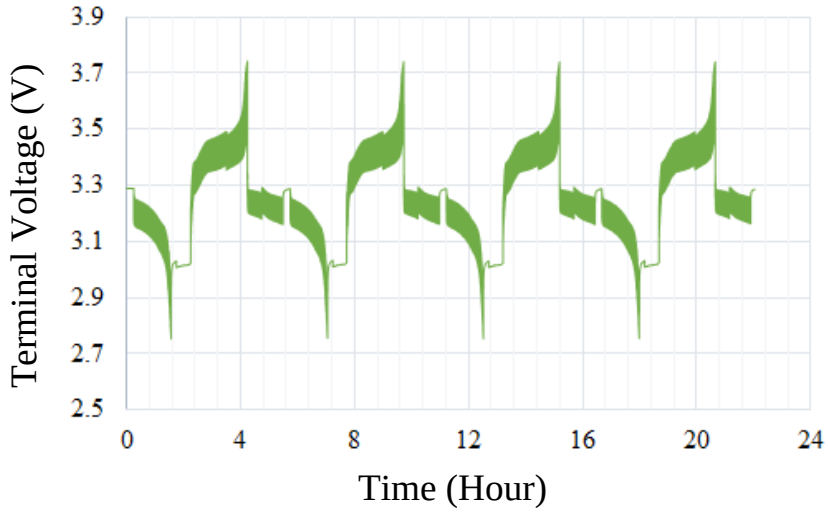

Fig. 6.13: Stress test for Cell#2 and Cell#4 (Pulsed) during a day

Fig. 6.14 and Fig. 6.15 represent the capacity-fading of the battery cells after 400 cycles of the stress test. In order to determine the amount of capacity loss of each battery, the elapsed time for each battery cell was used when the terminal voltage reached to 3.0Volts from fully charged status at about 1/20C discharge rate.

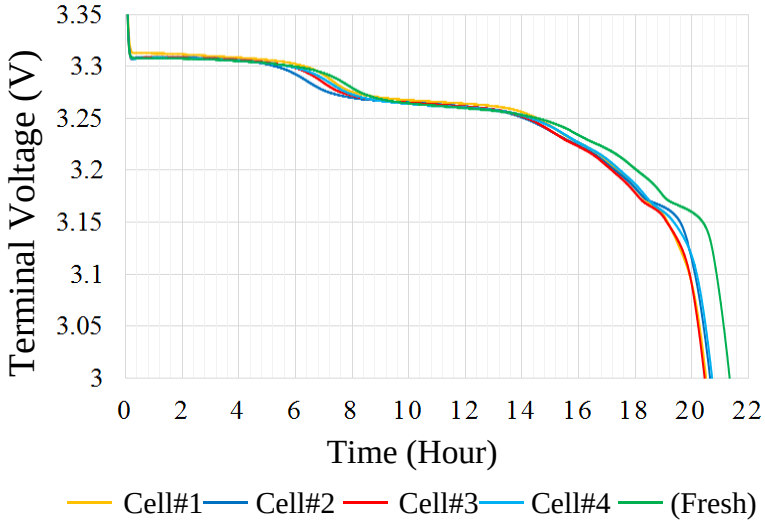

Fig. 6.14: Discharge curves for aged batteries after 400 cycles of stress test versus Fresh battery

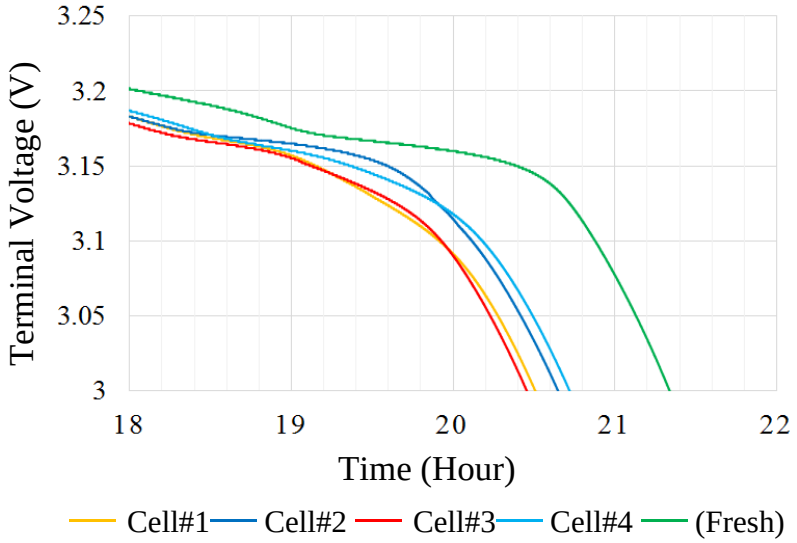

Fig. 6.15: Zoomed discharge curves for aged batteries after 400 cycles of stress test versus Fresh battery

Equation (7-1) was used again to calculate the capacity fading improvement for each battery set. The results show approximately 24% and 30% life time improvement for Cell #2 and Cell #4, respectively.

Chapter 7 : Conclusions and Recommendations

7.1 Research Outcomes

Conventional home energy storage systems can reduce the consumer's total electricity cost by harvesting maximum available free renewable energy sources such as solar or wind energy. In this thesis, a new strategy to improve the lifetime of Li-ion batteries for a renewable home energy storage system was suggested and implemented. The new HESS employed the split banks idea to employ pulsed charge-discharge method. This new HESS not only reduces the electricity cost for the consumers but also, it extends the life time of the Li-ion batteries which are usually the most expensive component of an energy storage system. Then, different modes of operation were introduced. Each mode of operation was discussed in details using MATLAB Simulink program and new HESS.

An experimental stress test set up was implemented to confirm the effectiveness of pulsed charge-discharge method for extending the lifetime of the Li-ion cells. The stress test was a very long process which charged and discharged two sets of Li-ion batteries from zero to about 100% SOC, using Continuous and Pulsed current methods. The same setup used to capture the Discharge curves to calculate capacity fading for each battery cell. The results showed 24% and 30% improvement in extending the lifetime for the two battery cells that after 400 stress test cycles, when Pulsed current method used versus the two cells that Continuous current method was used.

The prototype provides users to operate it as a conventional HESS or new HESS (Pulsed HESS) with a mobile, fully controllable, self-contained experimental platform that supports a spectrum of training and research initiatives.

7.2 Future Research

To improve and optimize the lifetime of the batteries, it is intended to replace the electromechanical relays with electronic switches like isolated gate bipolar transistors (IGBTs). This allows operating the pulsed charge-discharge method at higher frequencies. According to electrochemical impedance spectroscopy (EIS) test, the optimal frequency will cause minimum impedance value of the battery at each SOC value. So that, it is spectated to extend the batteries life time to the maximum possible time.

The operation of the HESS also can be optimized by selecting the appropriate size or capacity of the solar panels, battery banks, battery chargers and inverters to operate the system efficiently. Wind energy can also be added as an option for the consumers in rural areas.

Generally, increasing the size of the equipment can be considered to increase the capacity of the whole system. However, a compromise between the implementation cost for adding more hardware and reducing the total electricity cost has to be considered based on the demand from the loads.

Finally, the energy conversion devices can be customized such as using a bidirectional inverter to reduce the total cost and improve the efficiency of the whole system. Also, high voltage battery banks can be used to eliminate the boost converter in the inverter modules.

7.3 Publications

- Alimardani, M.; Narimani, M.; Al-Mutawaly, N., “A new approach to improve Lithium-ion battery lifetime in home energy storage system with photovoltaic modules”, Electrical and Computer Engineering Canadian Conference, in May 2018.

- Kordic M.; Narimani, M.; Alimardani, M., “A New Hybrid Multilevel Nested Neutral Point Clamped (NNPC) Converter”, Electrical and Computer Engineering Canadian Conference, in May 2018.

- Alimardani, M.; Narimani, “Pulsed Energy Storage System”, Provincial Patent Application number: 62735984, September 25. 2018.

References

[1] D.E. Olivares, A. Mehrizi-Sani, A.H. Etemadi, C.A. Cañizares, R. Iravani, M. Kazerani, A.H. Hajimiragha, O. Gomis-Bellmunt, M. Saeedifard, R. Palma-Behnke, G.A. Jiménez-Estévez, N.D. Hatziargyriou. (2014, July). "Trends in Microgrid Control," IEEE Tran.

[2] R. L. Fares, M. E. Webber. (2017, Jan.). "The impacts of storing solar energy in the home to reduce reliance on the utility," Nature Energy. Vol. 2, no. 17001..

[3] D. Keles, T. Telsnig, B. Fleischer, M. Baumann, D. Fraboulet, A. Faure, W. Fichtner. (2015, Jun). "Self-consumption of electricity from renewable sources," INSIGHT_E. [Online]. Available: http://www.insightenergy.org/system/publications/files/000/000/016/.

[4] S.V. Kuchak, A.N. Voroshilov, E.A. Chudinov. (2017). "Discharge Characteristics of Lithium-Ion Accumulators under Different Currents," IEEE 18th International Conference on Micro/Nanotechnologies and Electron Devices (EDM).

[5] L. Wu, W. Kihinet, E. Robelo, E. Bezabith, K. Longwood, M. Saeedifard, T. Tshimanga, F. Lambert, R. Harley. (2016, Sep). "Development of a solar-power-based nanogrid system for village hut in Haiti mountain area," IEEE 2016 North American Power Symposium.

[6] X. Wu, X. Hu, X.Yin, S.J. Moura. (2018, May). "Stochastic Optimal Energy Management of Smart Home With PEV Energy Storage," IEEE Transactions on Smart Grid. vol. 9, no. 3. pp.2065-2075..

[7] Hydro One. (2018, May). "Electricity Pricing and Costs'" Hydro One. [Online]. Available: https://www.hydroone.com/rates-and-billing/rates-and-charges/electricity-pricing-and-costs..

[8] A. Safdarian, M. Fotuhi-Firuzabad, M. Lehtonen, F. Aminifar. (2015, Nov). "Optimal Electricity Procurement in Smart Grids With Autonomous Distributed Energy Resources," IEEE Transactions on Smart Grid. vol. 6, no. 6. pp.2975-2984..

[9] A. Mateo, J.A. Villarejo, J. Jimenez, E. de Jodar.(2013). "Zero energy grid injection strategies using comercial inverters in solar energy power generation systems," IEEE International Conference on New Concepts in Smart Cities: Fostering Public and Priva.

[10] T. Jiang, Y. Cao, L. Yu, Z. Wang. (2014, Nov). "Load Shaping Strategy Based on Energy Storage and Dynamic Pricing in Smart Grid," IEEE Transactions on Smart Grid. vol. 5, no. 6. pp.1607-1618..

[11] I. Poole. (2018). "Lithium Ion Battery Advantages & Disadvantages," Radio-Electronics. [Online]. Available: https://batteryuniversity.com/learn/article/charging_lithium_ion_batteries.

[12] V. Karthigeyan, M. Aswin, L. Ptiyanjka, K.N. Dileep Sailesh, K. Palanisamy. (2017). “A comparative study of lithium ion (LFP) to lead acid (VRLA) battery for use in telecom power system,” IEEE 2017 International Conference (ICCPEIC). pp. 742-748.

[13] Battery University. (2018). " BU-409: Charging Lithium-ion,” [Online]. Battery University Available: https://batteryuniversity.com/learn/article/how_to_prolong_lithium_based_batteries.

[14] Toronto Hydro. (2018, May). “Billing’”. [Online]. Available: http://www.torontohydro.com/sites/electricsystem/residential/yourbilloverview/Pages/default.aspx.

[15] H. Hvidtfeldt Larsen, L. Sønderberg Petersen. (2013), “ENERGY STORAGE OPTIONS FOR FUTURE SUSTAINABLE ENERGY SYSTEMS,” DTU National Laboratory for Sustainable Energy. [Online]. Available: http://orbit.dtu.dk/files/60269108/DTU_International_Energy_Report_.

[16] Battery University. (2018). " BU-204: How do Lithium Batteries Work?” [Online]. Battery University Available: https://batteryuniversity.com/learn/article/lithium_based_batteries.

[17] N.Omar , M. Daowd , P. Van Den Bossche , O. Hegazy , J. Smekens , T. Coosemans., J. Van Mierlo, (2012, Aug). “Rechargeable Energy Storage Systems for Plug-in Hybrid Electric Vehicles—Assessment of Electrical Characteristics,” Energies. no. 5. pp.2952.

[18] Battery University. (2018). " BU-105: Battery Definitions and what they mean ,” [Online]. Battery University Available: https://batteryuniversity.com/learn/article/battery_definitions.

[19] MIT Electric Vehicle Team, (2008, Dec). "A Guide to Understanding Battery Specifications,” MIT University. [Online]. Available: http://web.mit.edu/evt/summary_battery_specifications.pdf.

[20] Battery University. (2018). " BU-402: What Is C-rate?,” [Online]. Battery University Available: https://batteryuniversity.com/learn/article/what_is_the_c_rate..

[21] I. Baccouche, S. Jemmali , A. Mlayah , B. A. Manai, N. E.B. Amara, (2018). “Implementation of an Improved Coulomb-Counting Algorithm Based on a Piecewise SOC-OCV Relationship for SOC Estimation of Li-Ion Battery,” International Journal of Renewable Ener.

[22] G.L. Plett, (2004, Jun). “Extended Kalman filtering for battery management systems of LiPB-based HEV battery packs Part 1. Background,” ELSEVIER. Journal of Power Source. no. 134 pp. 252-261..

[23] K. S. Ng, C.-S. Moo, Y. P. Chen, and Y.-C. Hsieh, “Enhanced coulomb counting method for estimating state-of-charge and state-of-health of lithium-ion batteries,” Applied energy, vol. 86, no. 9, pp. 1506–1511, 2009..

[24] PowerTech Systems. (2018). " Lithium Iron Phosphate (LiFePo4),” [Online]. PowerTech Systems. Available: https://www.powertechsystems.eu/home/tech-corner/lithium-iron-phosphate-lifepo4/.

[25] R. Xiong, J. Cao, Q. Yu, H. He, F. Sun, (2017, Jun). “Critical Review on the Battery State of Charge Estimation Methods for Electric Vehicles,” IEEE Access. Available: https://ieeexplore.ieee.org/stamp/stamp.jsp?arnumber=8168251.

[26] B. Xia, H. Wang, Y. Tian , M. Wang, W. Sun ,Z. Xu, (2015, Jun). “State of Charge Estimation of Lithium-Ion Batteries Using an Adaptive Cubature Kalman Filter,” Energy. pp. 5916-5936..

[27] T. Amietszajew, E. McTurk, J. Feleming, R. Bhagat. (2018, Feb). “Understanding the limits of rapid charging using instrumented commercial 18650 high-energy Li-ion cells,” ELSEVIER. Electrochimica Acta. Vol. 263, pp. 346-352..

[28] Battery University. (2018). " Fast and Ultra-fast Chargers,” [Online]. Battery University Available: https://batteryuniversity.com/learn/article/ultra_fast_chargers..

[29] Richtek (2018). " Understanding the characteristics of Li-ion batteries and Richtek power management solutions,” [Online]. Richtek. Available: https://batteryuniversity.com/learn/article/ultra_fast_chargers..

[30] Richtek (2018). " Li-ion Battery and Gauge Introduction,” [Online]. Richtek. Available: https://www.richtek.com/Design%20Support/Technical%20Document/AN024..

[31] Electropedia. (2018). " Lithium Battery Failures,” [Online]. Electropedia. Available: https://www.mpoweruk.com/lithium_failures.htm ..

[32] J. Li, E. Murphy, J. Winnick, P. A. Kohl. (2001, Dec) , "The effects of pulse charging on cycling characteristics of commercial lithium-ion batteries" ELSEVISER , Journal of Power Sources. vol. 102, no.2, pp. 302-309..

[33] J. M. Amanor-Boadu 1, A. Guiseppi-Elie, E. Sánchez-Sinencio. (2018, Aug). “The Impact of Pulse Charging Parameters on the Life Cycle of Lithium-Ion Polymer Batteries,” Energy..

[34] L. R. Chen. (2009, Feb). "Design of duty-varied voltage pulse charger for improving Li-Ion battery-charging response," IEEE Transactions on Industrial Electronics. vol. 56, no. 2. pp.480-487..

[35] X. Xu, C.Y. Qi, Z.D. Hao, H. Wang, J.T. Jiu, J.B. Liu, H. Yan, K. Suganuma, (2017, Aug), "The Surface Coating of Commercial LiFePO4 by Utilizing ZIF-8 for High Electrochemical Performance Lithium Ion Battery, " Springerlink.com..

[36] J.W. Kimball , B.T. Kuhn, P.T. Krein. (2008, June). "Increased Performance of Battery Packs by Active Equalization," IEEE Vehicle Power and Propulsion Conference. pp. 1938-8756..

[37] Alternative and Renewable Energy Tutorials. (2018). " Solar Cell I-V Characteristic," [Online]. Alternative and Renewable Energy Tutorials. Available: http://www.alternative-energy-tutorials.com/energy-articles/solar-cell-i-v-characteristic.html..

[38] Computer Controls. (2018). " IV and CV Characterizations of Solar/ Photovoltaic Cells Using the B1500A," [Online]. Computer Controls. Available: https://www.ccontrols.ch/cms/upload/applikationen/Solar-Cell/5990-4428EN.pdf, Application Note B1500A-14..

[39] Microchip Technology Inc. (2013). " Practical Guide to Implementing Solar Panel MPPT Algorithms," [Online]. Microchip Technology Inc. Available: http://ww1.microchip.com/downloads/en/appnotes/00001521a.pdf, DS00001521A..

[40] R. Faranda, S. Leva, V. Maugeri. (2008, Aug) "MPPT techniques for PV Systems: Energetic and cost comparison," IEEE Power and Energy Society General Meeting..

[41] M. A. Elgendy, B. Zahawi, and D. J. Atkinson. (2014, Jun). "Evaluation of incremental conductance MPPT algorithm at low perturbation rates," IEEE IET International Conference on Power Electronics, Machines and Drives..

[42] M. Lal Azad , S. Das, P.K. Sadhu, B. Satpati, A. Gupta, P. Arvind. (2107, Oct). "P&O algorithm based MPPT technique for solar PV System under different weather conditions," IEEE International Conference on Circuit ,Power and Computing Technologies..

[43] S. C. K. C. C. Yen, "Residential photovoltaic energy storage system," *IEEE Transactions on Industrial Electronics,* vol. 45, no. 3, pp. 385-394, 1998.

[44] M. C. d. Piazza, M. Luna, M. Pucci, G. L. Tona and A. Accetta, "Electrical Storage Integration into a DC Nanogrid Testbed for Smart Home Applications," in *2018 IEEE International Conference on Environment and Electrical Engineering and 2018 IEEE Industrial and Commercial Power Systems Europe (EEEIC / I&CPS Europe)*, Palermo, Italy, 2018.

[45] R. K. Lam, D. H. Tran and H.-G. Yeh, "Economics of residential energy arbitrage in california using a PV system with directly connected energy storage," in *2015 IEEE Green Energy and Systems Conference (IGESC)*, Long Beach, CA, USA, 2015.

[46] F. Peacock, "Is my grid connect solar system 100% compatible with a Tesla Powerwall 2 battery?," Tesla, [Online]. Available: https://support.solarquotes.com.au/hc/en-us/articles/115001986773-Is-my-grid-connect-solar-system-100-compatible-with-a-Tesla-Powerwall-2-battery-.

[47] A.T. Elsayed, C.R. Lashway, O.A. Mohammed. (2016, Mar). "Advanced Battery Management and Diagnostic System for Smart Grid Infrastructure," IEEE Transactions on Smart Grid. vol. 7, no. 2, pp, 897-905..

[48] D. Tran, A. M. Khambadkone. (2013, Sep). "Energy Management for Lifetime Extension of Energy Storage System in Micro-Grid Applications," IEEE Transactions on Smart Grid. vol. 4, no. 3. pp.1289-1296..

[49] Battery Space. (2018). " SPECIFICATION OF LFP-G40 / LFP-G4S40AH," [Online]. Battery Space. Available: https://www.batteryspace.com/prod-specs/6333-40Ah.pdf..

[50] Renogy. (2018). " Maximum Power Point Tracking Solar Charge Controller," [Online]. Renogy. Available: https://www.renogy.com/template/files/Manuals/20A-30A-40A-MPPT-Solar-Charge-Controller-Manual.pdf..

[51] B&K Precision. (2018). " 300W-360W Switching Bench DC Power Supplies," [Online]. B&K Precision. Available: http://www.bkprecision.com/products/power-supplies/1687B-1-36v-0-10a-dc-power-supply.html..

[52] Populace. (2018). " 300w grid tie micro inverter intelligent solar power inverter 300 watt," [Online]. Available: https://www.alibaba.com/product-detail/300w-grid-tie-micro-inverter-intelligent_60522689039.html?spm=a2700.7724857.normalList.13.7f249bb7zxq.

[53] COTEK. (2018). " 1KW Pure Sine Wave Power Inverter," [Online]. COTEK. Available: http://www.pmepower.com/wp-content/uploads/2015/11/COTEK-SR-1000-manual.pdf..

[54] A. E. Mejdoubi, A. Oukaour, H. Chaoui. (2016, Apr). "State-of-Charge and State-of-Health Lithium-Ion Batteries' Diagnosis According to Surface Temperature Variation," IEEE Transactions on Industrial Electronics. vol. 63, no. 4, pp. 2391-2402..

[55] N. Kakimoto, K. Goto. (2016, Jan). "Capacity-Fading Model of Lithium-Ion Battery Applicable to Multicell Storage Systems," IEEE Transactions on Sustainable Energy. vol. 7, no.1, pp. 108-117..

[56] Y.Wang, X. Lin, M. Pedram. (2014, Mar). "Adaptive Control for Energy Storage Systems in Households With Photovoltaic Modules," IEEE Transactions on Smart Grid. vol. 5, no. 2. pp.992-1001.

[57] PowerTech Systems. (2018). " 12v Lithium-Ion battery pack," [Online]. PowerTech Systems. https://www.powertechsystems.eu/wp-content/uploads/specs/PowerBrick_PRO+_12V_55Ah_Lithium-Ion_battery.pdf.

[58] Populace. (2018). " 300w grid tie micro inverter intelligent solar power inverter 300 watt," [Online]. Available: https://www.alibaba.com/product-detail/300w-grid-tie-micro-inverter-intelligent_60522689039.html?spm=a2700.7724857.normalList.13.7f249bb7zxq.

[59] M. Sechilariu, B. Wang, F. Locment. (2018, May). "Building Integrated Photovoltaic System With Energy Storage and Smart Grid Communication," IEEE Transactions on Industrial Electronics. vol. 60, no. 4. pp.1607-1618..

[60] M. Murnane, A. Ghazel (2018). "A Closer Look at State of Charge and State of Health (SOH) Estimation Techniques for Batteries," Analog Devices. [Online]. Available:https://www.analog.com/media/en/technical-documentation/technical-articles/A-Closer-Look-at.

[61] J.Zhang, J. Lee. (2011, Aug), "A review on prognostics and Health monitoring of Li-ion battery," ELSEVISER , Journal of Power Sources. Vol. 196, no.15, pp. 6007-6014..

[62] Battery University. (2018). "How to Prolong Lithium-based Batteries" [Online]. Battery University Available: https://batteryuniversity.com/learn/article/how_to_prolong_lithium_based_batteries.

[63] Battery Space. (2018). " Specification of LFP-G40 / LFP-G4S40AH," [Online]. Battery Space. Available: https://www.batteryspace.com/prod-specs/6333-40Ah.pdf..

[64] B. Fayed, B. A. Tar. (2016, Oct). "An Overview of the Fundamentals of Battery Chargers," IEEE 59th International Midwest Symposium on Circuits and Systems (MWSCAS)..

Appendix A

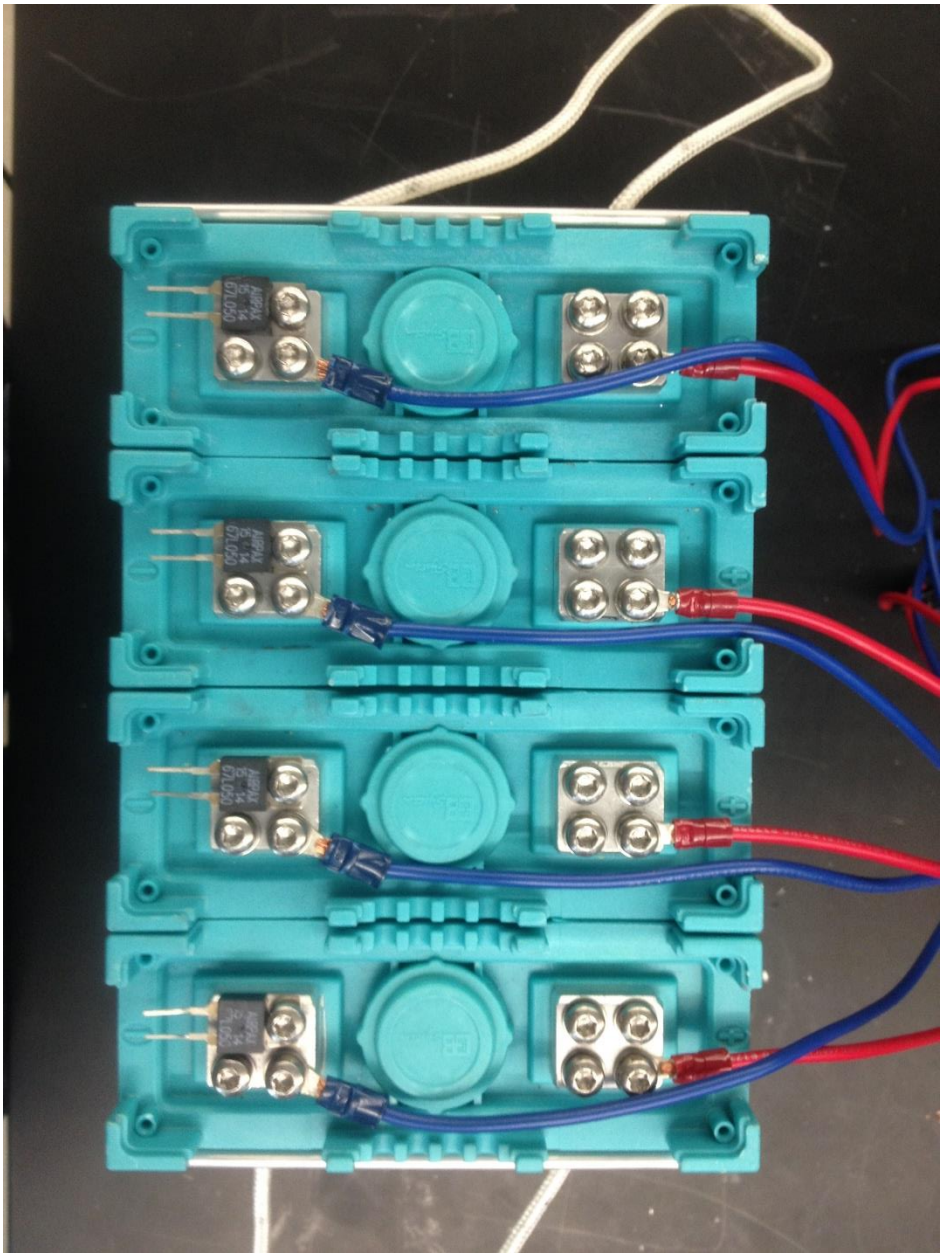

Fig. A. 1: Top view of one battery bank including Thermal Switches

Fig. A. 2: HESS Battery banks and cooling fans

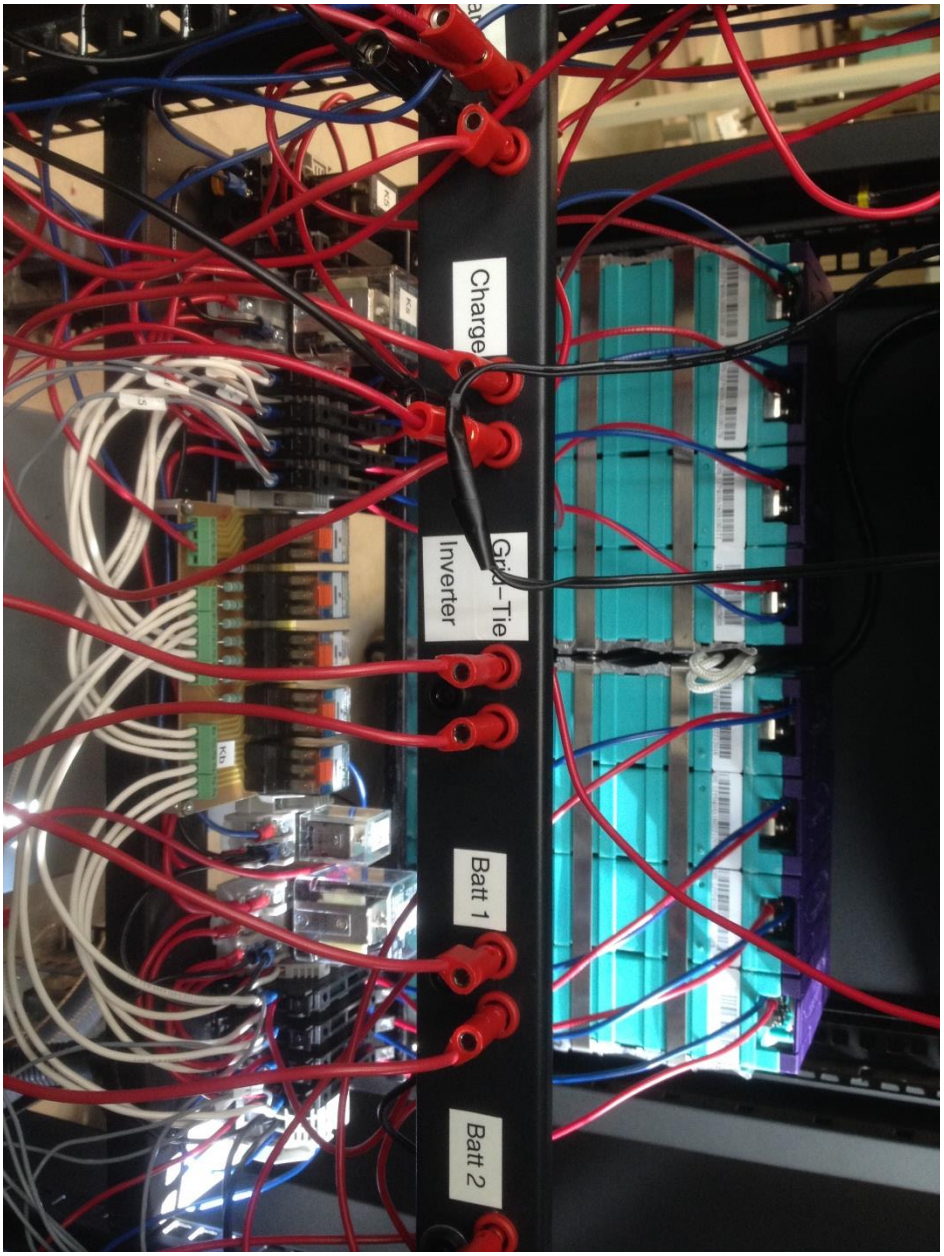

Fig. A. 3: HESS rear view of battery bank section